

# JOURNAL OF BIOMEDICINE AND TRANSLATIONAL RESEARCH

Available online at JBTR website: <https://jbtr.fk.undip.ac.id>

Copyright©2023 by Faculty of Medicine Universitas Diponegoro, Indonesian Society of Human Genetics and Indonesian Society of Internal Medicine

Original Research Article

## Analysis Of *Clerodendrum inerme* Plant Compounds as Anti Diabetes Mellitus Through Network Pharmacology Approach

Ahmad Shobrun Jamil<sup>1\*</sup>, Fauzan Hilmy<sup>2</sup>

<sup>1</sup>Department of Pharmacy, Faculty of Health Science, Universitas Muhammadiyah Malang, Indonesia

<sup>2</sup>Faculty of Health Science, Universitas Muhammadiyah Malang, Indonesia

### Article Info

#### History

Received: 08 Mar 2023

Accepted: 31 Oct 2023

Available: 31 Dec 2023

### Abstract

**Background:** Diabetes mellitus prevalence in Indonesia has surged. In 2021, an estimated 19.5 million people had diabetes, with a 10.6% age-adjusted prevalence. Projections indicate around 9.5 million cases by 2024. Diabetes medications, such as metformin, are commonly used, although these medications have adverse effects. A common choice for chronic diseases like DM is the use of natural medications. A plant known as *Clerodendrum inerme* has the potential to alleviate diabetes, but little is known about its molecular mechanisms.

**Objective:** The objective of this study was to investigate the chemical compound of *Clerodendrum inerme* and its molecular mechanism to treat diabetes mellitus.

**Methods:** The KNAPSAcK was used to analyze plant parts of *Clerodendrum inerme* to seek out chemicals present in plants. A screening was done to find compounds by estimating Absorption, Distribution, Metabolism, and Excretion (ADME) parameters using the canonical Simplified molecular-input line-entry system (SMILES) on the SwissADME. On the SwissTargetPrediction tool, predictions of target proteins from compounds that pass the screening are connected to various probable proteins. Utilizing the String-db to show the network between target proteins and associated diseases.

**Results:** The *Clerodendrum inerme* consists of 24 different compounds. The 24 compounds were screened, and the results showed that 4 of them, specifically (Z)-3-Hexenyl beta-D-glucopyranoside, Rhodioloside, Sammangaoside B, and Clerodermic acid, had the potential to develop into a therapeutic agent. The compound is then analyzed to find the protein target associated with diabetes mellitus and predict its networks. The findings indicate that multiple target proteins, including GSK3B, PPARG, DPP4, and STAT3, are connected to diabetes mellitus.

**Conclusion:** It has been shown that (Z)-3-Hexenyl beta-D-glucopyranoside, or Clerodermic acid, can attach to the proteins GSK3B, PPARG, DPP4, and STAT3, which are all linked to diabetes mellitus.

### Keywords:

*Clerodendrum inerme*; Diabetes Mellitus; molecular mechanism; potential; therapeutic

**Permalink/ DOI:** <https://doi.org/10.14710/jbtr.v9i3.17607>

### INTRODUCTION

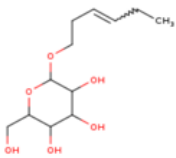

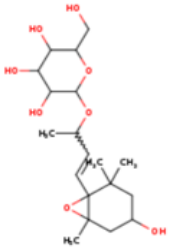

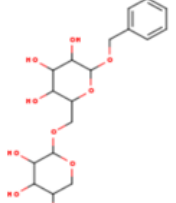

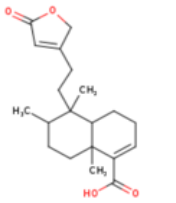

The prevalence of diabetes mellitus in Indonesia has been on the rise over time. In 2021, it was approximated that there were approximately 19.5 million individuals diagnosed with diabetes, which accounts for an age-adjusted comparative prevalence of 10.6%. It is

anticipated that by 2024, the diabetic population in Indonesia will reach an estimated 9.5 million individuals.<sup>1</sup>

\*Corresponding author:

E-mail: [shobrun@umm.ac.id](mailto:shobrun@umm.ac.id)  
(Ahmad Shobrun Jamil)

**Table 1.** List of substances that meet the Lipinski RoF (Rule of Five) for ADME selection. ADME evaluated 24 compounds, and four of them passed. These four substances have the potential to be used for developing novel DM drugs.

Metabolit	Compound Structure	Bioavailability Diagram	Pubchem CID	Molecule Weight	MLOGP	Bioavailability score	BBB permeant
(Z)-3-Hexenyl beta-D-glucopyranoside			5318045	262.3	-1.02	0.55	No
Rhodiolide			159278	388.45	-0.85	0.55	No
Sammangaoside B			102023621	402.39	-2.43	0.55	No
Clerodermic acid			16745295	332.43	3.53	0.85	Yes

Diabetes mellitus (DM) is a chronic metabolic disease or disorder with multiple etiologies characterized by high blood sugar levels and disturbances of carbohydrate, lipid, and protein metabolism as a result of insufficient insulin function.

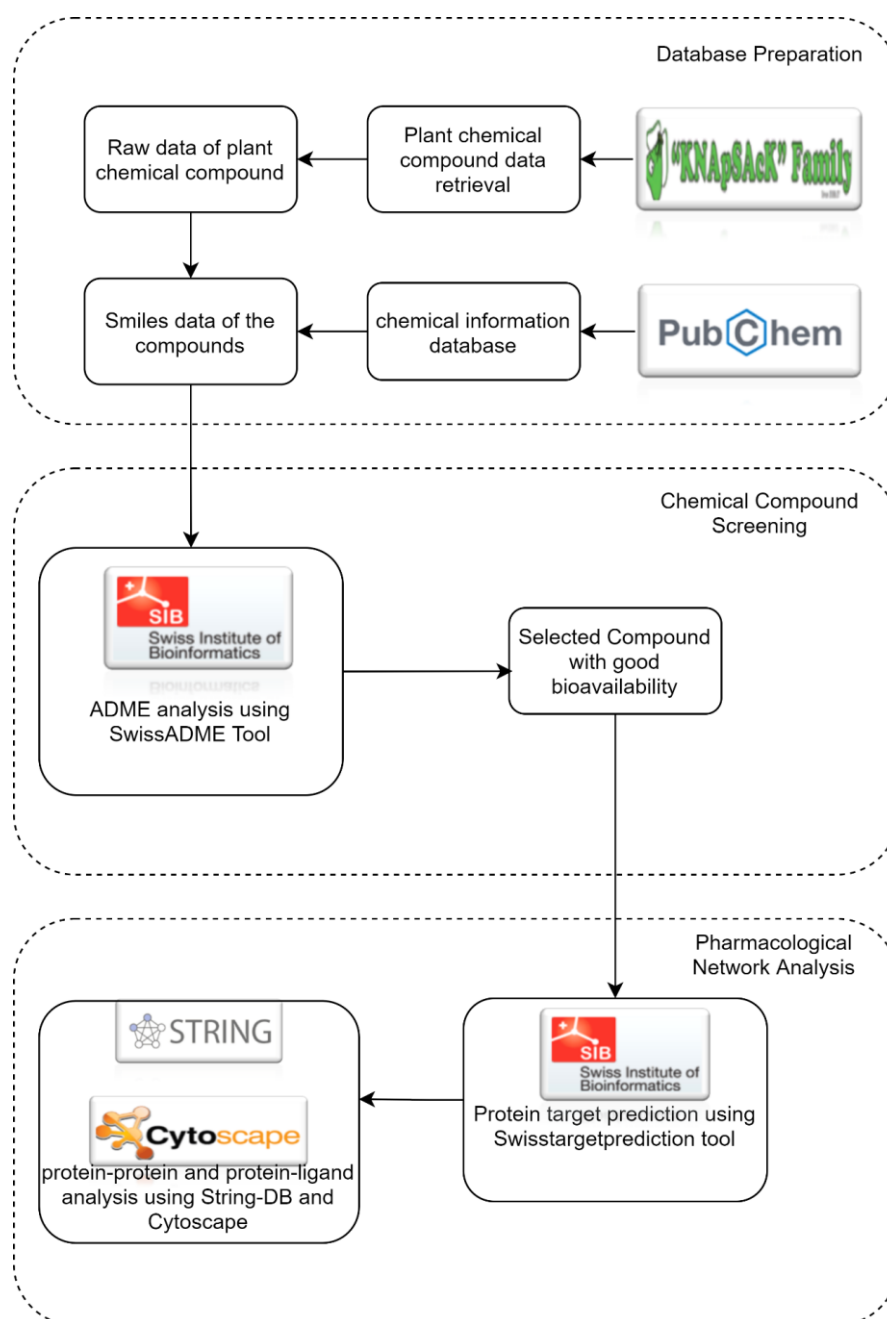
New therapies must be created and found to meet the need for health services, including those for promotion, prevention, treatment, and rehabilitation. Tens or even hundreds of new medications are released into the market each year after going through time-consuming and expensive development processes. DM is a common metabolic condition characterized by persistent hyperglycemia as a result of reduced insulin secretion, impaired glucose utilization, insulin resistance, and increased glucose synthesis.<sup>2</sup> The aim of the treatment of diabetes mellitus is to achieve normal insulin levels in plasma.<sup>3</sup> In network pharmacology approaches, important network proteins are targeted synergistically by two or more drugs acting mechanistically on the same causal signaling disease module.<sup>4</sup>

Diabetes mellitus is classified into two types: type 1 and type 2. Type 1 diabetes causes cell damage, resulting in the inability of the body to produce insulin. Insulin resistance, a condition in which cells fail to respond properly to insulin, is the starting point for type 2 Diabetes.<sup>5</sup> Another type of Diabetes is gestational diabetes. Gestational diabetes mellitus, often called

"Type 3 diabetes," emerges during pregnancy, typically vanishing after childbirth. It is characterized by insulin resistance and is linked to factors like interleukin-6 and C-reactive protein. It's essential to monitor and manage to ensure a healthy pregnancy and postpartum period.<sup>6</sup>

When fasting glucose exceeds 120 mg/dL or post-meal levels go beyond 200 mg/dL, it signifies diabetes. For venous blood, fasting levels over 140 mg/dL or post-meal levels over 200 mg/dL indicate diabetes. Impaired glucose tolerance (IGT) falls between 140-200 mg/dL after eating and less than 120-140 mg/dL when fasting. IGT doesn't need treatment but should be monitored.<sup>7</sup>

People are growing increasingly interested in network pharmacology, a brand-new subject based on system biology, bioinformatics, and high-throughput histology.<sup>8</sup> Important network proteins are targeted synergistically by two or more active compounds operating mechanistically on the same signaling disease module in pharmacology methods.<sup>4</sup> Network pharmacology, which recently linked corresponding targets to corresponding diseases and used them as three different types of nodes to construct a "component-target-disease" network, has combined the three active constituents of traditional Chinese medicine<sup>(9)</sup>.



**Figure 1.** Workflow chart of *Clerodendrum inerme* for the potential treatment of diabetes mellitus based on network pharmacology.

*Clerodendrum inerme*, often known as Indonesian Gambir Laut, belongs to the Verbenaceae family. Typically, these plants can be found in Australia, Asia, Malaysia, and the Pacific Islands. *Clerodendron inerme* is traditionally used to halt bleeding and treat asthma, hepatitis, ringworm, and colic. It is also used as a febrifuge, uterine stimulant, pest control agent, and antiseptic.<sup>10</sup> This study aims to determine what compounds in the *Clerodendrum inerme* plant have activity as therapeutic agents for individuals with diabetes mellitus.

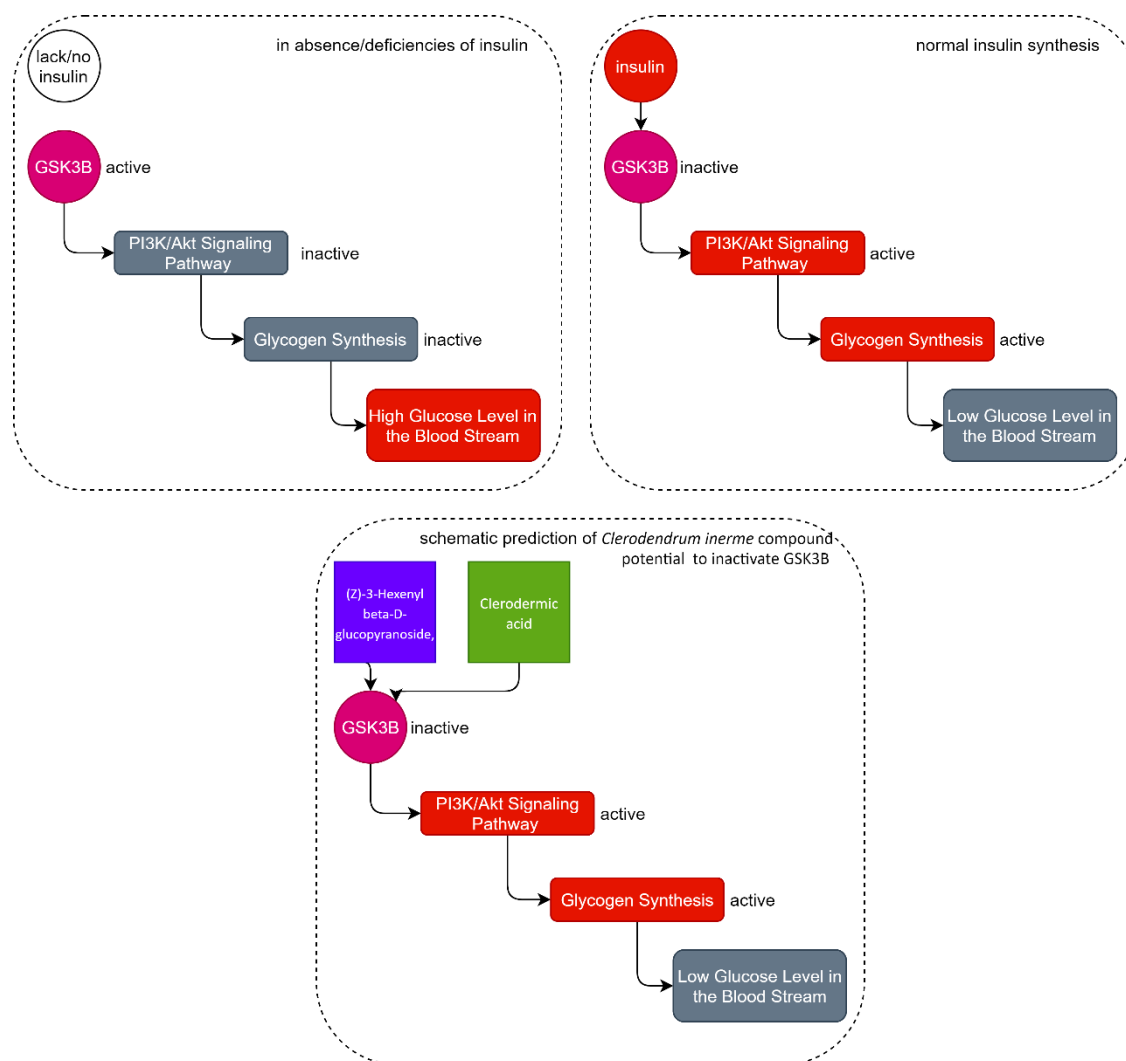
This study was carried out utilizing an *in-silico* approach, in which the compounds found in plants were initially searched using a web-based plant database. The compounds that meet the absorption, metabolism, distribution, and excretion (ADME) criteria are then screened based on their ADME properties. It continues

with proteins that can bind to compounds, and it will be investigated whether these proteins play a role in the mechanism of diabetes mellitus.

## MATERIALS AND METHODS

### Plant chemical compound data retrieval

*Clerodendrum inerme* chemical compound data were retrieved using the KNApSack database (accessed on 2023-01-20 at [http://www.knapsackfamily.com/knapsack\\_core/top.php](http://www.knapsackfamily.com/knapsack_core/top.php)).<sup>11</sup> Then, used the PubChem database (accessed on 2023-01-20 at <https://pubchem.ncbi.nlm.nih.gov>) to search the compound's canonical Simplified Molecular-Input Line-Entry System (SMILES).<sup>12</sup>



**Figure 2.** Predictive scheme for potential bioactive compounds in *Clerodendrum inerme* as candidates for diabetes mellitus treatment. GSK3B is a crucial protein in blood sugar regulation. The first scheme (top left) shows that with low or no insulin binding to GSK3B, glycogen synthesis is inactive. The second scheme (top right), with insulin binding to GSK3B, makes this protein inactive, activating glycogen synthesis and reducing blood glucose levels. The third scheme (bottom) suggests two compounds from *C. inerme*, (Z)-3-Hexenyl beta-D-glucopyranoside and Clerodermic acid, may potentially replace insulin's role by inhibiting GSK3B activity and activating the glycogen synthesis pathway, thus lowering blood glucose levels.

### Chemical Compound Screening

Chemical compound screening is used to find compounds that do not cause toxicity by predicting ADME characteristics, pharmacokinetic properties, drug-like qualities, and chemical friendliness of pharmaceuticals from one or more small molecules to aid in drug discovery using SwissADME tool (<http://www.swissadme.ch/index.php>, accessed on 2023-01-20).<sup>13</sup>

### Protein Target Prediction

Protein targets were predicted using the SwissTargetPrediction tool (<http://www.swisstargetprediction.ch>, accessed on 2023-01-20).<sup>14</sup> This tool estimates the most likely macromolecular targets of a small molecule that is thought to be bioactive. The prediction is based on a mix of 2D and 3D similarity with a library of 370,000 known actives on over 3000 distinct proteins from three different species.<sup>14</sup>

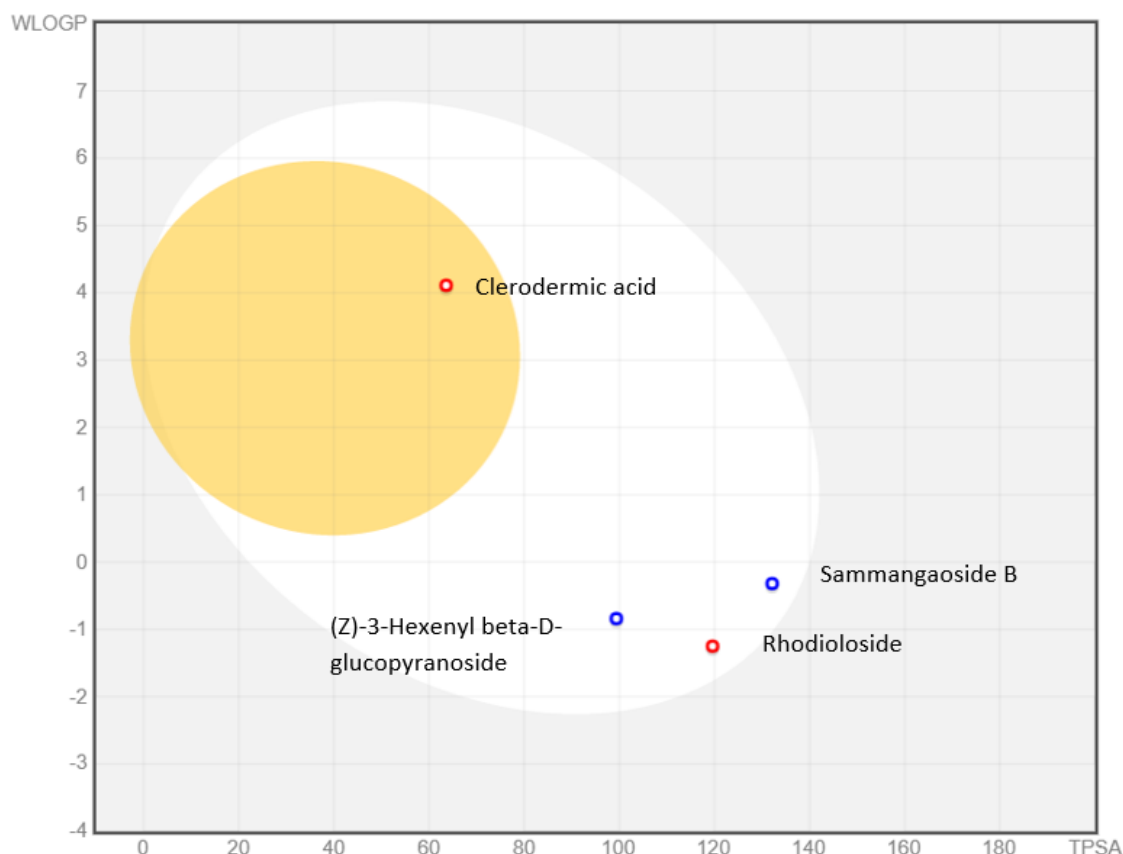
### Construction of target protein network and analysis

The following stage is to investigate functions and correlations between stage protein targets after discovering the protein targets for chemical compounds in plants. Utilizing String-DB and Cytoscape tools, it was possible to determine the link between the protein target and the chemical composition of plants. The online platform String-DB and the Cytoscape software version 3.1.1.9 can be utilized to perform direct (physical) and indirect (functional) connections related to this interaction.<sup>15,16</sup> The results of the correlation are built based on (1) Interaction between plant compounds and protein targets and (2) Interaction between protein targets and disease.

## RESULTS

### *Clerodendrum inerme* compound

The search for compounds contained in the *Clerodendrum inerme* plant was carried out through a database available on the KNApSACk website. Found 24 metabolite compounds and then carried out the next stage, namely the selection of compounds based on



**Figure 3.** Distribution of plant compounds using the BOILED-Egg visualization, to determine the lipophilicity of these compounds. There is one compound that can penetrate the blood-brain barrier, namely Clodermic acid. The other 3 compounds cannot penetrate the blood-brain barrier.

ADME. The requirements used are lipinski. Lipinski's Rule Of Five (RoF) is that the molecular weight is lower than 500 Da, the number of hydrogen bond donors is less than 5, the number of hydrogen bond acceptors is less than 10, and  $\chi \log P$  is lower than 5.<sup>17</sup> Detailed result can be found in table 1.

The 4 compounds were examined for their lipophilicity using the Brain or Intestinal EstimateD Permeation (BOILED-Egg) method. For this purpose, BOILED-Egg is proposed as an accurate predictive model that works by calculating the lipophilicity and polarity of small molecules.<sup>18</sup> From these results, it was found that 1 compound could penetrate the Blood-brain barrier, that is Clodermic Acid. For full details, it can be seen in Figure 2.

#### Correlation between compounds and protein targets

The four compounds that passed ADME will be tested to see if they can bind to any protein target associated with diabetes. The String-DB database is used to perform data mining. String-DB intends to prioritize scope (applying thousands of genome-sequenced organisms), evidence source richness (including automated text mining), and usability features (such as customization, enrichment detection, and programmatic access).<sup>15</sup> The target protein that have a probability to bind to protein target is shown in figure 3. The predicted targets of the four compounds include several proteins relevant to diabetes mellitus. They include GSK3B, PPARG, STAT3, ACE, and DPP4.

Apart from diabetes mellitus, other diseases were found that had a relationship with protein targets predicted from plant compounds that can be seen in figure 4. So, there is potential as a drug candidate apart from diabetes mellitus. In diabetes mellitus, there are 2 metabolites from the *Clerodendrum inerme* plant that are predicted to bind to target proteins, it is (Z)-3-Hexenyl beta-D-glucopyranoside (PubChem ID: 5318045) and Clodermic acid (PubChem ID: 16745295).

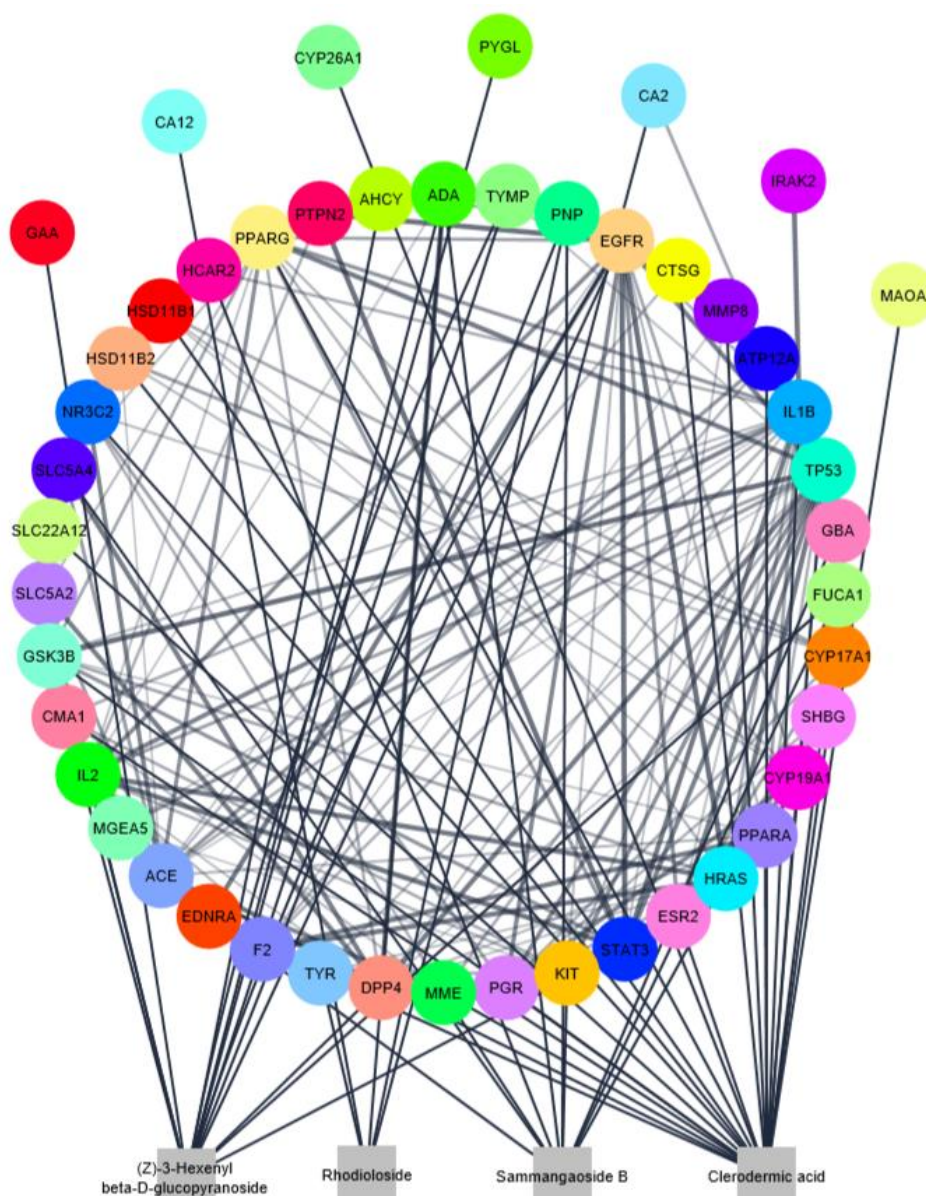
#### Correlation between protein targets and diabetes mellitus

Figures 2 and 3 reveal a relationship between the substance (Z)-3-Hexenyl beta-D-glucopyranoside and the proteins GSK3B, PPARG, DPP4, and STAT3 that have a role in controlling diabetes mellitus. Clodermic acid appears to interact with PPARG and GSK3B.

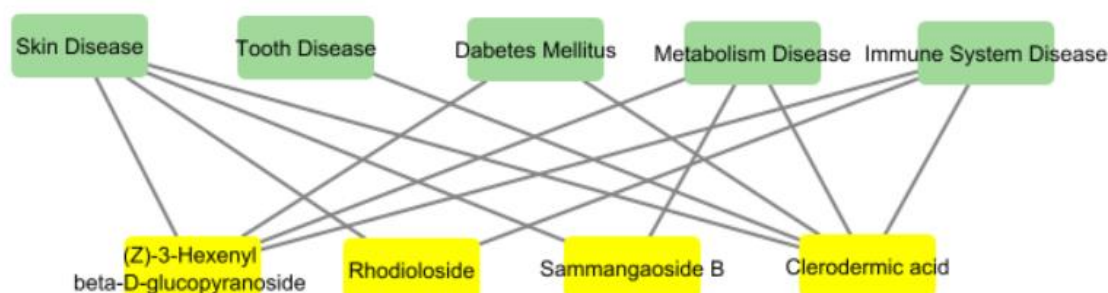
## DISCUSSION

GSK3B, also known as glycogen synthase kinase-3, is a proline-directed serine-threonine kinase that has been linked to the phosphorylation and inactivation of glycogen synthase, insulin signaling, glycogen synthesis, neurotrophic factor signaling, Wnt signaling, neurotransmitter signaling, and microtubule dynamics. microtubule dynamics, neurotrophic factor, Wnt, neurotransmitter signaling, and insulin and glycogen synthesis.<sup>19</sup> GSK3B is important in the treatment of diabetes. In insulin-related signaling pathways, GSK3B is considered a negative regulator, and phosphorylation renders GSK3B inactive. One of the major downstream targets of AKT signaling is GSK3B. Figure 5 shows





**Figure 4.** The correlation between *Clerodendrum inerme* metabolites and protein targets, which are shown in gray are plant metabolites called (Z)-3-Hexenyl beta-D-glucopyranoside, Rhodiolside, Sammangaoside B, Clerodermic acid. The colors of the rainbow are the target protein resulting from the prediction of the protein target.



**Figure 5.** Correlation between disease and metabolites of *Clerodendrum inerme*.

diabetes influences cell death through disruption of insulin signaling pathways.<sup>20</sup> Compounds from the *Clerodendrum inerme* plant will act as inhibitors on GSK3B so that the glycogen protein synthase is not inhibited and there is no decrease in glycogen synthesis.

Peroxisome proliferator-activated receptor gamma (PPAR $\gamma$ - or PPARG) is a type II nuclear receptor that acts as a transcription factor and is encoded by the PPARG gene in humans. It is also known as glitazone reverse insulin resistance receptor or NR1C3 (nuclear receptor

subfamily 1, group C, member 3).<sup>21</sup> Several lines of evidence have shown that the SNPs of the PPARG (nuclear receptor) have an important role in controlling lipid and glucose metabolism.<sup>22</sup> PPARG promotes adiponectin collection from fat cells, increases fatty acid storage in fat cells (reduces lipotoxicity), induces FGF21, and enhances nicotinic acid adenine dinucleotide phosphate synthesis by increasing the CD38 enzyme.<sup>23</sup> The role of plant compounds in PPARG is as a ligand on PPARG (receptor). Once activated by the plant compound *Clerodendrum inerme*, the nuclear receptor binds to DNA-specific PPAR response elements (PPRE) and modulates the transcription of its target genes, such as acyl-CoA oxidase. Hence, it controls the peroxisome beta-oxidation pathway of fatty acids.

The STAT3 gene encodes signal transducers and activators of transcription that mediate cellular responses to growth factors such as interleukins, KITLG/SCF, LEP, and others. Coactivators such as NCOA1 or MED1 to the promoter region of target genes upon activation. According to research, the JAK2/STAT3/SOCS-1 signaling pathway is activated to cause hepatic insulin resistance and is also involved in the treatment of T2DM and insulin resistance.<sup>24</sup> Studies showing that activation or loss of STAT3 leads to insulin resistance, loss of muscle mass, or increased satellite cell repair depending on STAT3 stimulation and penning length are proof of this. In the framework of myotubes made from people with impaired glucose tolerance, IL-6 causes insulin resistance. Insulin sensitivity is increased and muscle regeneration is facilitated by STAT3 inhibition in muscles.<sup>25</sup>

Adenosine Deaminase Complexing Protein-2 and T cell CD26 antigen are related to dipeptidyl peptidase 4, commonly referred to as Gen DPP4. This is a type II intrinsic glycoprotein transmembrane enzyme that breaks down the protein X-proline from the N polypeptide's starting codon. Dipeptidyl peptidase 4 plays a significant role in the metabolism of glucose and insulin as well as the immune system. The surface cell receptor glycoprotein found in synaptic vesicles is essential for mediating cell-to-cell receptor activation (TCR). Acts as a positive regulator of T-cell coactivation by binding to at least ADA, CAV1, IGF2R, and PTPRC. The connection between CAV1 and CARD11 promotes T cell proliferation and NF-kappa-B activation in T cell receptors/caras that are concentrated on CD3. Interaction with ADA also changes the adhesion of the limfosit-epitel adhesion. Compounds in the *Clerodendrum inerme* plant function as DPP4 inhibitors, so increasing or prolonging GLP-1 levels can potentiate insulin secretion by the pancreas. In addition, inhibition of DPP4 can reduce the production of  $\alpha$  cells, so that glucagon and glucose in plasma also decrease.<sup>26</sup>

From the extensive elucidation of cellular molecular mechanisms related to the interaction between bioactive compounds in *C. inerme* and target proteins, particularly in the context of diseases like diabetes mellitus, it's important to understand that this research is *in-silico* or computationally predictive, utilizing artificial intelligence. Subsequent in vitro and in vivo studies are imperative to confirm and bolster the evidence presented by this research.

In vitro and in vivo research are essential to corroborate *in-silico* findings. While *in-silico* provides valuable predictions, in vitro and in vivo studies validate these predictions in real biological systems. They offer insights into how substances or interventions affect living organisms, their safety, and potential side effects. In vivo research, in particular, is crucial for testing therapies' effectiveness on experimental animals or humans, providing a deeper understanding of their therapeutic potential. By combining data from these three research approaches, we gain a more comprehensive understanding, reduce errors, and support the development of safer and more effective treatments.

## CONCLUSION

Compounds contained in the *Clerodendrum inerme* plant, that are (Z)-3-Hexenyl beta-D-glucopyranoside, Clerodermic acid can bind to proteins associated with diabetes mellitus (GSK3B, PPARG, DPP4, STAT3). These compounds bind by inhibiting or activating the function of the target protein. So the *Clerodendrum inerme* plant has potential as a diabetic drug candidate.

The use of computer models, which may oversimplify complicated biological processes, is one restriction of *in-silico* research. It doesn't account for real-world unpredictability and could produce inaccurate predictions. Additionally, data quality and model validation are significant challenges that need additional experimental validation to produce reliable results. Recommend strengthening *in-silico* research through model complexity enhancement, actual variability involvement, and robust experimental accuracy validation through in vitro and in vivo research.

## ACKNOWLEDGMENTS

The author would like to thank the Faculty of Health Sciences at the University of Muhammadiyah Malang for sponsoring this research.

## REFERENCES

1. IDF. Diabetes facts and figures show the growing global burden for individuals, families, and countries. 2023. p. 1–6.
2. Monobe K, Noso S, Babaya N, Hiromine Y, Taketomo Y, Niwano F, et al. Clinical and genetic determinants of urinary glucose excretion in patients with diabetes mellitus. *J Diabetes Investig.* 2021 May;12(5):728–37.
3. Ferguson D, Finck BN. Emerging therapeutic approaches for the treatment of NAFLD and type 2 diabetes mellitus. *Nat Rev Endocrinol.* 2021 Aug;17(8):484–95.
4. Nogales C, Mamdouh ZM, List M, Kiel C, Casas AI, Schmidt HHHW. Network pharmacology: curing causal mechanisms instead of treating symptoms. *Trends Pharmacol Sci.* 2022 Feb;43(2):136–50.
5. Tanase DM, Gosav EM, Costea CF, Ciocoiu M, Lacatusu CM, Maranduca MA, et al. The Intricate Relationship between Type 2 Diabetes Mellitus (T2DM), Insulin Resistance (IR), and Nonalcoholic Fatty Liver Disease (NAFLD). *J Diabetes Res.* 2020;2020.

6. Szmuiłowicz ED, Josefson JL, Metzger BE. Gestational Diabetes Mellitus. *Endocrinol Metab Clin North Am.* 2019 Sep;48(3):479–93.
7. Yosmar R, Almasdy D, Rahma F. Survei Risiko Penyakit Diabetes Melitus Terhadap Masyarakat Kota Padang. *J Sains Farm Klin.* 2018 Aug;5(2):134–41.
8. Liu J, Liu J, Tong X, Peng W, Wei S, Sun T, et al. Network Pharmacology Prediction and Molecular Docking-Based Strategy to Discover the Potential Pharmacological Mechanism of Huai Hua San Against Ulcerative Colitis. *Drug Des Devel Ther.* 2021;15:3255–76.
9. Wu N, Yuan T, Yin Z, Yuan X, Sun J, Wu Z, et al. Network Pharmacology and Molecular Docking Study of the Chinese Miao Medicine Sidaxue in the Treatment of Rheumatoid Arthritis. *Drug Des Devel Ther.* 2022;16:435–66.
10. Kar P, Dutta S, Chakraborty AK, Roy A, Sen S, Kumar A, et al. The antioxidant-rich active principles of *Clerodendrum* sp. control haloalkane xenobiotic-induced hepatic damage in murine model. *Saudi J Biol Sci.* 2019 Nov;26(7):1539–47.
11. Nakamura Y, Mochamad Afendi F, Kawsar Parvin A, Ono N, Tanaka K, Hirai Morita A, et al. KNApSACk metabolite activity database for retrieving the relationships between metabolites and biological activities. *Plant Cell Physiol.* 2014;55(1):1–9.
12. Kim S, Thiessen PA, Cheng T, Yu B, Shoemaker BA, Wang J, et al. Literature information in PubChem: Associations between PubChem records and scientific articles. *J Cheminform.* 2016 Jun 10;8(1).
13. Daina A, Michielin O, Zoete V. SwissADME: A free web tool to evaluate pharmacokinetics, drug-likeness and medicinal chemistry friendliness of small molecules. *Sci Rep.* 2017;7(October 2016):1–13.
14. Gfeller D, Grosdidier A, Wirth M, Daina A, Michielin O, Zoete V. SwissTargetPrediction: A web server for target prediction of bioactive small molecules. *Nucleic Acids Res.* 2014 Jul 1;42(W1).
15. Szklarczyk D, Gable AL, Nastou KC, Lyon D, Kirsch R, Pyysalo S, et al. The STRING database in 2021: customizable protein-protein networks, and functional characterization of user-uploaded gene/measurement sets. *Nucleic Acids Res.* 2021 Jan;49(D1): D605–12.
16. Ono K. Introduction to Biological Network Analysis and Visualization with Cytoscape. 2016.
17. Nogara PA, Saraiva RDA, Caeran Bueno D, Lissner LJ, Lenz Dalla Corte C, Braga MM, et al. Virtual screening of acetylcholinesterase inhibitors using Lipinski's rule of five and ZINC databank. *Biomed Res Int.* 2015 Jan;2015.
18. Daina A, Zoete V. A BOILED-Egg To Predict Gastrointestinal Absorption and Brain Penetration of Small Molecules. *ChemMedChem.* 2016;1117–21.
19. An WF, Germain AR, Bishop JA, Nag PP, Metkar S, Ketterman J, et al. Discovery of Potent and Highly Selective Inhibitors of GSK3 $\beta$ . *Probe Reports from NIH Mol Libr Progr.* 2010;
20. Zhu YR, Jiang XX, Ye P, Wang ZM, Zheng Y, Liu Z, et al. Knockout of AKAP150 improves impaired BK channel-mediated vascular dysfunction through the Akt/GSK3 $\beta$  signaling pathway in diabetes mellitus. *J Cell Mol Med.* 2020 Apr;24(8):4716–25.
21. Greene ME, Blumberg B, McBride OW, Yi HF, Kronquist K, Kwan K, et al. Isolation of the Human Peroxisome Proliferator-Activated Receptor Gamma cDNA: Expression in Hematopoietic Cells and Chromosomal Mapping. *Gene Expr.* 1995;4(4–5):281.
22. Sarhangi N, Sharifi F, Hashemian L, Hassani Doabsari M, Heshmatzad K, Rahbaran M, et al. PPARG (Pro12Ala) genetic variant and risk of T2DM: a systematic review and meta-analysis. *Sci Rep.* 2020 Dec;10(1).
23. Ahmadian M, Suh JM, Hah N, Liddle C, Atkins AR, Downes M, et al. PPAR $\gamma$  signaling and metabolism: the good, the bad, and the future. *Nat Med.* 2013;19(5):557–66.
24. Zhang Y, Lin C, Chen R, Luo L, Huang J, Liu H, et al. Association analysis of SOCS3, JAK2, and STAT3 gene polymorphisms and genetic susceptibility to type 2 diabetes mellitus in Chinese population. *Diabetol Metab Syndr.* 2022 Dec;14(1).
25. Gurzov EN, Stanley WJ, Pappas EG, Thomas HE, Gough DJ. The JAK/STAT pathway in obesity and diabetes. *FEBS J.* 2016 Aug;283(16):3002–15.
26. Zhong J, Maiseyeu A, Davis SN, Rajagopalan S. DPP4 in Cardiometabolic Disease. *Circ Res.* 2015 Apr;116(8):1491–504.



# JOURNAL OF BIOMEDICINE AND TRANSLATIONAL RESEARCH

Available online at JBTR website: <https://jbtr.fk.undip.ac.id>

Copyright©2023 by Faculty of Medicine Universitas Diponegoro, Indonesian Society of Human Genetics and Indonesian Society of Internal Medicine

Original Research Article

## Comparative Analysis of Kidney Histomorphometry Utilizing Two Distinct Image Processing Software

Ageng Brahmadi<sup>1\*</sup>, Ira Citra Ningrom<sup>2</sup>

<sup>1</sup>Histology Laboratory, Faculty of Medicine, Universitas Muhammadiyah Purwokerto, Indonesia

<sup>2</sup>Patology Anatomy Laboratory, Faculty of Medicine, Universitas Muhammadiyah Purwokerto, Indonesia

### Article Info

History

Received: 08 Jun 2023

Accepted: 21 Nov 2023

Available: 31 Dec 2023

### Abstract

**Background:** Histopathological examination is critical to evaluate tissue condition. An accurate assessment is necessary for diagnosis establishment. Nowadays, both quantitative and qualitative scoring are enhanced with computer-assisted image analysis to reduce bias. Various software was developed to assist in image analysis. The question of whether the measurement results from one software will be comparable to those from another software may come up, given the wide variety of software options. Nevertheless, this subject is only occasionally discussed.

**Objective:** This study aimed to compare the measurement results from two open-source software, Fiji and QuPath software in kidney histomorphometry.

**Methods:** Five histological slides of normal kidney were observed. Selected histological structures, including the renal corpuscle area, glomerular area, Bowman space area, inner diameter of proximal, distal, and Henle loop, were measured using QuPath (version 0.3.2) and Fiji (version 1.53c) software. The measurement results from the two software were compared for value differences and agreement analysis.

**Results:** The renal corpuscle means the area was  $12.7 \times 10^3 \mu\text{m}^2$  in QuPath and  $12.5 \times 10^3 \mu\text{m}^2$  in Fiji. The glomerular area was  $7.8 \times 10^3 \mu\text{m}^2$  for both software. The proximal tubule's inner diameters varied from 18.7 to 150.8  $\mu\text{m}$ . Smaller inner diameters were observed in distal tubules (17.1-80.5  $\mu\text{m}$ ) and The Henle loop (15.5-69.6  $\mu\text{m}$ ). There was no significant difference in measurement results of particular structures between the compared software (P-value > 0.05). The further confirmational analysis supported the similarity between the two measurement results.

**Conclusion:** the measurement result of kidney microstructures using QuPath and Fiji were identical.

**Keywords:** Kidney; Histology; Computer-assisted; Histomorphometry

**Permalink/ DOI:** <https://doi.org/10.14710/jbtr.v9i3.18554>

### INTRODUCTION

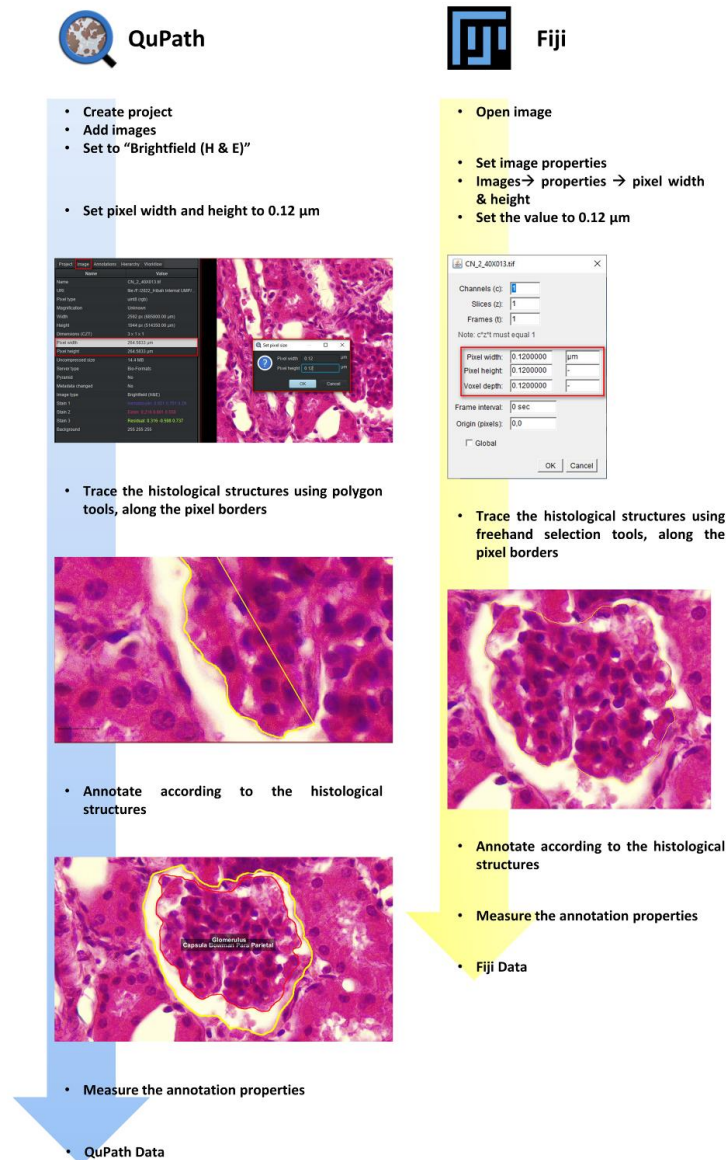
Histopathological examination is critical to evaluate the condition of cells, tissues, and organs. An accurate assessment is necessary for diagnosis establishment or determining disease progression. Generally, a histological examination can be performed semi-quantitatively or quantitatively using virtual images and measuring tissue histology parameters.

Both quantitative and qualitative methodologies have advantages and disadvantages. The qualitative diagnosis is based on identifiable morphological changes in the tissue area of interest and requires trained experts

or pathologists.<sup>1</sup> In the semi-quantitative scoring, the qualitative tissue data are converted into numerical data which enables more reliable group comparison.<sup>2</sup> The semi-quantitative approach is widely used in preclinical and clinical research. However, a decent experimental design and a reliable scoring system are a must in order to enhance reproducibility and limit result bias.<sup>2</sup>

\*Corresponding author:

E-mail: [brahmadi@ump.ac.id](mailto:brahmadi@ump.ac.id)  
(Ageng Brahmadi)

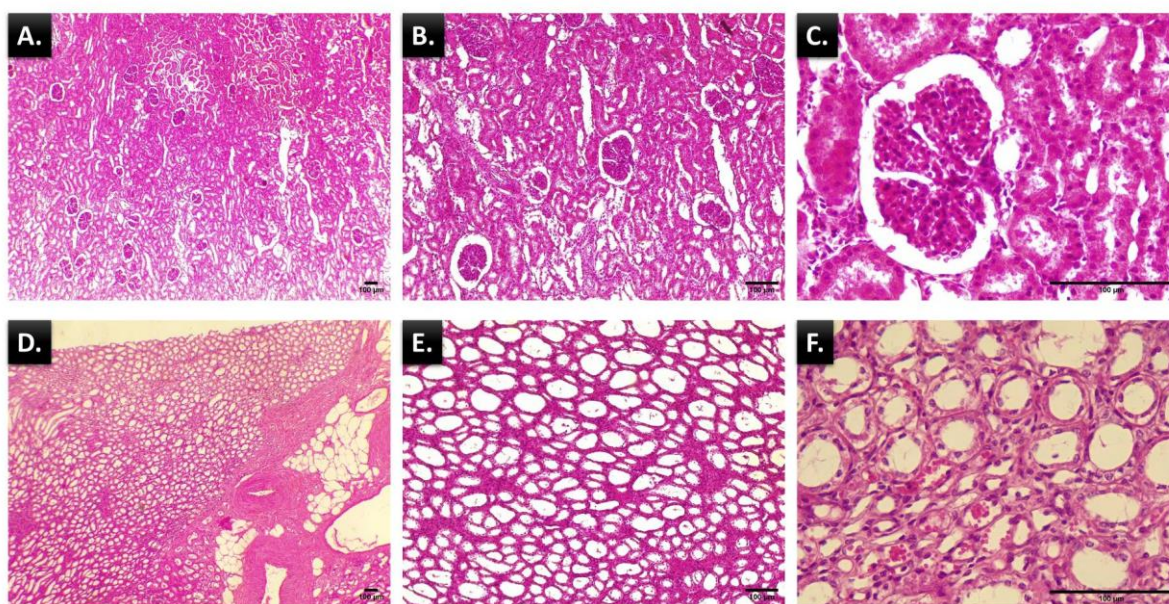


**Figure 1.** Data acquisition procedures using QuPath and FIJI

Along with technological advancement, either quantitative or qualitative scoring might be enhanced with computer-assisted image analysis to lessen the bias. Various software such as ImageJ2,<sup>3</sup> Fiji,<sup>4</sup> QuPath,<sup>4</sup> Cell profiler analyst,<sup>5</sup> Advanced cell classifier,<sup>6</sup> Ilastik,<sup>7</sup> Cell Cognition Explorer<sup>8</sup> and many more were developed to assist in image analysis. Typically, two-dimensional sections are used for image analysis, which may produce skewed results. As a result, more advanced methods such as unbiased stereology and whole slide images (WSI) analysis were introduced in histology. Unbiased stereology and WSI analysis provide more reliable data than traditional qualitative and semi-quantitative analysis. However, applying these two methods might not be feasible in some laboratories for several reasons, including method complexity, technology and human resource limitation,<sup>9</sup> the high initial cost of the scanners, the cost of acquisition, deployment, and operational costs of WSI.<sup>10</sup>

Considering the aforementioned limitations, some researchers or laboratories continue to use qualitative or

semi-quantitative tissue assessment. Open-source software is preferable to accommodate the analysis demands. ImageJ was known as one of the pioneers of image analysis software. Along with the technology development, ImageJ was developed further to ImageJ2 and currently known as Fiji. As the next generation of ImageJ, Fiji is equipped with various built-in plug-ins. Another option for open-source software for analysis is QuPath. QuPath is reliable software for digital pathology and is designed to accommodate WSI analysis. However, QuPath is less popular compared to Fiji. The question of whether the measurement results from one software will be comparable to those from another software may come up given the wide variety of software options. To the author's knowledge, this subject is only occasionally discussed. Therefore, this study aims to compare the measurement results from Fiji and QuPath software in kidney histomorphometry.



**Figure 2.** Kidney histological examination in various magnifications. A. Renal cortex at low magnification (4x); B. Renal cortex at medium magnification (10x); C. Renal cortex at high magnification (40x); D, E, and F respectively represent the renal medulla at low, medium, and high magnification.

## MATERIALS AND METHODS

Haematoxylin eosin-stained human kidney histological slide was purchased from Ginkomed Taiwan. Five slides (CAT NO H110010) were used in this study. The observation was performed in the cortical and medulla region using Leica DM500. Description of specific tissue characteristics and histological structures in 4x, 10x, and 40x objective magnification were compared.

For histomorphometry analysis, areas containing the renal corpuscle and medulla region were photographed in 40x objective magnification using Leica ocular camera (LCC50E). Leica LAS EZ software was used to obtain calibrated images. The images then proceed further for histomorphometry measurements using open-source software QuPath version 0.3.2 (<https://qupath.github.io/>) and Fiji version 1.53c (<https://fiji.sc/>). Selected histological structures, including the renal corpuscle area, glomerular area, inner diameter of distal tubules, proximal tubules, and Henle loop were measured using QuPath and Fiji (Figure 1). The Bowman space area was calculated by subtracting the renal corpuscle area from glomerular area and expressed in  $\mu\text{m}^2$ . The inner diameter of tubules was stated in  $\mu\text{m}$ .

The measurement results from the two software were analysed for data normality using Kolmogorov–Smirnov test and then compared for value differences. The renal corpuscle area, glomerular area and Bowman capsule area were analysed with t-test. The tubules inner diameters were analysed with Mann-Whitney test because the data were not normally distributed. Deming regression and Bland-Altman plot for agreement analysis. P-value < 5% was considered as significant difference between values. The study was approved by the Medical and Health Research Ethics Committee of Faculty of Medicine Universitas Muhammadiyah Purwokerto (No: KEPKK/FK/052/VIII/2023).

## RESULTS

### Renal histology

Renal tissue examinations were carried out thoroughly, covering the renal cortex to the renal medulla. At low magnification (4x), dark-red tissue parenchyma was seen in the renal cortex. The renal corpuscles were seen as spherical structures, scattered through the cortex. The cortical labyrinth appears as dense parenchyma with a white-colored lumen. However, it is still difficult to distinguish the type of kidney tubules at this magnification. As the magnification increases, the histological structure details become more visible (Figure 2B and C). The glomerulus structure is identified, and the parietal layer of Bowman's capsules can be distinguished from the surrounding renal tubules. Higher magnification enables renal tubule identification. As shown in Figure 2C, the proximal convoluted tubule with a brush border on its lumen can be distinguished from the distal tubule. A contrasting histological appearance is exhibited in the medulla. In low and medium magnification observation, the renal medulla parenchyma was paler-colored and looser than the cortex (Figure 2D and E). Renal tubules with varying lumen diameters were seen. The collecting tubules, distal tubule, and Henle loop segments appear to predominate in the renal medulla (Figure 2F). However, the proximal tubule is also occasionally found in this region.

### Renal structures histomorphometry

Measurement of selected histological structures was performed at 40x objective magnification. In the cortical region, the measurements focused on renal corpuscles, distal tubules, and proximal tubules. The area covered by the parietal layer and renal glomerulus was determined. The area of Bowman space was calculated by subtracting the area contained in the Bowman capsule parietal layer area from the glomerular area. In the medulla region, the measurements were subjected mainly to the inner diameters of the Henle loop.



**Table 1.** Histomorphometry parameters of kidney microstructures

Histological structures	QuPath	Fiji	<i>p-value</i>
<b>Renal corpuscle area (<math>\times 10^3 \mu\text{m}^2</math>)</b>			
Min	6.3	6.3	0.8440 <sup>a)</sup>
Max	18.9	18.8	
Mean $\pm$ SD	12.7 $\pm$ 2.9	12.5 $\pm$ 3.0	
<b>Glomerular area (<math>\times 10^3 \mu\text{m}^2</math>)</b>			
Min	3.3	3.3	0.9914 <sup>a)</sup>
Max	13.3	13.3	
Mean $\pm$ SD	7.8 $\pm$ 2.1	7.8 $\pm$ 2.2	
<b>Bowman space area (<math>\times 10^3 \mu\text{m}^2</math>)</b>			
Min	1.7	2.0	0.6539 <sup>a)</sup>
Max	8.3	7.8	
Mean $\pm$ SD	4.8 $\pm$ 1.5	4.7 $\pm$ 1.5	
<b>TP inner diameter (<math>\mu\text{m}</math>)</b>			
Min	20.2	18.7	0.8288 <sup>b)</sup>
Max	142.4	150.8	
Mean $\pm$ SD	47.7 $\pm$ 25.46	47.5 $\pm$ 26.3	
<b>TD inner diameter (<math>\mu\text{m}</math>)</b>			
Min	17.1	17.8	0.9207 <sup>b)</sup>
Max	80.5	79.3	
Mean $\pm$ SD	36.8 $\pm$ 15.0	36.6 $\pm$ 15.0	
<b>HL inner diameter (<math>\mu\text{m}</math>)</b>			
Min	15.7	15.5	0.9322 <sup>b)</sup>
Max	68.8	69.6	
Mean $\pm$ SD	35.1 $\pm$ 10.7	34.9 $\pm$ 10.7	

<sup>a)</sup> *p-values* were obtained from independent *T-test*

<sup>b)</sup> *p-values* were obtained from Mann-Whitney test

TP: Proximal tubule; TD: Distal tubule; HL: Henle loop.

The measurement showed that the renal corpuscle means areas were  $12.7 \pm 2.9 \times 10^3 \mu\text{m}^2$  and  $12.5 \pm 3.0 \times 10^3 \mu\text{m}^2$  for QuPath and Fiji respectively. The glomerular area was  $7.8 \pm 2.1 \times 10^3 \mu\text{m}^2$  for QuPath and  $7.8 \pm 2.2 \times 10^3 \mu\text{m}^2$  for Fiji. The calculated mean Bowman space area was  $4.8 \pm 1.5 \times 10^3 \mu\text{m}^2$  and  $4.7 \pm 1.5 \times 10^3 \mu\text{m}^2$  for QuPath and Fiji respectively. The T-test showed there was no difference in the measurement from both software (*p*-value > 0.05) (Table 1).

The detailed values of renal tubules' inner diameters are shown in Table 1. Based on our examination using two software, the inner diameter of the proximal tubule ranged from 18.7-150.8  $\mu\text{m}$ . The distal tubules' inner diameter was smaller compared to the proximal tubule, ranging from 17.1-80.5  $\mu\text{m}$ . The Henle loop had the smallest diameter among the other kidney tubules, in the range of 15.5-69.6  $\mu\text{m}$ . From the renal tubule measurements, we also did not find any statistical differences between the two software measurement results (*p*-value > 0.05).

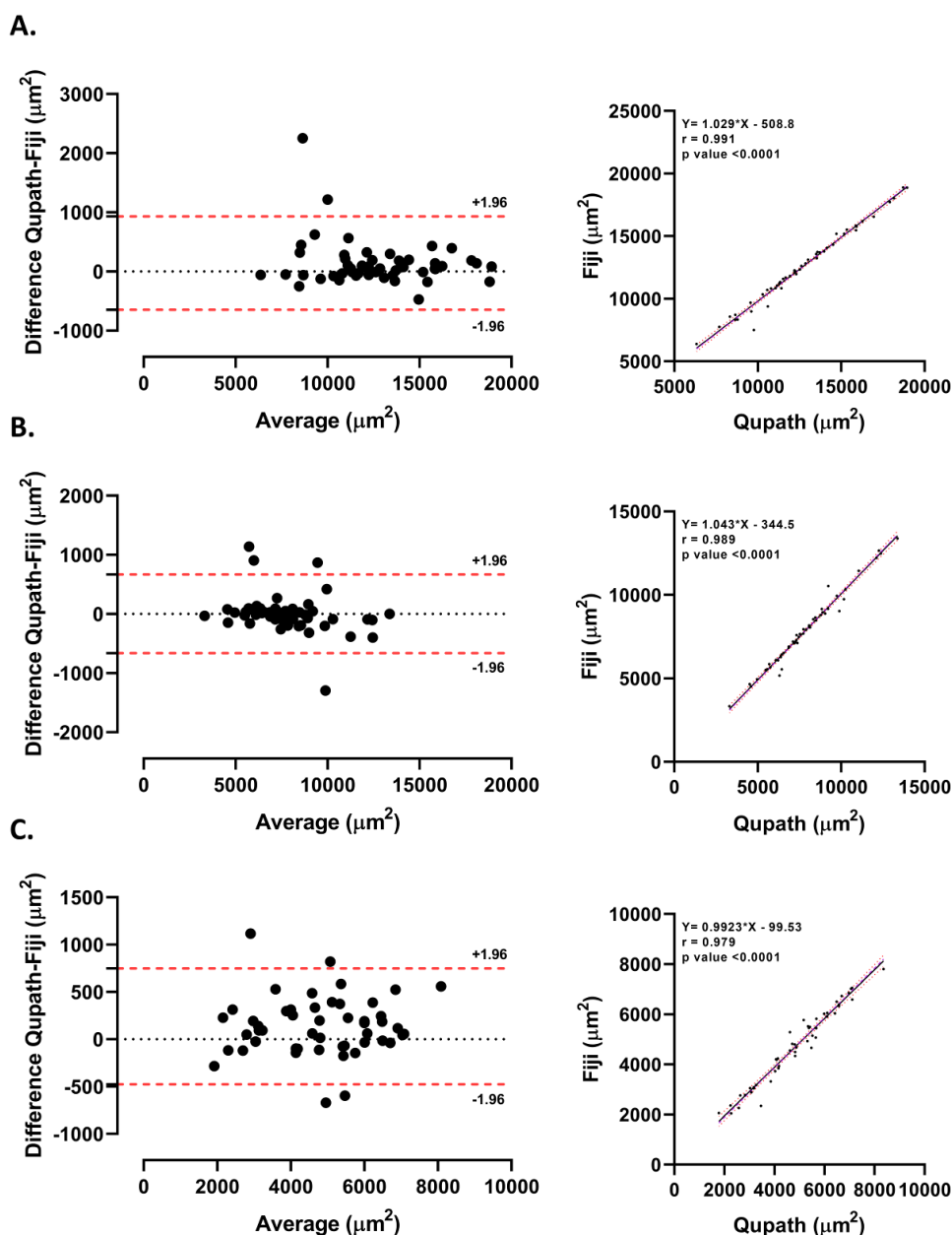
To further confirmed that the measurement from QuPath and Fiji were identical. We analysed the quantification results using Deming regression and the Bland-Altman plot. The Deming regression exhibited linear correlation for quantification of renal corpuscle area (Figure 3A), glomerular area (Figure 3B), and Bowman space area (Figure 3C) in both software. In addition, Pearson's rho values were beyond 0.979 (Figure 3A-C, right panel). The Bland-Altman plot showed most of the measurement values from both software were within the lower and upper limits of agreements. Only a small percentage of values were outside the limit of the agreements range. The off-limit values were 4% for the value of the renal corpuscle area and 8% for either the glomerular or Bowman capsule area value (Figure 3A-C, left panel).

The correlation and linearity from two measurements were also demonstrated for the values of the inner diameter of renal tubules. Pearson's rho values greater than 0.995 was obtained for the distal tubule (Figure 4A) and proximal tubule (Figure 4B). For Henle loop inner diameter, the lower Pearson's rho value was obtained (*r* = 0.880) (Figure 4C). The majority of paired data were within the lower and upper limits of agreement of the Bland-Altman plot. However, we observed 4% off limit values in the distal tubule (Figure 4A left panel), and 8% in proximal tubule and Henle loop inner diameter value (Figure 4B and C, left panel).

## DISCUSSION

All slides showed normal kidney histology. Under normal circumstances, histological structures including renal corpuscle, renal tubules, various types of vessels, in the cortical and medulla regions were identified under a bright field microscope. Magnification adjustment might require to gain greater details on the structures. Particular lesion or histological structures, might best be viewed in specific magnification, for example glomerular lesions it is usually observed at 400-1000x magnification while tubulointerstitial lesions is generally analysed at 100-400x magnification.<sup>11</sup>

We obtained renal corpuscle means areas of  $12.7 \pm 2.9 \times 10^3 \mu\text{m}^2$  in QuPath and  $12.5 \pm 3.0 \times 10^3 \mu\text{m}^2$  from Fiji measurement. The glomerular areas were  $7.8 \pm 2.1 \times 10^3 \mu\text{m}^2$  and  $7.8 \pm 2.2 \times 10^3 \mu\text{m}^2$  for QuPath and Fiji respectively. The glomerulus has a round figure and approximately 200  $\mu\text{m}$  diameter.<sup>12,13</sup> The larger glomerular area was reported in patients with IgA nephropathy ( $28.9 \times 10^3 \mu\text{m}^2$ ), Focal segmental glomerulosclerosis ( $31.1 \times 10^3 \mu\text{m}^2$ ), Membranous glomerulonephritis ( $27.9 \times 10^3 \mu\text{m}^2$ ),<sup>14</sup> and in Secondary focal segmental glomerulosclerosis ( $3.1 \times 10^4 \mu\text{m}^2$ ).<sup>15</sup>



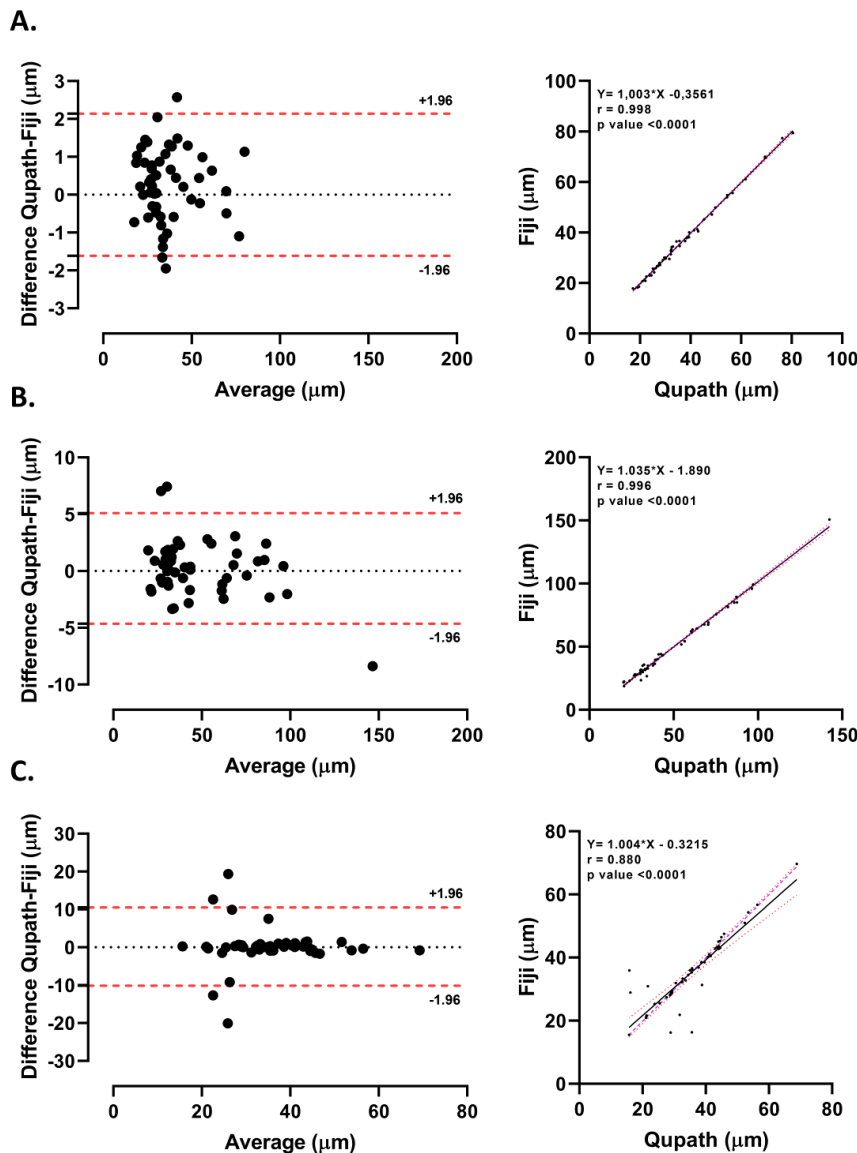
**Figure 3.** Bland-Altman plot (left panel) and Deming regression (right panel) between measurement results using QuPath and Fiji. (A) Renal corpuscle area (B) Glomerular area (C) Bowman space area. The red dashed line in Bland-Altman plot indicates the 95% of the upper and lower limits of agreements. In Deming regression panel, the black dot indicates data points, purple dash indicates Deming regression line, black line indicates simple regression line, and red dot indicates error bar for simple regression line.

The renal tubules varied in diameter and histological appearance. Based on our measurements, the proximal tubule's inner diameters ranged from 18.7 to 150.8  $\mu\text{m}$ . Smaller inner diameters were observed in distal tubules (17.1-80.5  $\mu\text{m}$ ) and The Henle loop (15.5-69.6  $\mu\text{m}$ ). There are variations in lumen diameter according to the previous report, the mean diameter of the human tubular lumen was  $39.6 \pm 1.8 \mu\text{m}$ .<sup>16</sup> The smaller mean diameter was reported at  $29.5 \pm 9.2 \mu\text{m}$  within the 30 - 60  $\mu\text{m}$  diameter range.<sup>17</sup> Specified renal tubule segment, such as the proximal convoluted tubule was about 15 mm long and 55  $\mu\text{m}$  in diameter.<sup>18</sup> Contrary to popular belief, the renal convoluted tubules are elliptical rather than round due to the difference in mean length between the short

axis and the long axis. This issue should be considered when analyzing tubular area or diameter.<sup>19</sup>

The renal tubule diameters are often compared to other species in the animal model for kidney diseases. In mice, the normal proximal convoluted tubules' mean diameter was  $37.4 \pm 0.5 \mu\text{m}$  (minimum diameter) and  $44.0 \pm 0.7 \mu\text{m}$  (maximum diameter). For distal convoluted tubules, the mean minimum diameter was  $32.2 \pm 0.6 \mu\text{m}$  and the mean maximum diameter was  $40.2 \pm 0.9 \mu\text{m}$ .<sup>19</sup> Meanwhile the mean diameter for rat tubular lumen in the kidney cortex was rat  $32.5 \pm 2.9 \mu\text{m}$ .<sup>16</sup> The external diameter of the Henle loop's thin section is about 12  $\mu\text{m}$ . The near end collecting tube is 200  $\mu\text{m}$  in diameter, while the small collecting tubule has a diameter of roughly 40  $\mu\text{m}$ .<sup>20</sup>





**Figure 4.** Bland-Altman plot (left panel) and Deming regression (right panel) between measurement results using QuPath and Fiji (renal tubules). (A) Distal tubule (B) Proximal tubule (C) Henle loop. The red dashed line indicates the 95% of the upper and lower limits of agreements. The red dashed line in Bland-Altman plot indicates the 95% of the upper and lower limits of agreements. In Deming regression panel, the black dot indicates data points, purple dash indicates Deming regression line, black line indicates simple regression line, and red dot indicates error bar for simple regression line.

In this study, we compare the measurement results of kidney microscopic structures using QuPath and Fiji. From our observation this two software were resulting comparable values. There was no significant difference in measurement results of renal corpuscle area, glomerular area, Bowman space area, luminal diameter of proximal tubules, distal tubules, and Henle loop between the compared software ( $p\text{-value} > 0.05$ ). Further confirmational analysis supported the similarity between two measurement results. We analysed the quantification results using Deming regression and the Bland-Altman plot. Strong correlation and linearity from two measurements were also demonstrated in all observed kidney structures with Pearson's rho values greater than 0.995 for most structures except for the Henle loop ( $r = 0.880$ ). We observed some values were outside the upper or lower limit of agreement. However, the majority of paired data lies within the lower and

upper limits of agreement of the Bland-Altman plot and only less than 10% off-limit values. The evidence supports that both measurement values were identical.

Based on our experience, both QuPath and Fiji are user-friendly and reliable for renal histomorphometric analysis. However, our team found that QuPath provides better workspace visualization compared to Fiji. Which affects our navigation performance or response while working on the project. In addition, annotating, object measurement, and project management were more convenient to perform in QuPath.

We note limitations in our study. Since WSI analysis is not feasible in our team setting. We were not able to compare the measurement results of both software with the WSI result as the "gold standard".

In conclusion, the measurement result of kidney microstructures using QuPath and Fiji were identical. The researcher can select QuPath or Fiji for kidney

histomorphometry and expect relatively similar measurement results. For researchers who are constrained to conducting research using unbiased stereology or WSI, the availability of reliable and user-friendly software can aid in carrying out histomorphometry analysis.

## ACKNOWLEDGEMENT

The author would like to acknowledge the Lembaga Penelitian dan Pengabdian pada Masyarakat (LPPM) of Universitas Muhammadiyah Purwokerto for funding this research.

## REFERENCES

1. Klopfeisch R. Multiparametric and semiquantitative scoring systems for the evaluation of mouse model histopathology--a systematic review. *BMC Vet Res*. 2013;9:123. doi: 10.1186/1746-6148-9-123.
2. Meyerholz DK, Beck AP. Fundamental Concepts for Semiquantitative Tissue Scoring in Translational Research. *ILAR J*. 2018;59(1):13-7. doi: 10.1093/ilar/ily025.
3. Rueden CT, Schindelin J, Hiner MC, DeZonia BE, Walter AE, Arena ET, et al. ImageJ2: ImageJ for the next generation of scientific image data. *BMC Bioinformatics*. 2017;18(1):1-26. doi: 10.1186/s12859-017-1934-z.
4. Schindelin J, Arganda-Carreras I, Frise E, Kaynig V, Longair M, Pietzsch T, et al. Fiji: an open-source platform for biological-image analysis. *Nat Methods*. 2012;9(7):676-82. doi: 10.1038/nmeth.2019.
5. Jones TR, Kang IH, Wheeler DB, Lindquist RA, Papallo A, Sabatini DM, et al. CellProfiler Analyst: data exploration and analysis software for complex image-based screens. *BMC Bioinformatics*. 2008;9(1):482. doi: 10.1186/1471-2105-9-482.
6. Piccinini F, Balassa T, Szkalisity A, Molnar C, Paavolainen L, Kujala K, et al. Advanced Cell Classifier: User-Friendly Machine-Learning-Based Software for Discovering Phenotypes in High-Content Imaging Data. *Cell Syst*. 2017;4(6):651-5. doi: 10.1016/j.cels.2017.05.012.
7. Berg S, Kutra D, Kroeger T, Straehle CN, Kausler BX, Haubold C, et al. ilastik: interactive machine learning for (bio)image analysis. *Nat Methods*. 2019;16(12):1226-32. doi: 10.1038/s41592-019-0582-9.
8. Sommer C, Hoefler R, Samwer M, Gerlich DW. A deep learning and novelty detection framework for rapid phenotyping in high-content screening. *Mol Biol Cell*. 2017;28(23):3428-36. doi: 10.1091/mbc.E17-05-0333.
9. Farahani N, Parwani A, Pantanowitz L. Whole slide imaging in pathology: advantages, limitations, and emerging perspectives. *Pathol Lab Med Int*. 2015;7:23-33. doi: 10.2147/PLMI.S59826.
10. Kumar N, Gupta R, Gupta S. Whole Slide Imaging (WSI) in Pathology: Current Perspectives and Future Directions. *J Digit Imaging*. 2020;33(4):1034-40. doi: 10.1007/s10278-020-00351-z.
11. Rangan GK, Tesch GH. Quantification of renal pathology by image analysis (Methods in Renal Research). *Nephrology*. 2007;12(6):553-8. doi: 10.1111/j.1440-1797.2007.00855.x.
12. Cho K-O, Lee SH, Jang H-J. Feasibility of fully automated classification of whole slide images based on deep learning. *Korean J Physiol Pharmacol*. 2019;24(1):89-99. doi: 10.4196/kjpp.2020.24.1.89.
13. Samuel T, Hoy WE, Douglas-Denton R, Hughson MD, Bertram JF. Applicability of the glomerular size distribution coefficient in assessing human glomerular volume: the Weibel and Gomez method revisited. *J Anat*. 2007;210(5):578-82. doi: 10.1111/j.1469-7580.2007.00715.x.
14. Turgut D. Measurement of glomerular area in primary glomerular diseases with a digital pathology software. *Journal of clinical and experimental investigations*. 2021;48(1):9-16. doi: 10.5798/dicletip.887368.
15. Zamami R, Kohagura K, Kinjyo K, Nakamura T, Kinjo T, Yamazato M, et al. The Association between Glomerular Diameter and Secondary Focal Segmental Glomerulosclerosis in Chronic Kidney Disease. *Kidney Blood Press Res*. 2021;46(4):433-40. doi: 10.1159/000515528.
16. Morozov D, Parvin N, Charlton JR, Bennett KM. Mapping kidney tubule diameter ex vivo by diffusion MRI. *Am J Physiol Renal Physiol*. 2021;320(5):F934-F46. doi: 10.1152/ajprenal.00369.2020.
17. Li Q, Onozato ML, Andrews PM, Chen CW, Paek A, Naphas R, et al. Automated quantification of microstructural dimensions of the human kidney using optical coherence tomography (OCT). *Opt Express*. 2009;17(18):16000-16. doi: 10.1364/oe.17.016000.
18. Barrett KE, Barman SM, Yuan JXJ, Brooks H. Ganong's review of medical physiology. 26th ed. ed. New York, N.Y: McGraw-Hill Education LLC.; 2019.
19. Ortega-Martinez M, Gutierrez-Davila V, Gutierrez-Arenas E, Niderhauser-Garcia A, Cerda-Flores RM, Jaramillo-Rangel G. The Convolute Tubules of the Nephron Must Be Considered Elliptical, and Not Circular, in Stereological Studies of the Kidney. *Kidney Blood Press Res*. 2021;46(2):229-35. doi: 10.1159/000515051.
20. Alicelebić S. Proximal convolute tubules of the rats kidney--a stereological analysis. *Bosn J Basic Med Sci*. 2003;3(1):36-9. doi: 10.17305/bjbms.2003.3568.

# JOURNAL OF BIOMEDICINE AND TRANSLATIONAL RESEARCH

Available online at JBTR website: <https://jbtr.fk.undip.ac.id>

Copyright©2023 by Faculty of Medicine Universitas Diponegoro, Indonesian Society of Human Genetics and Indonesian Society of Internal Medicine

Original Research Article

## Comparison of SARS-CoV-2 Variant Screening and Whole Genome Sequencing at an Indonesian Tertiary Hospital

Rebriarina Hapsari<sup>1,2,3\*</sup>, Irfan Kesumayadi<sup>1</sup>, Desvita Sari<sup>1,4</sup>, Dwi Utami Anjarwati<sup>1,4,5</sup>, Nesia Hani Alfiyuliani<sup>1,4</sup>, Mujahidah Mujahidah<sup>1,4</sup>, Iva Puspita Sari<sup>1,4</sup>, Purnomo Hadi<sup>1,4</sup>

<sup>1</sup>Department of Microbiology, Faculty of Medicine, Universitas Diponegoro, Indonesia

<sup>2</sup>Microbiology Laboratory, Diponegoro National Hospital, Indonesia

<sup>3</sup>Microbiology Laboratory, KRMT Wongsonegoro Hospital, Indonesia

<sup>4</sup>Department of Clinical Microbiology, Kariadi Hospital, Indonesia

<sup>5</sup>Department of Microbiology, Faculty of Medicine, Universitas Jendral Soedirman, Indonesia

### Article Info

#### History

Received: 03 Jul 2023

Accepted: 31 Oct 2023

Available: 31 Dec 2023

### Abstract

**Background:** The global COVID-19 pandemic, caused by the severe acute respiratory syndrome coronavirus 2 (SARS-CoV-2), experienced a surge in cases with the emergence of the Omicron variant. Despite increasing vaccination coverage, Indonesia witnessed peaks in COVID-19 cases. Variant screening and whole genome sequencing (WGS) play a crucial role in identifying SARS-CoV-2 variants and monitoring their spread.

**Objective:** The objective of this study was to compare variant screening results with WGS data and assess the prevalence of subvariants.

**Methods:** Between November 7th and 18th, 2022, variant screening and WGS were conducted on samples with CT values below 30. Variant screening utilized the mBioCov-19+ VarScreen assay, while WGS was performed on the Oxford Nanopore Technologies (ONT) platform. Bioinformatics analysis was performed using epi2melabs. Demographic data were analyzed.

**Results:** Out of 89 subjects, all tested positive for the Omicron variant through variant screening. The variant screening identified two subvariants: Omicron BA.2 (64%) and Omicron B.1.1.529.1 (36%). WGS revealed that the XBB subvariant was the most dominant (52.8%), followed by BQ.1 (22.5%) and BA.5 (13.5%). When VarScreen indicated BA.2, the majority of WGS results showed XBB (82.5%), while for B.1.1.529.1, the majority of WGS results were BQ.1 (59.4%), followed by BA.5 (37.5%). XBB was the most prevalent variant in both females and males, while BQ.1 was more dominant in females (80%). No infections were detected among children aged 1-5 years.

**Conclusion:** Variant screening provides accurate and quick results for detecting the Omicron variant in laboratories without WGS capacity. However, it is important to continuously update the screening methodology based on the prevailing circulating variants. During the study period, XBB emerged as the predominant subvariant of the Omicron variant.

**Keywords:** Variant screening; Whole Genome Sequencing; Omicron, XBB

**Permalink/ DOI:** <https://doi.org/10.14710/jbtr.v9i3.19147>

### INTRODUCTION

By the end of 2021, there was a significant increase in the daily worldwide cases of severe acute respiratory

syndrome coronavirus 2 (SARS-CoV-2), surpassing one million cases.

\*Corresponding author:

E-mail: [r.hapsari@fk.undip.ac.id](mailto:r.hapsari@fk.undip.ac.id)  
(Rebriarina Hapsari)

This surge was largely attributed to the emergence and spread of the Omicron variant, also known as B.1.1.529<sup>1</sup>. Due to the lower fatality rate of the Omicron variant and the increasing number of vaccinated individuals, it is expected that the global pandemic will eventually reach to an end following the Omicron wave<sup>2</sup>. However, the number of COVID-19 cases in Indonesia continues to increase after the introduction of the Omicron variant, with three peaks occurring in 2022, specifically in February, August, and November, with the highest number of confirmed cases being ten of thousand cases.<sup>1</sup>

By the end of 2022, various SARS-CoV-2 variants, including Alpha (B.1.1.7), Beta (B.1.351), Gamma (P.1), Delta (B.1.617.2), and Omicron (B.1.529) along with its subvariants, have been identified. Despite the availability of vaccines, certain subvariants have shown the ability to evade immunity, leading to infections in vaccinated individuals or reinfection in COVID-19 survivor.<sup>3,4</sup> Among all the variants, Omicron is believed to possess the highest potential for immune evasion due to its significant spike protein mutations. Therefore, the identification of SARS-CoV-2 variants through genome sequencing plays a crucial role in controlling the spread of the virus.<sup>5</sup>

Genomic epidemiology has played a crucial role in the SARS-CoV-2 pandemic as it has proven to be a powerful technique for monitoring the emergence and transmission of new viruses, as well as assessing outbreaks.<sup>6</sup> The initial identification of SARS-CoV-2 occurred through whole genome shotgun sequencing of a pneumonia patient in Wuhan, China, in December 2019. Prior to this, six coronaviruses (HCoV-OC43, HCoV-HKU1, HCoV-NL63, HCoV-229E, SARS-CoV, and MERS-CoV) had been identified as infecting humans.<sup>7</sup> In comparison, SARS-CoV-2 shares approximately 94.4% of its genome sequence with SARS-CoV, and it was initially predicted to be a zoonotic infection originating from bats, given its 96.2% similarity to the genome sequence of SARSr-CoV RaTG13 and 97% similarity in the spike glycoprotein.<sup>8,9</sup>

Whole genome sequencing (WGS) is currently considered the most accurate method for identifying mutations in the SARS-CoV-2 virus.<sup>10</sup> However, due to limited resources and time-consuming, WGS is not commonly performed to identify SARS-CoV-2 variants. To address this, variant screening methods have been developed as alternatives to WGS. These methods include RT-PCR-based assays and Virus-Receptor-Based Electrical Biosensors, which can help identify variants before conducting WGS tests.<sup>11,12</sup> In Indonesia, we have developed an RT-PCR-based assay called mBioCov-19+ VarScreen, which can identify several SARS-CoV-2 variants, including Alpha (B.1.1.7), Beta (B.1.351)/Gamma (P1), Mu (B.1.621), Delta/Delta Plus (B.1.617.2), B.1.620, Lambda (C.37), Omicron (B.1.1.529.1), and BA.2. However, it is important to note that this variant assay may not be able to identify specific subvariants such as BA.5, BQ.1, and XBB. In Asia, Omicron variant quickly replaced previous circulating strain after its introduction, and then followed by its subvariants, namely BA.1, BA.2, BA.4, BA.5, BQ.1, and XBB. Among those, XBB became the most predominating subvariants in October 2022.<sup>13,14</sup>

In our study, we conducted both variant screening and whole genome sequencing (WGS) tests. We examined the prevalence of subvariants identified through WGS and compared it with the results obtained from variant screening. Additionally, we investigated the correlation between these subvariants and demographic data.

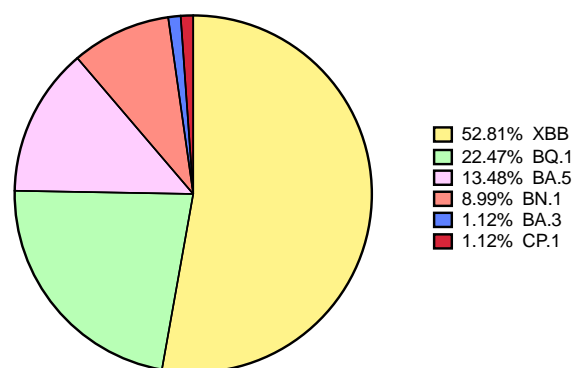
## MATERIALS AND METHODS

During 7<sup>th</sup> and 18<sup>th</sup> November 2022, we performed SARS-CoV-2 variant screening test and whole genome sequencing using the ONT platform (Oxford Nanopore Technologies, New York, NY, USA) on samples with CT value <30 (Bio Farma, Bandung, Indonesia).

SARS-CoV-2 variant screening was done using mBioCov-19+ VarScreen according to the manufacturer's instruction (Bio Farma, Bandung, Indonesia). mBioCov-19+ VarScreen kit was intended to identify Alpha (B.1.1.7), Beta (B.1.351)/Gamma (P1), Mu (B.1.621), Delta/Delta plus (B.1.617.2), B.1.620, Lambda (C.37), Omicron (B.1.1.529.1), and BA.2 variants. This kit incorporated two reactions targeting Helicase gene to detect SARS-CoV-2; and H69/V70, E484K/Q/A, N501Y, T478K, ORF1ab SGF3675-3677-mutations to determine variants and subvariants.

Whole genome sequencing was done using the PCR tiling of SARS-CoV-2 virus with rapid barcoding and Midnight RT PCR Expansion protocol on GridION (Oxford Nanopore Technologies, New York, NY, USA). Bioinformatics analysis, i.e., quality control check, ARTIC workflow run, and nextclade analysis, were performed by epi2melabs.<sup>15</sup> Gender and age were collected on this study and analyzed based on the group of SARS-CoV-2 variants.

This study has been approved by the Institutional Review Board of the Dr. Kariadi Hospital, Semarang, Indonesia (Number 1363/EC/KEPK-RSDK/2022).



**Figure 1.** Distribution frequency of Omicron subvariants based on WGS

## RESULTS

A total of 89 subjects were enrolled during the study period. Variant screening revealed that all the subjects were infected by the Omicron variant. Among them, 57 (64%) were identified as Omicron BA.2, whereas 32 (36%) were identified as Omicron B.1.1.529.1 by mBioCov-19+ VarScreen. Based on WGS and lineage assignment, XBB was the most dominant subvariant, accounting for 47 (52.81%), followed by BQ.1 and BA.5, which accounted for 20 (22.47%) and 20 (13.48%),

**Table. 1** Crosstabulation of VarScreen and WGS

VarScreen	Whole Genome Sequencing Lineages					
	XBB	BQ.1	BA.5	BN.1	BA.3	CP.1
BA.2	47 (82.5%)	1 (1.8%)	0 (0%)	8 (14%)	1 (1.8%)	0 (0%)
Omicron B.1.1.529.1	0 (0%)	19 (59.4%)	12 (37.5%)	0 (0%)	0 (0%)	1 (3.1%)

**Table. 2** Demographic among Omicron Lineages

	XBB	BQ.1	BA.5	BN.1	BA.3	CP.1
<b>Gender</b>						
Male	18 (52.9%)	4 (11.8%)	7 (20.6%)	5 (14.7%)	0 (0%)	0 (0%)
Female	29 (52.7%)	16 (29.1%)	5 (9.1%)	3 (5.5%)	1 (1.8%)	1 (1.8%)
<b>Age, years (Mean±SD)</b>	44.64±22.71	39.33±23.68	32.63±20.2	58.88±21.74	31*	34*
≤1 years	6 (66.7%)	2 (22.2%)	1 (11.1%)	0 (0%)	0 (0%)	0 (0%)
1-5 years	0 (0%)	0 (0%)	0 (0%)	0 (0%)	0 (0%)	0 (0%)
6-18 years	0 (0%)	1 (33.3%)	2 (66.7%)	0 (0%)	0 (0%)	0 (0%)
18-60 years	29 (52.7%)	12 (21.8%)	8 (14.5%)	4 (7.3%)	1 (1.8%)	1 (1.8%)
>60 years	12 (54.5%)	5 (22.7%)	1 (4.5%)	4 (18.2%)	0 (0%)	0 (0%)

\*Data obtained only from one subject

respectively. The less frequent variants were BN.1, BA.3, and CP.1, which accounted for 8 (8.99%), 1 (1.12%), and 1 (1.12%), respectively (Figure 1).

According to the variant screening results, the BA.2 subvariant was primarily comprised of XBB and BN.1, accounting for 47 (82.5%) and 8 (14%), respectively. On the other hand, the variant screening results for Omicron B.1.1.529.1 indicated that the dominant subvariants were BQ.1 and BA.5, accounting 19 (59.4%) and 12 (37.5%), respectively. Interestingly, there was one subject where the BQ.1.1 subvariant was detected within the BA.2 variant screening. A cross-tabulation between variant screening and WGS is shown in Table 1.

#### Demographics among Omicron subvariants

Based on the data presented in Table 2, we can conclude that XBB was the most dominant variant observed in both females and males across different age groups during the study period. Among females, BQ.1 was more dominant, accounting for 16 (80%), compared to males where it accounted for 4 (20%). No infections were detected among children aged 1-5 years in our study.

## DISCUSSION

Variant screening for SARS-CoV-2 refers to the process of detecting and identifying genetic variant groups or mutations of the virus. Some SARS-CoV-2 variants may be associated with increased virulence, or increased transmissibility, or decreased efficacy of current diagnostics, vaccinations, or treatments, the

variants which are known as variants of concern. To date, there have been five variants of concern of SARS-CoV-2 i.e., Alpha (B.1.1.7), Beta (B.1.351), Gamma (P.1), Delta (B.1.617.2), and Omicron (B.1.529). Variant screening has helped in monitoring the spread and prevalence of different SARS-CoV-2 variants (especially during the Delta variant outbreak and early Omicron outbreak). It provided valuable information for public health interventions and the implementation of control measures. By understanding the prevalence and characteristics of different variants, public health authorities can make informed decisions to mitigate the spread of the virus and adapt response efforts accordingly.<sup>16,17</sup>

Significant mutations in the SARS-CoV-2 virus leading to highly transmissible virus were identified in November 2021, in which the resulting strain has been called as Omicron variant (B.1.1.529) and considered as a variant of concern by the World Health Organization. The first confirmed case was reported in South Africa, and subsequent cases were identified globally, leading to the displacement of the Delta variant in many countries.<sup>18</sup> Despite extensive mutations in the spike protein, Omicron appears to have lower pathogenicity due to alterations in the non-RBD portion of its S protein, affecting cellular tropism. Compared to previous variants, the Omicron variant is suspected to enter cells via an endosomal entry route in the upper respiratory tract (where TMPRSS2 expression is low), as opposed to a plasma membrane entry route in lung tissue with high



TMPrSS2 expression. This altered entry route is believed to contribute to its high transmissibility.<sup>19,20</sup>

Before the Omicron outbreak occurred, Indonesia experienced 4 months with relatively few cases. However, when Omicron struck, there was a sudden surge in positive COVID-19 cases in Indonesia, accompanied by an increase in hospitalizations and deaths. VarScreen testing plays a role in the early stages of the Omicron outbreak due to the limited availability of WGS facilities. Health authorities require rapid epidemiological data on the spread of the SARS-CoV-2 virus to understand its transmission and effectively address it.

Our study revealed that all subjects enrolled during the study period were infected with the Omicron variant, as indicated by both the Variant Screening and WGS results. Initially, the Omicron variant has been categorized into BA.1 and BA.2 sub-lineages. As time passes, mutations continue to occur, leading to the discovery of other major sub-lineages, including BA.3, BA.4, BA.5, and XBB. In our study, the most prevalent sub-lineage of the Omicron variant was XBB, followed by BQ.1. During the study period, when VarScreen results showed BA.2, the majority of WGS results were XBB (82.5%), and for Omicron B.1.1.529.1 in VarScreen, the majority of WGS results were BQ.1 (59.4%), followed by BA.5 (37.5%).

A previous study documented that using a RT-PCR based SARS-CoV-2 variant screening assays can quickly provide the probable variant of SARS-CoV-2, but it requires careful quality control and interpretation.<sup>21</sup> Previously, the assay in our study has been carefully evaluated against Omicron variant by using the spike (S)- gene target failure (SGtF) and S-gene target positive (SGtP) with the principle of the single nucleotide polymorphism (SNP)-probe test. Here in our study, we did practical analysis in performing both variant screening and WGS examination.

The XBB subvariant of Omicron is considered a recombinant strain originating from the BA.2 lineage. It is formed through recombination of two specific sublineages, namely BA.2.10.1 and BA.2.75. This recombinant strain is characterized by several mutations in the Spike protein, which play a crucial role in the virus's infectivity and interaction with the host cells.<sup>22</sup> BQ.1 is a sublineage derived from BA.5, and it is characterized by specific spike mutations occurring in significant antigenic sites, such as K444T and N460K. Furthermore, the BQ.1.1 sublineage carries an extra spike mutation in another crucial antigenic site, namely R346T.<sup>22,23</sup> BQ.1 was previously noted to be more prevalent in the United States. It has been proposed that the virus has the ability to evolve uniquely in each geographic area, resulting in the emergence of variants that are better adapted to specific local communities.<sup>24</sup> Our study also showed that XBB is equivalently distributed among sex and ages. Meanwhile, BQ.1 is more dominant in female. There is no current study describe the association of BQ.1 and female sex, thus it might be coincidence.

The current VarScreen has limited effectiveness in today's (July 2023 when this article is prepared) context due to the predominant presence of mutations originating from XBB sublineages and not from others.

With the emergence of the Omicron subvariants, there is a pressing need to enhance the capabilities of VarScreen to accurately detect and identify the strains currently circulating. This adaptation is crucial to provide timely and relevant information for effective public health interventions. By updating and modifying VarScreen to target the specific genetic markers and mutations associated with the Omicron subvariants, we can improve its sensitivity and specificity in identifying the currently circulating strains. This would enable healthcare professionals and public health authorities to quickly identify cases, implement appropriate isolation measures, and conduct contact tracing to prevent further transmission.

## CONCLUSION

Variant screening provides accurate and quick result of Omicron variant in the laboratories with no WGS capacity. During the study period, a BA.1.1.529.1 found in the variant screening would be more likely to be a BQ.1, while BA.2 would be more likely to be an XBB variant. Variant screening reagents should be continuously updated based on the predominating circulating variants.

## ACKNOWLEDGMENTS

We thank the Agency for Health Policies Development, the Ministry of Health of the Republic of Indonesia for providing reagents and systems to perform SARS-CoV-2 whole genome sequencing and VarScreen in our laboratories. This study was partially funded by the research grant of the Faculty of Medicine Universitas Diponegoro (4509/UN7.5.4.2.1/PP/PM/2020).

## REFERENCES

1. Covid WHO. Dashboard. Geneva: World Health Organization. 2020;2020. <https://covid19.who.int/region/searo/country/id>
2. Murray CJL. COVID-19 will continue but the end of the pandemic is near. *The Lancet*. 2022;399(10323):417-9. [https://doi.org/10.1016/s0140-6736\(22\)00100-3](https://doi.org/10.1016/s0140-6736(22)00100-3)
3. Mlcochova P, Kemp SA, Dhar MS, Papa G, Meng B, Ferreira IATM, et al. SARS-CoV-2 B.1.617.2 Delta variant replication and immune evasion. *Nature*. 2021;599(7883):114-9. <https://doi.org/10.1038/s41586-021-03944-y>
4. Lazarevic I, Pravica V, Miljanovic D, Cupic M. Immune Evasion of SARS-CoV-2 Emerging Variants: What Have We Learnt So Far? *Viruses*. 2021;13(7). <https://doi.org/10.3390/v13071192>
5. Ke H, Chang MR, Marasco WA. Immune Evasion of SARS-CoV-2 Omicron Subvariants. *Vaccines*. 2022;10(9):1545. <https://doi.org/10.3390/vaccines10091545>
6. Gardy JL, Loman NJ. Towards a genomics-informed, real-time, global pathogen surveillance system. *Nat Rev Genet*. 2018;19(1):9-20. <https://doi.org/10.1038/nrg.2017.88>

7. Su S, Wong G, Shi W, Liu J, Lai ACK, Zhou J, et al. Epidemiology, Genetic Recombination, and Pathogenesis of Coronaviruses. *Trends Microbiol.* 2016;24(6):490-502. <https://doi.org/10.1016/j.tim.2016.03.003>
8. Zhou P, Yang XL, Wang XG, Hu B, Zhang L, Zhang W, et al. A pneumonia outbreak associated with a new coronavirus of probable bat origin. *Nature.* 2020;579(7798):270-3. <https://doi.org/10.1038/s41586-020-2012-7>
9. Wan Y, Shang J, Graham R, Baric RS, Li F. Receptor Recognition by the Novel Coronavirus from Wuhan: an Analysis Based on Decade-Long Structural Studies of SARS Coronavirus. *J Virol.* 2020;94(7). <https://doi.org/10.1128/jvi.00127-20>
10. Ong DSY, Koeleman JGM, Vaessen N, Breijer S, Paltansing S, de Man P. Rapid screening method for the detection of SARS-CoV-2 variants of concern. *J Clin Virol.* 2021;141:104903. <https://doi.org/10.1016/j.jcv.2021.104903>
11. Park S, Kim H, Woo K, Kim JM, Jo HJ, Jeong Y, et al. SARS-CoV-2 Variant Screening Using a Virus-Receptor-Based Electrical Biosensor. *Nano Lett.* 2022;22(1):50-7.
12. Camp JV, Buchta C, Jovanovic J, Puchhammer-Stöckl E, Benka B, Griesmacher A, et al. RT-PCR based SARS-CoV-2 variant screening assays require careful quality control. *J Clin Virol.* 2021;141:104905. <https://doi.org/10.1021/acs.nanolett.1c03108.s001>
13. Singapore MoH. Update on COVID-19 situation and measures to protect healthcare capacity 2022 [Cited 2023 Sept 24]. Available from: <https://www.moh.gov.sg/news-highlights/details/update-on-covid-19-situation-and-measures-to-protect-healthcare-capacity>.
14. Nextstrain. Genomic epidemiology of SARS-CoV-2 with subsampling focused on Asia over the past 6 months . Available from: <https://nextstrain.org/ncov/gisaid/asia/6m?dmax=2022-11-17&dmin=2022-01-01&l=scatter&p=full>.
15. SARS-Cov-2 Analysis Workflow [Cited 2023 March 24]. Available from: [https://labs.epi2me.io/notebooks/SARS\\_CoV\\_2\\_Analysis\\_Workflow.html](https://labs.epi2me.io/notebooks/SARS_CoV_2_Analysis_Workflow.html).
16. Boudet A, Stephan R, Bravo S, Sasso M, Lavigne JP. Limitation of Screening of Different Variants of SARS-CoV-2 by RT-PCR. *Diagnostics (Basel).* 2021;11(7). <https://doi.org/10.3390/diagnostics11071241>
17. Zhou Y, Zhang L, Xie YH, Wu J. Advancements in detection of SARS-CoV-2 infection for confronting COVID-19 pandemics. *Lab Invest.* 2022;102(1):4-13. <https://doi.org/10.1038/s41374-021-00663-w>
18. Fan Y, Li X, Zhang L, Wan S, Zhang L, Zhou F. SARS-CoV-2 Omicron variant: recent progress and future perspectives. *Signal Transduct Target Ther.* 2022;7(1):141. <https://doi.org/10.1038/s41392-022-00997-x>
19. Meng B, Abdullahi A, Ferreira IATM, Goonawardane N, Saito A, Kimura I, et al. Altered TMPRSS2 usage by SARS-CoV-2 Omicron impacts infectivity and fusogenicity. *Nature.* 2022;603(7902):706-14. <https://doi.org/10.1038/s41586-022-04474-x>
20. Peacock TP, Brown JC, Zhou J, Thakur N, Newman J, Kugathasan R, et al. The SARS-CoV-2 variant, Omicron, shows rapid replication in human primary nasal epithelial cultures and efficiently uses the endosomal route of entry. *BioRxiv.* 2022:2021-12. <https://doi.org/10.1016/j.jcv.2021.104905>
21. Camp JV, Buchta C, Jovanovic J, Puchhammer-Stöckl E, Benka B, Griesmacher A, et al. RT-PCR based SARS-CoV-2 variant screening assays require careful quality control. *Journal of Clinical Virology.* 2021;141:104905.
22. Focosi D, McConnell S, Casadevall A. The Omicron variant of concern: Diversification and convergent evolution in spike protein, and escape from anti-Spike monoclonal antibodies. *Drug Resist Updat.* 2022;65:100882. <https://doi.org/10.1016/j.drug.2022.100882>
23. WHO. TAG-VE statement on Omicron sublineages BQ.1 and XBB 2022 [Cited 2023 March 24]. Available from: <https://www.who.int/news/item/27-10-2022-tag-ve-statement-on-omicron-sublineages-bq.1-and-xbb>.
24. Ngiam JN, Al-Mubaarak A, Maurer-Stroh S, Tambyah PA. Does the COVID-19 XBB Omicron subvariant signal the beginning of the end of the pandemic? *Singapore Med J.* 2022. <https://doi.org/10.4103/singaporemedj.smj-2022-180>

# JOURNAL OF BIOMEDICINE AND TRANSLATIONAL RESEARCH

Available online at JBTR website: <https://jbtr.fk.undip.ac.id>

Copyright©2023 by Faculty of Medicine Universitas Diponegoro, Indonesian Society of Human Genetics and Indonesian Society of Internal Medicine

Original Research Article

## High Pre-treatment Neutrophil-to-Lymphocyte ratio (NLR) and Platelet-to-Lymphocyte ratio (PLR) Show Lower Progressive-free Survival and Overall Survival in Tyrosine Kinase Inhibitor-treated Lung Adenocarcinoma

Erna Kusumawardhani<sup>1,2</sup>, Haryati Haryati<sup>1,2</sup>, Fidya Rahmadhany Arganita<sup>1,2\*</sup>

<sup>1</sup>Gastroentero-Hepatology Division, Department of Internal Medicine, Dr. Kariadi General Hospital, Indonesia

<sup>2</sup>Faculty of Medicine, Universitas Diponegoro, Indonesia

### Article Info

#### History

Received: 16 Jul 2023

Accepted: 22 Dec 2023

Available: 31 Dec 2023

### Abstract

**Background:** The role of Neutrophil-to-Lymphocyte ratio (NLR) and Platelet-to-Lymphocyte ratio (PLR) as an easy and inexpensive prognostic examination modality has different results. While the combination of the two has never been done.

**Objective:** This study investigated the association between NLR/PLR and outcomes in advanced lung adenocarcinoma Epidermal Growth Factor Receptor (EGFR) mutation-positive with Tyrosine Kinase Inhibitor (TKI) treatment.

**Methods:** This retrospective study enrolled 40 medical records of lung adenocarcinoma patients treated with TKI in Ulin General Hospital from 2017-2019, with follow-up until April 1, 2021. A receiver operating curve (ROC) was performed to determine the optimal cut-off and parallel tests of NLR/PLR combination. The Kaplan-Meier was used to evaluate the impact on progressive-free survival (PFS) and overall survival (OS).

**Results:** The optimal cut-off was 6.25 for NLR and 451.5 for PLR with sensitivity and specificity of PFS (31.6%, 100%, and 18.4%, 100%) and OS (32.4%, 100% and 8.9%, 100%) (AUC 0.362, 0.329 and 0.482, 0.477) respectively. Patients in NLR <6.25 and PLR <451.5 groups presented longer PFS (10 months, 95% CI:7.783 -12.217, vs. 8 months, 2.908-13.092, p=0.821; 10 months, 7.508 – 12.492 vs. 9 months, 6.434-11.566, p=0.513) and OS (20 months, 14.017-25.983 vs.16 months, 11.474-20.526, p=0.378; 20 months, 14.629-25.371 vs. 14 months, 3.735-24.265, p=0.382) but not significantly correlated.

**Conclusion:** High pre-treatment NLR and PLR showed shorter PFS and OS, although not significant as a prognostic marker for PFS and OS of EGFR-mutant lung adenocarcinoma treated with TKI.

### Keywords:

Lung Adenocarcinoma; NLR; PLR; progressive-free survival; and overall survival

Permalink/ DOI: <https://doi.org/10.14710/jbtr.v9i3.19403>

### INTRODUCTION

About 85% of new lung cancer cases are non-small cell lung cancer (NSCLC). One of the most typical forms of NSCLC is adenocarcinoma.<sup>1</sup> One type of adenocarcinoma is with an Epidermal Growth Factor Receptor (EGFR) mutation. The highest frequency of EGFR mutations was found in Asia (51.4%). This mutation is most commonly found in women who are not smokers. Consideration for examining mutations in

never-smoker Asian females diagnosed with lung adenocarcinoma was recommended before initiation of first-line therapy for advanced NSCLC.<sup>2,3</sup>

\*Corresponding author:

E-mail: [fidya.arganita@ulm.ac.id](mailto:fidya.arganita@ulm.ac.id)  
(Fidya Rahmadhany Arganita)

EGFR-Tyrosine Kinase Inhibitor (TKI) is the first-line therapy in NSCLC patients with EGFR mutations. EGFR-TKI offers a better quality of life in lung cancer patients than chemotherapy.<sup>4</sup> Treatment with EGFR TKI will provide a more prolonged overall survival (OS) if the type of lung cancer is adenocarcinoma, younger ageless advanced clinical stage, and there are fewer comorbidities. It was suggested that adenocarcinoma with EGFR TKI has a better life expectancy.<sup>5</sup> However, more research is needed regarding the modalities of prognostic examinations that are easy and cheap to determine the best intervention.

A routine haematological examination has become necessary in patient management. Assessment of Neutrophil-to-Lymphocyte ratio (NLR) and Platelet-to-Lymphocyte ratio (PLR) as inflammatory markers are often used to assess stratification and prognostic in patients with malignancies. The development and tumor growth was highly indicated by marker driven by inflammation, such as NLR and PLR. A large cohort study in Korea found a relationship between NLR and lung cancer deaths in lung cancer-free adults.<sup>6</sup> Some studies on different subjects have been done. A study in NSCLC advanced patients, not specific to any therapeutic modalities,<sup>7</sup> and with modalities of immune checkpoint inhibitor therapy (nivolumab and pembrolizumab),<sup>8,9</sup> found that NLR and PLR were significantly related to PFS and OS. Research on NSCLC with surgically resected non-small cell lung cancer found that NLR and PLR were associated with OS.<sup>11</sup> Several studies that assessed NLR and PLR as prognostic markers in NSCLC showed different results.<sup>6-8</sup>

There has been limited research on lung adenocarcinoma treated by EGFR TKI. A study in adenocarcinoma treated with TKI found NLR related to PFS.<sup>9</sup> The combination of NLR and PLR against PFS and OS in EGFR-TKI-treated lung adenocarcinoma patients has not been conducted in previous studies.<sup>10</sup> This study investigated the association between NLR, PLR, and parallel test of both the PFS and OS in advanced lung adenocarcinoma EGFR mutation-positive with TKI treatment. This study was essential to maximize the management of lung adenocarcinoma patients.

## MATERIALS AND METHODS

### Study Design and Subjects

This is observational analytic research with cohort retrospective design. The sample population was 40 adenocarcinoma lung cancer patients newly diagnosed with positive EGFR mutations who will undergo TKI therapy at Ulin General Hospital. This study data was from outpatient and inpatient medical records of patients treated at Ulin General Hospital from January 2017 to December 2019. This study was conducted with the subject's inclusion: adenocarcinoma lung cancer patients with positive EGFR mutations who received TKI target therapy at Ulin General Hospital from January 1, 2017, to December 1, 2019, and followed until April 1, 2021. The exclusion criteria were (1) Adenocarcinoma lung cancer patients with positive EGFR mutations who had previously undergone targeted TKI therapy or received

chemotherapy. (2) Diagnosed with hematological malignancies (3) Diagnosed with infection (4) Got additional corticosteroid therapy or other immunosuppressant drugs.

**Table 1.** Characteristics of Subjects

Characteristic	N (%)
Age	
<50	8 (20)
≥50	32 (80)
Gender	
Male	28 (70)
Female	12 (30)
Smoking Status	
Smokers	25 (62.5)
Non-smokers	15 (37.5)
Tumor Stage	
IIIC	1 (2.5)
IVA	39 (97.5)
EGFR Mutation status	
18	0 (0)
19	26 (65)
20	0 (0)
21	14 (35)
ECOG Performance Status	
0	2 (5)
1	37 (92.5)
2	1 (2.5)
TKI	
Afatinib	12 (30)
Erlotinib	2 (5)
Gefitinib	26 (65)

ECOG, Eastern Cooperative Oncology Group; TKI, Tyrosine Kinase Inhibitor.

### Data Collection

Positive EGFR Mutation was defined by the detection of EGFR mutations based on PCR test from Formalin-Fixed Paraffin-Embedded (FFPE) blocks or cytology specimens of the patients with lung adenocarcinoma. DNA was assayed using Polymerase Chain Reaction (PCR) Rotor-Gene Q system (Qiagen, Hilden, Germany) with Qiagen therascreen® EGFR RGQ PCR kit (Qiagen, Manchester, UK) to qualitatively detect the following 29 somatic mutation on exon 18, 19, 20, and 21 mutations. NLR was determined by the count of neutrophils divided by the count of lymphocytes. PLR was determined by the total number of platelets divided by lymphocytes. Progression-free survival (PFS) was defined as the length of time during and after the treatment that the condition does not worsen or progressive. Overall Survival (OS) was the length of time from either the date of diagnosis and the patients are still alive.

**Table 2.** Cut-Off Value, Sensitivity and Specificity of NLR and PLR with ROC Curve Analysis

Variable	Cut Off	PFS			OS				
		Sensitivity (%)	Specificity (%)	AUC	P-Value 95% CI	Sensitivity (%)	Specificity (%)	AUC	P-Value 95% CI
NLR	6.25	31.6	100	0.362	0.515 (0.200-0.524)	32.4	100	0.482	0.918 (0.253-0.711)
PLR	451.5	18.4	100	0.329	0.420 (0.088-0.569)	18.9	100	0.477	0.898 (0.187-0.768)
NLR+ PLR	-	31.6	100	0.395	0.620 (0.211-0.579)	32.4	100	0.523	0.898 (0.280-0.765)

CI, Confidence Interval

**Table 3.** Clinicopathology Characteristic based on NLR and PLR

Variable	NLR			PLR		
	<6.25	≥6.25	<i>P Value</i>	<451.5	≥451.5	<i>P Value</i>
<b>Age</b>						
<50	7	1	0.369	7	1	1.0
≥50	21	11		26	6	
<b>Gender</b>						
Male	8	4	1.0	10	2	1.0
Female	20	8		23	5	
<b>Smoking Status</b>						
Non-smokers	11	4	1.0	13	2	0.691
Smokers	17	8		20	5	
<b>Mutation Status</b>						
Del – 19	19	7	0.720	21	5	1.0
Exon 21 L858R	9	5		12	2	

Fisher exact test

## Data Analysis

The normality of data was analyzed using the Shapiro-Wilk test. Determination of the optimal cut-off value of NLR and PLR for PFS and OS uses Receiving Operating Characteristics (ROC) Curves. A parallel test of NLR and PLR was also performed against PFS and OS using ROC curves. NLR and PLR are categorized according to the cut-off point and tested with chi-square or Fisher exact test. NLR and PLR's relationship with Median Survival Time (MST) in PFS and OS were analyzed using Kaplan–Meier's analysis. The difference in each survival time is assessed based on the log-rank test.

This research was approved by Health Research Ethics Committee of Ulin General Hospital, Universitas Lambung Mangkurat (No.50/VII-Reg Riset/RSUDU/2021).

## RESULTS

There were a total of 40 subjects included in this study with clinical characteristics in table 1 showed that the majority of the sample was over 50 years old (80%), male (70%), smoker (62.5%), stage IVA (97.5%) with exon mutation 19 (65%), and has Eastern Cooperative Oncology Group Performance Status (ECOG PS) 1 (92.5%). The most frequent use of TKI was gefitinib at 65%, afatinib at 30%, and erlotinib at 5%.

As seen in table 2, we found the same cut-off value of NLR for PFS and OS, 62.5, while PLR for PFS and OS is also the same, which is 451.5. In parallel tests, showing concurrent assessment of NLR and PLR values can increase sensitivity and specificity to PFS and OS.

### Analysis of clinicopathological characteristics associated with NLR, PLR and PFS, and OS

Patients with high NLR and high PLR were found at age ≥50, male sex, smoker, and exon mutation 19 (table 3). However, there were no significant differences in NLR and PLR values based on clinicopathological characteristics.

Based on table 4, ages over 50 years, females, smokers, exon deletion mutation 19, and treated with erlotinib were found to have a longer PFS time, but there was no significant difference. Meanwhile, the longer OS was obtained in female patients, smoking and using the erlotinib type of TKI but did not significantly different.

### Analysis of NLR and PLR with PFS and OS

The analysis of NLR and PLR values with PFS was described in table 5. Kaplan Meier's curve analysis in figure 1 (A) and (B) showed median PFS in the group with NLR <6.25 was 10 months (95% CI: 7.783 – 12.217), and the group with NLR ≥ 6.25 was eight months (95% CI: 2.908–13.092). PFS in groups with PLR <451.5 was 10 months (95% CI: 7.508–12.492),



**Table 4.** Potential Factor of Characteristic Clinicopathology related to PFS and OS

Variable	Progression-Free Survival			Overall Survival		
	N	MST(months)	P	N	MST (months)	P
<b>Age</b>						
<50	8	9	0.952	8	19	0.777
≥50	32	10		32	19	
<b>Gender</b>						
Male	28	8	0.774	12	14	0.944
Female	12	10		28	20	
<b>Smoking Status</b>						
Non-smokers	15	9	0.944	15	15	0.826
Smokers	25	12		25	23	
<b>Mutation Status</b>						
Del – 19	26	12	0.221	26	19	0.286
Exon 21	14	7		14	19	
<b>TKI</b>						
Afatinib	12	10	0.099	12	24	0.494
Gefitinib	26	8		26	19	
Erlotinib	2	13		2	25	

MST, Median Survival Time. TKI, Tyrosine Kinase Inhibitor

**Table 5.** The Univariate Analysis between NLR and PLR for PFS and OS

Variables	Progression-Free Survival			Overall Survival		
	Median	95% CI	P value	Median	95% CI	P value
NLR < 6.25	10 months	7.783 – 12.217	0.821	20	14.017-25.983	0.378
NLR ≥ 6.25	8 months	2.908 – 13.092		16	11.474-20.526	
PLR < 451.5	10 months	7.508 – 12.492	0.513	20	14.629-25.371	0.382
PLR ≥ 451.5	9 months	6.434 – 11.566		14	3.735-24.265	

CI, Confidence Interval

and the group with PLR ≥ 451.5 was 9 months (95% CI: 6.434–11.566). The difference in PFS between high and low NLR and PLR is not significant.

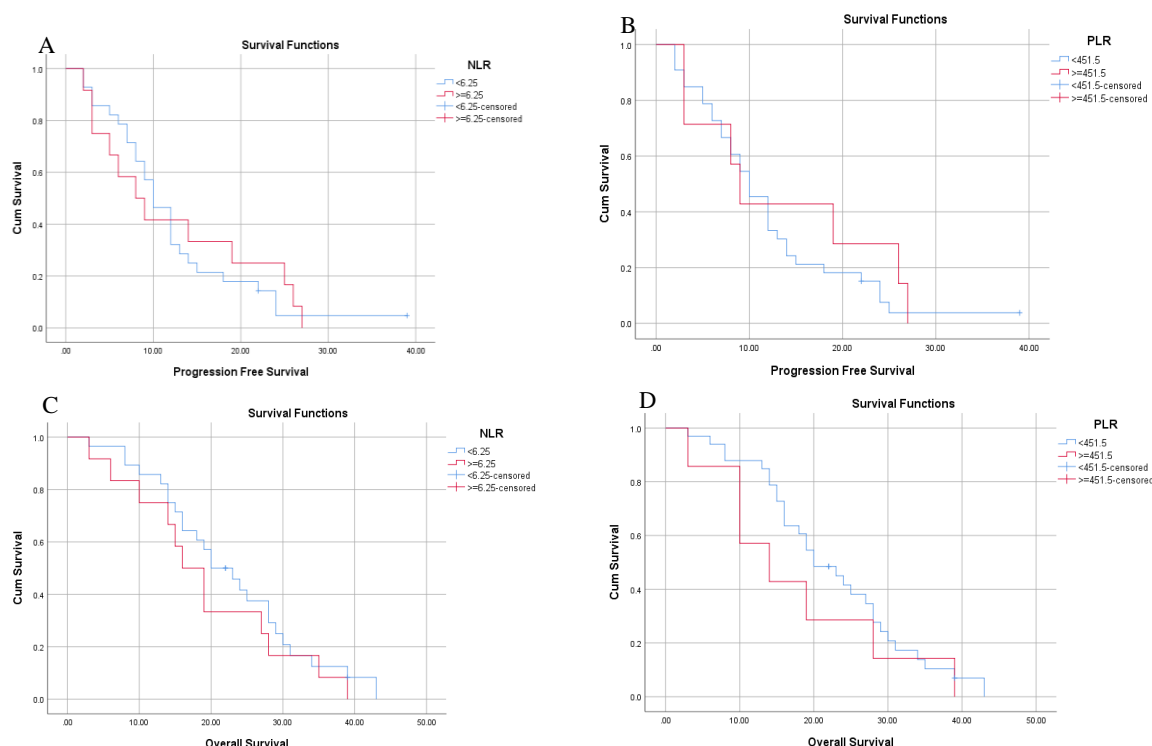
The analysis of NLR and PLR with median OS was in table 5, with Kaplan Meier in Figure 1 (C) and (D). Groups with NLR <6.25 obtained median OS 20 months (95% CI: 14.017-25.983), the group with NLR ≥6.25 obtained the median OS 16 months (95% CI: 11.474-20.526). A group with PLR ≥451.5 obtained an median OS of 14 months (95% CI: 3.735-24.265), while PLR <451.5 had a longer median OS of 20 months (95% CI: 14.629-25.371). However, the difference in the length of OS between the two NLR and two PLR groups was not significant.

## DISCUSSION

Based on sample characteristics in adenocarcinoma patients with positive EGFR mutations who underwent TKI therapy in the period 2017 to 2019, this study was, on average, over 50 years old. In accordance with other research, lung adenocarcinoma patients with EGFR mutations were more common in the population of patients ≥ age 50 years.<sup>13</sup> The findings of the present study was also in accordance with a study conducted in dr. Soetomo General Hospital which found that most adenocarcinoma patients were male active smokers with age ≥ 50 years.<sup>11</sup> In this study, the most common type of mutation was the deletion of Exon 19 in both men and women.

Several studies on NLR and PLR as prognostic biomarkers in NSCLC treated with different therapeutic modalities have been conducted. Prognostic biomarkers studied in advanced NSCLC patients, not specific in therapeutic modalities, found that high NLR and PLR are significantly associated with poor OS. High NLR is significantly associated with poor OS post-treatment.<sup>7</sup> Another study on NSCLC subjects treated with immune checkpoint inhibitors (nivolumab and pembrolizumab) found that high NLR and PLR pre-treatment values were independently associated with shortening PFS and OS.<sup>9</sup> In NSCLC patients treated with nivolumab, it was found that the increase in NLR and PLR was associated with shorter PFS and OS. While patients with surgically resected NSCLC found that NLR and PLR were associated with OS, only Systemic Inflammation Index (SII) was promising as a prognostic predictor for patients with surgically resected, and its significance persisted only in subgroups of pulmonary adenocarcinoma.<sup>12</sup> In NSCLC with dominant subtype epidermoid carcinoma on the sample, NLR values were independently associated only with survival disease, and PLR was associated with only overall survival.

There was only one study on the subjects of EGFR mutation lung adenocarcinoma treated with EGFR TKI and found NLR, PLR, and SII were predictors of PFS; however, only SII was a predictor in the OS. The cut-off values found in the study were ≥4.40 (NLR) and ≥182.595 (PLR).



**Figure 1.** Kaplan–Meier curves of PFS according to NLR (A) and PLR (B), and OS according to NLR (C) and PLR (D).

Several characteristic variables in NSCLC subjects affect NLR and PLR values, including ECOG PS related to higher NLR and smoking history related to higher PLR.<sup>10</sup>

The present study found that the characteristics of subjects, such as age, gender, smoking status, and mutation status, were not significantly associated with high NLR and high PLR. With the cut-off values of  $\geq 6.25$  (NLR) and  $\geq 451.5$  (PLR) that we found, Kaplan Meier analyzed log-rank tests and found no significant differences in PFS and OS. However, both show shorter median values in high NLR groups and high PLR. So far, there are minimal publications of research on lung adenocarcinoma subjects with EGFR mutations: In this study, a parallel test combining NLR and PLR values in adenocarcinoma patients found an increase in Area Under the Curve (AUC) to 0.523 (sensitivity=31.6%, specificity=100%), higher than the use of NLR or PLR alone. A study combining prognostic NLR and PLR scores in NSCLC subjects found that higher NLR was associated with poor prognosis. Low to normal NLR with high PLR was related to moderate risk, while lower NLR and lower PLR were an excellent prognosis.<sup>12</sup>

The relationship between NLR and PLR to the OS showed no significant relationship. Lower and higher NLR has OS 20 and 16 months, respectively. Meanwhile, lower and higher PLR had OS of 20 and 14 months, respectively. In a previous study, a significant relation was not found in PLR with OS, 29 months in low PLR and 17.3 months in high PLR. There were significant results in NLR and SII with longer OS in low-value groups. There have not been many other studies with similar research subjects compared to this study.<sup>10</sup> The difference in the results of this study compared with the previous studies could be caused by several factors.

As is known, NSCLC is a type of 85% of lung cancer, and adenocarcinoma is the most common NSCLC. The incidence of EGFR mutations in the lung cancer subgroup adenocarcinoma in Asia-Pacific also has the highest frequency of 47%, and many factors can affect prognostic patients.<sup>13</sup> However, the characteristics of clinicopathology (age, gender, smoking status, type of mutation, and type of TKI therapy) in this study showed no meaningful relationship with the PFS and OS, indicating that it was not significant to interfere with the research.

Another factor related to PFS and OS but not assessed in this study was the nutritional status of subjects where systemic inflammation due to cancer is known to affect immune status while inducing metabolic disorders and resulting in malnutrition. Cancer-related cachexia also affected prognosis.<sup>14</sup> Cachexia was frequent in advanced cancer patients, corresponding with reduced life and bad prognosis.<sup>15</sup> As a complication of cancer, cachexia manifests as a loss of muscle and fat mass.<sup>16</sup> Another study examining immune-inflammation-nutritional parameters (PNI) was significantly associated with overall survival.<sup>17</sup>

Another factor that can be related to prognosis is the type of mutation; a *multi-centre* study in Korea showed that the most EGFR mutations were Exon-19 (51%) followed by Exon-21 (42%). Deletion of Exon-19 is the only significant factor that decreases mortality, while mutation of Exon-21 is associated with the highest increase in mortality.<sup>18</sup> In this study, all samples that did not experience progressiveness in this study also had a type of deletion exon-19 only. Although the type of lung cancer has been homogeneous in previous studies, the kind of mutation with a different potential effect on prognosis may be one factor affecting the outcomes.

Other studies showed a prognosis link with genes and protein markers that play an essential role in lung adenocarcinoma, i.e.: UBE2C, MCM2, MCM6, FEN1, and TPX.<sup>18</sup> Other research on gene *signatures* demonstrates strong prognostic abilities and can be an independent predictor for lung adenocarcinoma patients in all datasets except GSE31210. In addition, the gene *signature* can predict lung adenocarcinoma patients' overall survival (OS) in different subgroups.<sup>19</sup> The identification of numerous inactivating mutations in genes that regulate the epigenome was a recent result of whole exome sequencing of thousands of patient malignancies. These mutations may affect nucleosome placement, histone modifications, and DNA methylation patterns, altering gene expression. Given that epigenomes play a significant part in the hierarchy of gene regulatory mechanisms, mutations may affect various pathways connected to the cancer phenotype.<sup>20</sup> These gene protein markers were also associated with poor prognoses; we have not studied them further. More research about other related factors like nutritional state and genetic factors needs to be done to confirm further research.

## CONCLUSION

In conclusion, high pre-treatment NLR and PLR showed slightly shorter PFS and OS, although they were not significant as a prognostic marker for PFS and OS of EGFR-mutant lung adenocarcinoma treated with TKI.

## ACKNOWLEDGMENTS

All authors have accepted responsibility for the content of the manuscript. The authors have not received any funding and report no conflicts of interest in this study.

## REFERENCES

1. Sung H, Ferlay J, Siegel RL, et al. Global Cancer Statistics 2020: GLOBOCAN Estimates of Incidence and Mortality Worldwide for 36 Cancers in 185 Countries. *CA Cancer J Clin* 2021; 71: 209–249.
2. Shi Y, Au JSK, Thongprasert S, et al. A Prospective, Molecular Epidemiology Study of EGFR Mutations in Asian Patients with Advanced Non-Small-Cell Lung Cancer of Adenocarcinoma Histology (PIONEER). *Journal of Thoracic Oncology* 2014; 9: 154–162.
3. Ha SY, Choi SJ, Cho JH, et al. Lung cancer in never-smoker Asian females is driven by oncogenic mutations, most often involving EGFR. *Oncotarget* 2015; 6: 5465.
4. Greenhalgh J, Dwan K, Boland A, et al. First-line treatment of advanced epidermal growth factor receptor (EGFR) mutation positive non-squamous non-small cell lung cancer. *Cochrane Database of Systematic Reviews*; 2016. Epub ahead of print 25 May 2016. DOI: 10.1002/14651858.CD010383.PUB2.
5. Bergqvist M, Christensen HN, Wiklund F, et al. Real world utilization of EGFR TKIs and prognostic factors for survival in NSCLC during 2010–2016 in Sweden: A nationwide observational study. *Int J Cancer* 2020; 146: 2510–2517.
6. Kang J, Chang Y, Ahn J, et al. Neutrophil-to-lymphocyte ratio and risk of lung cancer mortality in a low-risk population: A cohort study. *Int J Cancer* 2019; 145: 3267–3275.
7. Mandaliya H, Jones M, Oldmeadow C, et al. Prognostic biomarkers in stage IV non-small cell lung cancer (NSCLC): neutrophil to lymphocyte ratio (NLR), lymphocyte to monocyte ratio (LMR), platelet to lymphocyte ratio (PLR) and advanced lung cancer inflammation index (ALI). *Transl Lung Cancer Res* 2019; 8: 886.
8. Guo W, Cai S, Zhang F, et al. Systemic immune-inflammation index (SII) is useful to predict survival outcomes in patients with surgically resected non-small cell lung cancer. *Thorac Cancer* 2019; 10: 761–768.
9. Amaral SR, Moura MC, Carvalho J, et al. Prognostic significance of neutrophil-to-lymphocyte ratio (NLR) and platelet-to-lymphocyte ratio (PLR) in non-small cell lung cancer (NSCLC) treated with immune checkpoint inhibitors. *Annals of Oncology* 2019; 30: i3.
10. Deng C, Zhang N, Wang Y, et al. High systemic immune-inflammation index predicts poor prognosis in advanced lung adenocarcinoma patients treated with EGFR-TKIs. *Medicine (United States)*; 98. Epub ahead of print 1 August 2019. DOI: 10.1097/MD.00000000000016875.
11. Wu S-G, Chang Y-L, Yu C-J, et al. Lung adenocarcinoma patients of young age have lower EGFR mutation rate and poorer efficacy of EGFR tyrosine kinase inhibitors. *ERJ Open Res* 2017; 3: 92–2016.
12. Diem S, Schmid S, Krapf M, et al. Neutrophil-to-Lymphocyte ratio (NLR) and Platelet-to-Lymphocyte ratio (PLR) as prognostic markers in patients with non-small cell lung cancer (NSCLC) treated with nivolumab. *Lung Cancer* 2017; 111: 176–181.
13. Zheng Y, Chen Y, Chen J, et al. Combination of Systemic Inflammation Response Index and Platelet-to-Lymphocyte Ratio as a Novel Prognostic Marker of Upper Tract Urothelial Carcinoma After Radical Nephroureterectomy. *Front Oncol* 2019; 0: 914.
14. Midha A, Dearden S, McCormack R. EGFR mutation incidence in non-Small-cell lung cancer of adenocarcinoma histology: A systematic review and global map by ethnicity (mutMapII). *Am J Cancer Res* 2015; 5: 2892–2911.
15. Madeddu C, Mantovani G, Gramignano G, et al. Muscle wasting as main evidence of energy impairment in cancer cachexia: Future therapeutic approaches. *Future Oncology* 2015; 11: 2697–2710.
16. Van Der Meij BS, Schoonbeek CP, Smit EF, et al. Pre-cachexia and cachexia at diagnosis of stage III non-small-cell lung carcinoma: an exploratory study comparing two consensus-based frameworks. Epub ahead of print 2021. DOI: 10.1017/S0007114512004527.
17. Cohen S, Nathan JA, Goldberg AL. Muscle wasting in disease: Molecular mechanisms and promising therapies. *Nat Rev Drug Discov* 2014; 14: 58–74.

- 
18. Li D, Yuan X, Liu J, et al. Prognostic value of prognostic nutritional index in lung cancer: a meta-analysis. *J Thorac Dis* 2018; 10: 5298.
  19. Yoon HY, Ryu JS, Sim YS, et al. Clinical significance of EGFR mutation types in lung adenocarcinoma: A multi-centre Korean study. *PLoS One*; 15. Epub ahead of print 1 February 2020. DOI: 10.1371/journal.pone.0228925.
  20. Song Q, Shang J, Yang Z, et al. Identification of an immune signature predicting prognosis risk of patients in lung adenocarcinoma. *J Transl Med* 2019; 17: 70.
-

# JOURNAL OF BIOMEDICINE AND TRANSLATIONAL RESEARCH

Available online at JBTR website: <https://jbtr.fk.undip.ac.id>

Copyright©2023 by Faculty of Medicine Universitas Diponegoro, Indonesian Society of Human Genetics and Indonesian Society of Internal Medicine

Original Research Article

## Analysis Interaction of Immunoglobulin G and Immunoglobulin A Against *PstS1* as a Basis Specimen Selection for *M. tuberculosis* Rapid Test Diagnostic Agent

Nabila Rahmadani<sup>1\*</sup>, Tri Yudani Mardining Raras<sup>2</sup>, Maimun Zulhaidah Arthamin<sup>3</sup>

<sup>1</sup>Faculty of Medicine, Universitas Brawijaya, Indonesia

<sup>2</sup>Departement of Biochemistry and Molecular Biology, Faculty of Medicine, Universitas Brawijaya, Indonesia

<sup>3</sup>Departement of Clinical Pathology, Faculty of Medicine, Universitas Brawijaya, Indonesia

### Article Info

History

Received: 17 Jul 2023

Accepted: 08 Dec 2023

Available: 31 Dec 2023

### Abstract

*PstS1* is a 38-kDa phosphate-binding periplasmatic protein which developed from the recombinant Ag38 protein in local strain of *Mycobacterium tuberculosis*. *PstS1* has great potential to be used as a sero-diagnosis agent to be antigen rapid test because it has several epitopes that bind to antibodies. However, it is not yet known which antibody Ag38-recombinant binds maximally between IgA and IgG.

**Objective:** The aim of this study is to compare the interaction between IgG and IgA on *PstS1* in silico as a basis for the selection of sero-diagnosis agents in *M. tuberculosis*.

**Methods:** Protein-protein docking simulations using HDock and PDBSum

**Result:** The results show that the protein *PstS1* has a higher binding sensitivity to IgG based on one of the docking models which shows a docking score of -229.70, a confident score of 0.8312 and RMSD 1.060 Å. Ramachandran plot also shows that testing on this model has a protein structure that is good, with disallowed regions values of 0.5% (less than 0.8%). The results of this analysis show that the most favored regions are 90.5% with a G-factor of -0.27. The quality of the structure 3D mooring model can be said to be good because it fulfills the ideal structure requirements.

**Conclusion:** *PstS1* *M. tuberculosis* H37Rv binds to IgG more strongly than IgA.

### Keywords:

*M. tuberculosis*; *PstS1*; Immunoglobulin G; Immunoglobulin A; Protein docking

**Permalink/ DOI:** <https://doi.org/10.14710/jbtr.v9i3.19431>

### INTRODUCTION

Diagnosis of TB in is a challenge for health workers, because it has *paucibacillary* properties, then the symptoms that appear are usually non-specific and there are many limitations to existing diagnostic tests.<sup>1,2,3</sup> This is due to the difficulty of diagnosis which reaches 90%.<sup>4</sup> The main problem with is the difficulty of identifying infected individuals due to the *paucibacillary* nature of *M. tuberculosis* bacteria and also the limited sensitivity of tests.<sup>5</sup> In some case, some studies suggested that antibodies have possibility play protective role in at least a proportion of otherwise healthy individuals who have a history exposure of *M. tuberculosis*.<sup>6</sup> Using commercial serological tests for active TB have a poor

accuracy in endemic setting.<sup>7</sup> Sero-diagnosis is applicable in many infectious diseases such as hepatitis, AIDS etc. But no successful sero-diagnosis methods have been commercialized for TB based on *M. tuberculosis* antigen-specific IgG responses<sup>8,9</sup> or IgA responses. Antigen-based diagnostic tests have received special attention recently because of their high potency. One of them is the development of non-sputum-based diagnostic tests such as blood, urine, feces and saliva which have also been prioritized by the world health organization.<sup>10</sup>

\*Corresponding author:

E-mail: [nabila1998@student.ub.ac.id](mailto:nabila1998@student.ub.ac.id)

(Nabila Rahmadani)



**Table 1.** IgG and IgA docking analysis with PstS1 using HDOCK

Sample	Docking score	Confident score	RMSD
Model 1 IgG	-231.57	0.8364	36.10
Model 2 IgG	-229.70	0.8312	1.06
Model 3 IgG	-226.27	0.8213	39.81
Model 1 IgA	-55.42	0.1311	94.07
Model 2 IgA	-53.38	0.1265	86.31
Model 3 IgA	-52.43	0.1244	58.06

**Table 2.** IgG docking analysis with the PstS1 epitope using HDOCK

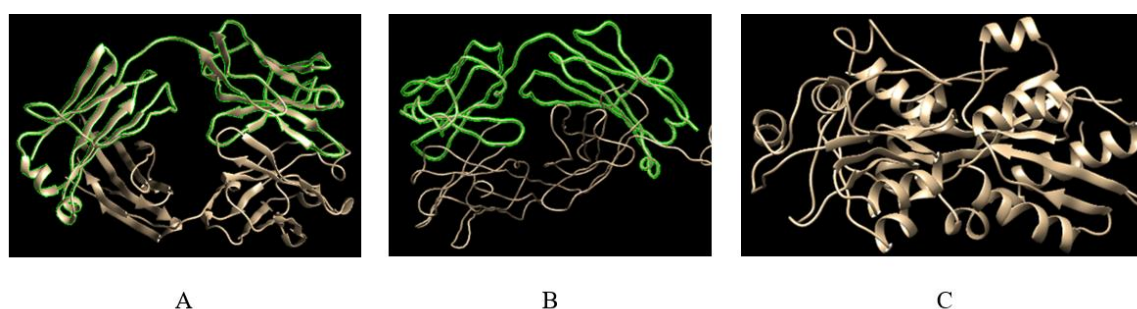
Sample	Model	Docking score	Confident score	RMSD
Epitope 1	1	-159.69	0.5483	47.20
	2	-153.66	0.5183	51.91
	3	-151.86	0.5093	49.49
Epitope 2	1	-120.29	0.3557	61.29
	2	-117.78	0.3443	60.76
	3	-115.75	0.3351	63.10
Epitope 3	1	-153.49	0.5174	49.94
	2	-150.64	0.5032	38.63
	3	-149.98	0.4999	39.19
Epitope 4	1	-239.45	0.8568	119.35
	2	-220.59	0.8040	116.79
	3	-220.57	0.8040	84.45

**Table 3.** IgA docking analysis with the PstS1 epitope using HDOCK

Sample	Model	Docking score	Confident score	RMSD
Epitope 1	1	-39.89	0.0996	90.88
	2	-39.67	0.0992	89.70
	3	-39.23	0.0984	83.67
Epitope 2	1	-30.57	0.0840	79.23
	2	-27.62	0.0796	79.52
	3	-27.16	0.0789	7079
Epitope 3	1	-34.07	0.0896	80.91
	2	-33.42	0.0885	82.88
	3	-32.14	0.0865	70.37
Epitope 4	1	-47.83	0.1147	118.04
	2	-45.99	0.1110	87.09
	3	-45.96	0.1052	105.10

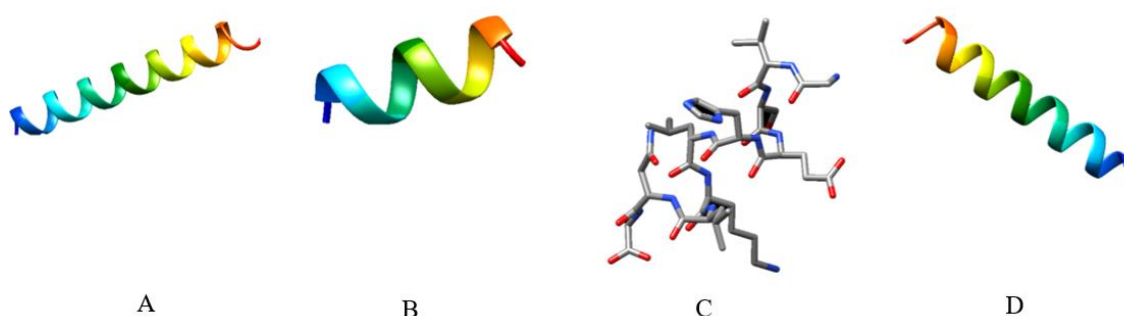
Ag38-recombinant from a local strain has been developed at the Laboratory of Biochemistry-Molecular Biology, Faculty of Medicine, Universitas Brawijaya.<sup>11</sup> This protein was successful in differentiating the saliva

of smear-positive TB patients and healthy people using the dot blot method.<sup>12</sup> However, it failed to differentiate the saliva of children suspected of having TB from the saliva of healthy children.



\* Green: light chain

**Figure 1.** Protein data, Immunoglobulin G (A), Immunoglobulin A (B), PstS1 protein (C)



**Figure 2.** Visualization of the 4 highest predicted epitopes with Chimera 1.17.1, GSKPPSGSPETGAGAGTVATTPASSPV (A), YLSEGDMAAHK (B), GVSEHLKLNG (C), QGTIKTWDDPQIAALNPGVNLNLP (D)

*PstS1* is an immunodominant epitope<sup>13</sup> which is a phosphate-binding subunit of *M. tuberculosis* (ATP-binding cassette) transporter. It is a glycosylated lipoprotein that can be found both intracellular and secreted extracellular. In this study, the Ag-38 protein or also called *PstS1* was shown to be able to trigger the appearance of IgG and IgA antibodies, both of which can recognize epitope complexes from Ag38-rec. The combination antibodies IgG and IgM had a stronger immunoreactivity to *PstS1*, this suggest that IgG is more ideal to bind *PstS1* than IgA. *PstS1* is a 38-kDa phosphate-binding periplasmatic protein, immunodominant marker for ATB<sup>14</sup> and plays role in *M. tuberculosis* immune evasion.<sup>15</sup> In active infection, serum antibodies against the *M. tuberculosis* phosphate transporter *PstS1* are detected.

Bioinformatics predictions of how the *PstS1* immunogenic epitope *in silico* binds to antibodies show results that may indicate further immunogenicity. It can thus be used to predict the inherent complexity of the immune presentation and epitope recognition process. Accurate prediction of the binding between the ligand and protein is critical to assisting how the target ligand interacts with the protein. The selected docking software application must be promising and provide accurate results. This requires fast and reliable computational methods using complex molecular research applications.<sup>16</sup> In this study a comparison will be made between the binding of immunoglobulin G and immunoglobulin A to *PstS1 in silico*. These results will represent how the prediction of bonding performance occurs such as sensitivity, specificity, accuracy of IgG and IgA, so that comparisons between the two can be known and can be used as the basis for developing a

diagnostic kit saliva-based antigen antibody for *M. tuberculosis*.

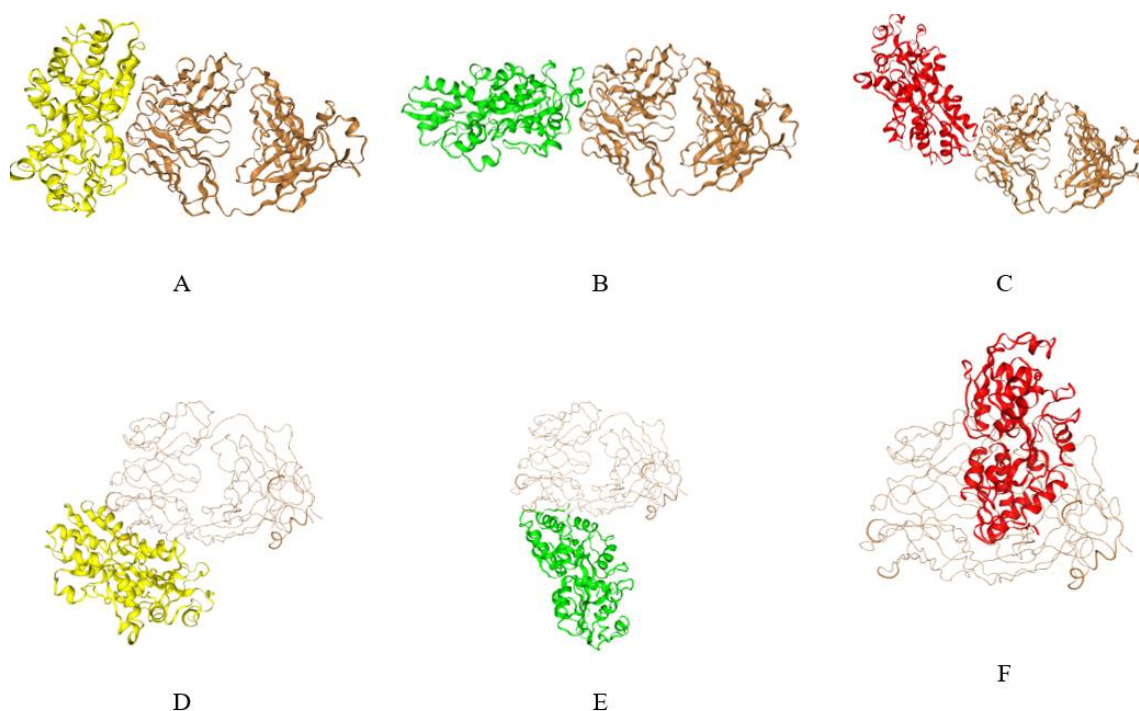
## MATERIALS AND METHODS

### Tools and materials

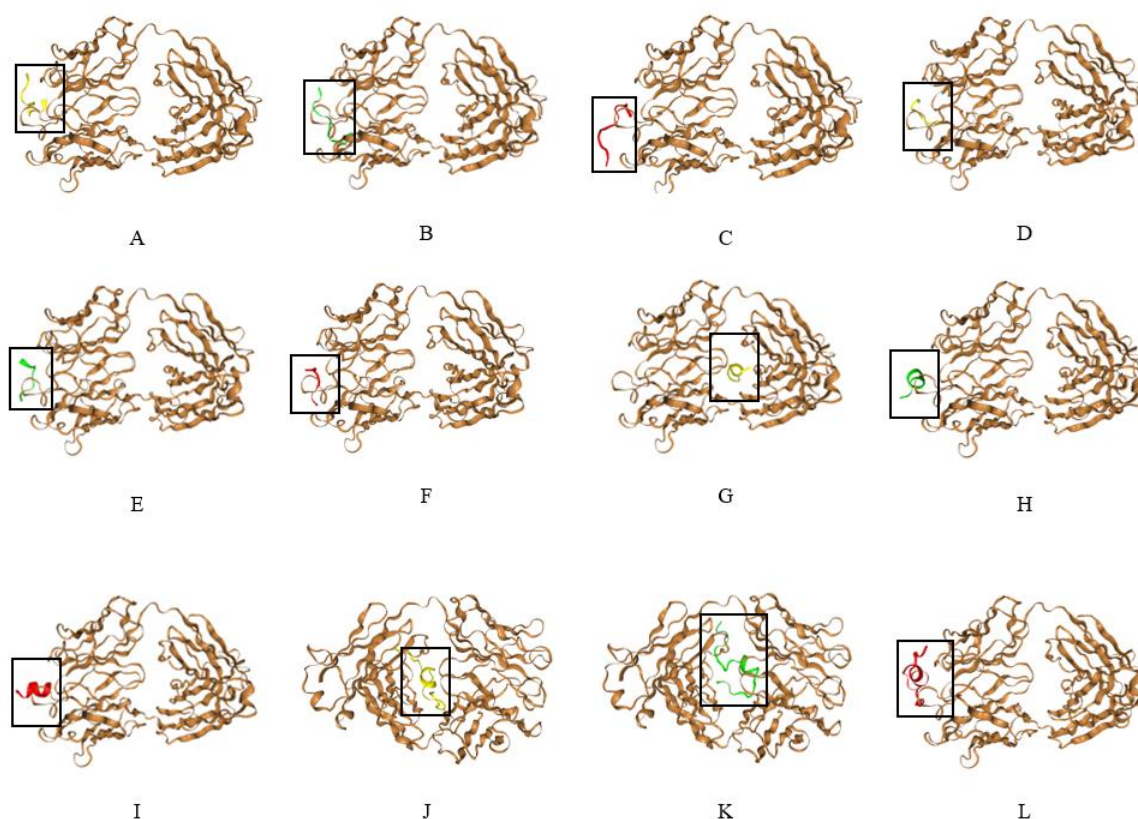
The hardware used in this research were a Windows 10 pro computer with specifications Intel(R) Celeron(R) CPU N3350 @ 1.10GHz 1.10 GHz, 4.00 GB RAM, 64-bit operating system, x64-based processor. The software and website used were Protein Data Bank (PDB) <https://www.rcsb.org/>, National Institute of Health (NCBI) <https://www.ncbi.nlm.nih.gov/>, Mycobrowser <https://mycobrowser.epfl.ch/>, Yet Another Scientific Artificial Reality Application (Yasara) 2003, Chimera 1.17.1, Immune Epitope Database and Analysis Resource (IEDB) with tools prediction B Cell Epitope method Bepipred Linear Epitope Prediction 2.0 (<https://www.iedb.org/>), HDOCK <http://hdock.phys.hust.edu.cn/>, PDBSum <http://www.ebi.ac.uk/thornton-srv/databases/pdbsum/>.

### Protein and ligand data

The data used were immunoglobulin G (IgG), Immunoglobulin A (IgA) and sequence protein of *PstS1*. Protein data used a type of protein-ligand docking and the proteins used were taken from PDB with database 7DM1 for immunoglobulin G and 7k75 for immunoglobulin A. Immunoglobulin sequence modeling was analyzed using Yasara. Then the *PstS1* sequence was taken from the data in *Mycobrowser*, and an analysis of the prediction of the epitope was carried out using IEDB and visualization of the epitope with Chimera 1.17.1.



**Figure 3.** Modeling of IgG binding with PstS1 Model 1 (A), Model 2 (B) Model 3 (C); Modeling IgA docking with PstS1 Model 1 (D), Model 2 (E), Model 3 (F)

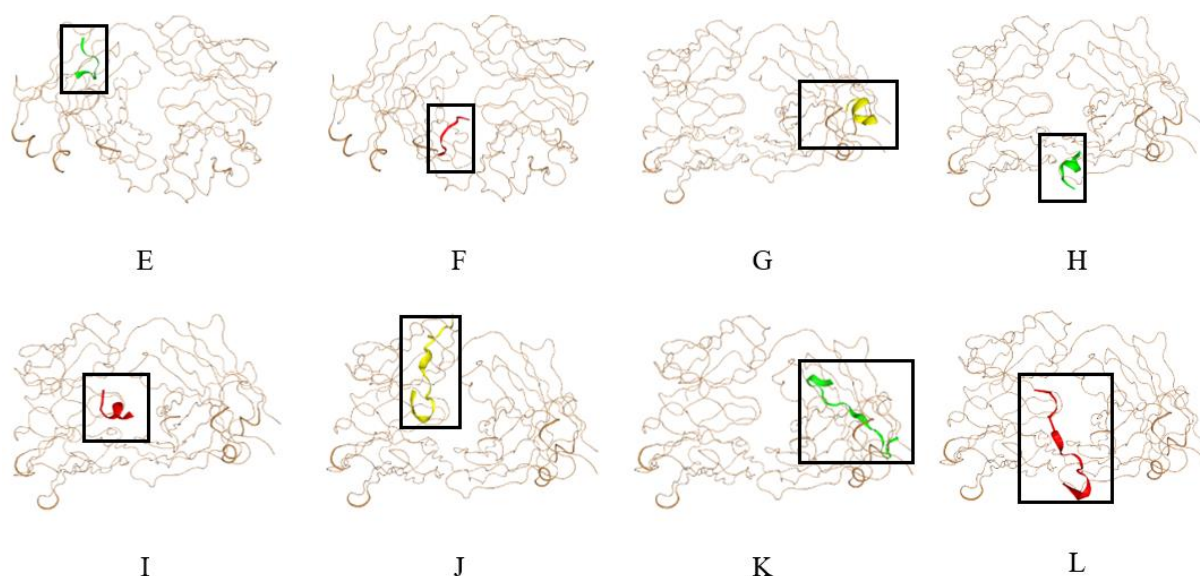


**Figure 4.** Visual docking of IgG with 4 highest prediction epitope of PstS1, model 1 IgG with epitope 1(A), model 2 IgG and epitope 1 (B) model 3 IgG and epitope 1 (C), model 1 IgG and epitope 2 (D), model 2 IgG and epitope 2 (E), model 3 IgG and epitope 2 (F), model 1 IgG and epitope 3 (G), model 2 IgG and epitope 3 (H), model 3 IgG and epitope 3 (I), model 1 IgG and epitope 4 (J), model 2 IgG and epitope 4 (K), model 3 IgG and epitope 4 (L)

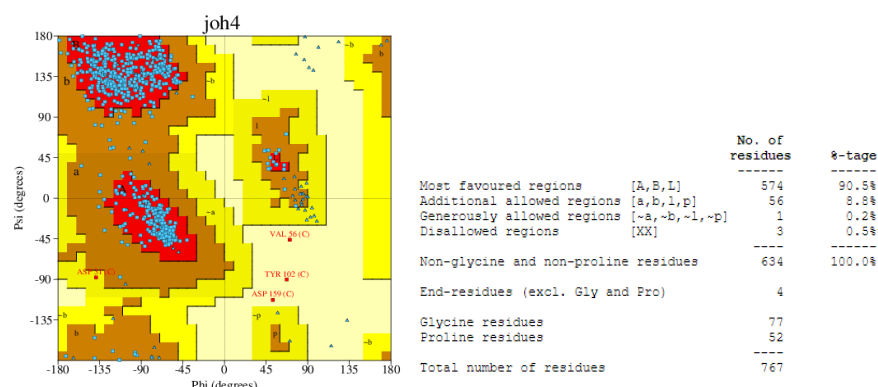
#### Docking

Protein-protein docking simulations were carried out with the aim of observing, exploring, and evaluating as well as comparing the molecular interactions and affinity formed between the ligand-protein complexes obtained previously. The docking software used in this study is

HDOCK and PDBSum. The success of the docking algorithm in holding the ligand binding pose can be seen from 3 parameters. The first is the value of the confidence score or the confident score which also shows the possibility of bonding 2 molecules.



**Figure 5.** Visual docking of IgA with 4 highest prediction epitope of PstS1, model 1 IgA with epitope 1 (A), model 2 IgA and epitope 1 (B) model 3 IgA and epitope 1 (C), model 1 IgA and epitope 2 (D), model 2 IgA and epitope 2 (E), model 3 IgA and epitope 2 (F), model 1 IgA and epitope 3 (G), model 2 IgA and epitope 3 (H), model 3 IgA and epitope 3 (I), model 1 IgA and epitope 4 (J), model 2 IgA and epitope 4 (K), model 3 IgA and epitope 4 (L)



**Figure 6.** Ramachandran plot docking on IgG with PstS1 protein

A value of 0.7 and above indicates a very high bonding ability, a value of 0.5 to 0.7 indicates the presence of moderate strength molecular bonds, and a value below 0.5 indicates a weak bond that may not even occur. The second is in the form of root-mean-square deviation (RMSD) between the positions of the heavy atoms of the ligands observed experimentally and those predicted by the algorithm. The flexibility system is a major challenge in finding the correct pose. The number of degrees of freedom involved in conformational search is a central aspect that determines search efficiency. Good performance is usually considered when the RMSD is less than.<sup>17</sup> Lastly is the value of the docking energy score, which is smaller than -200, the binding will be more likely to occur.

#### Protein Bond Conformation Analysis

Ramachandran plots were used to visualize the three-dimensional coordinates of proteins that have been determined experimentally into internal coordinates and also visualization of a function, by identifying the plots of non-glycine residues located in the dihedral corner disallowed regions. A protein structure is declared good if the number of residue plots contained in disallowed regions is less than 0.8%.<sup>18</sup>

## RESULTS

The analysis of the mooring sites of immunoglobulin G and immunoglobulin A are shown in Figures 1A and 1B. Furthermore, the results of the *PstS1 M. tuberculosis* H37Rv sequence analysis from *Mycobrowser* which has been visualized with Chimera 1.17.1 are shown in Figure 1C. From the *PstS1* sequence, epitopes were predicted with IEDB and the 4 highest predictions were taken. The results of the prediction of the epitopes are GSKPPSGSPETGAGAGTVATTPASSPV, YLSEGDMAAHK, GVSEHLKLNG, and QGTIKTWDDPQIAALNPGVNLNLP. The sequence was then visualized with Chimera 1.17.1 which is presented in Figure 2. Docking of IgG, IgA with *PstS1* using the HDock presented in Table 1 and Figure 3. Then binding was carried out on the 4 highest predicted results of the *PstS1* epitope with IgG presented in Table 2 and Figure 4. In addition, the 4 highest predictive results for the *PstS1* epitope were also analyzed for IgA binding which is presented in Table 3 and Figure 5. Finally, the best modeling results were analyzed using the Ramachandran plot in Figure 6.



## DISCUSSION

This *in silico*-based research was carried out with the aim of observing, exploring, and evaluating the structural mechanism of action of two molecular compounds between immunoglobulin, *PstS1* protein and *PstS1* epitope, as well as identifying the ability of these molecules to interact at the active binding site of the protein. The important stages of this research include the simulation of ligand-protein docking which forms a protein-ligand bond between immunoglobulin and *PstS1* protein. IgG and IgA immunoglobulin proteins that have been prepared from PDB data are prepared before removing water molecules. This preparatory stage aims to ensure the formation of molecular interactions that are able to achieve optimal stability in the active binding sites of the protein during the ligand-protein docking simulation stage and could increase the accuracy of docking.<sup>19</sup>

Docking begins with IgG and IgA which have been cut by light chains and heavy chains which are tethered with *PstS1* protein ligands using HDOCK. The value of the docking energy score is presented, which is smaller than -200, then the binding will be more likely to occur. From the results of the comparison between IgG and IgA the most negative docking energy score was found in model 1 on IgG binding with a value of -231.57, which means that IgG has a higher binding ability with *PstS1* than IgA. Then a confidence score is also presented which reflects the possibility of 2 molecule bonds. A value of 0.7 and above indicates a very high bonding ability, a value of 0.5 to 0.7 is for the presence of molecular bonds, and a value below 0.5 for a weak bond may not even occur. From the data that has been obtained, it is known that IgG binding has a confidence score above 0.7 in all 3 models, so IgG is considered to have the most likely bond with *PstS1*. The RMSD value shows that the second IgG model has an RMSD value below 20 or 1.060, which means that the belaying of the second model on IgG with *PstS1* has the highest probability.

In addition to docking IgG and IgA of protein *PstS1*, ligand binding was also performed on the *PstS1* epitope using HDOCK. The tethering uses the 4 selected epitopes with highest predictions from IEDB based on the *PstS1 M. tuberculosis* H37Rv sequence from *Mycobrowser*. For each epitope, 3 of the highest binding results will be taken. In ligand binding between IgG and the *PstS1* epitope, the most likely result is the binding with the predicted epitope 4 because the results of the docking score and confidence score were the best, even though the RMSD (Root mean square deviation) did not meet the standard. That is, the docking score is above -200 with a confidence score above 0.7. However, in the results of the IgA test, all docking results were not in accordance with the standard, so that docking IgA with the *PstS1* epitope was considered to have less affinity when compared to IgG.

The analysis of docking IgG and IgA against *PstS1* protein and the epitope, was found that the most probable model was IgG belay with *PstS1* protein. These results were then carried out by docking analysis with the help of PDBsum. The Ramachandran plot is used to visualize the three-dimensional coordinates of proteins that have been determined experimentally into internal

coordinates. The internal coordinates consist of the dihedral angle  $\Phi$  (phi) as the x-axis and the  $\psi$  (psi) angle as the y-axis of the amino acid residues of the protein structure. Mathematically, the Ramachandran plot is a visualization of a function, by identifying the plot of non-glycine residues located in dihedral regions that are disallowed (disallowed regions). A protein structure is declared good if the number of residue plots contained in disallowed regions is less than 0.8%.<sup>20</sup> The evaluation on IgG with *PstS1* protein has a good protein structure, if from the plot the residues found in disallowed regions are less than 0.8%, namely 0.5%. Structures with good quality are expected to have more than 90% residue in the most favored regions with G-factors above -0.5. Values below -0.5 unusual and values below -1.0 highly unusual. The results of this test show that the value of the most favored regions is 90.5% with a G-factor of -0.27. So that the structural quality of the 3D anchorage model can be said to be good because it fulfills the ideal structure requirements, namely having a residue distribution of more than 90% in the most favored regions, having little residue in the disallowed regions and having an overall G-Factors value above -0.5. From this result, IgG have more ideal binding to *PstS1* as in study in vivo results performed exclusively in mice revealed that *PstS1* antigen is a good inducer of antigen-specific Ab responses. In addition, in mice immunized with *PstS1*, adjuvant LTK63 could increase the production of anti-*PstS1* Ab and induce production CD4<sup>+</sup>, CD8<sup>+</sup> memory T cells, also amplifies secretion of IFN- $\gamma$  and IL-22 and IL-17 production by effector memory cells in an Ag-unrelated manner in vitro and in vivo<sup>21</sup>. The other study, show that *PstS1* glycoprotein was significantly lower in IgA than IgG for detecting bovine TB, although there is no significant difference. But in that study still support feasibility using IgA and suggested an approach using tests for IgA and IgG antibodies could improve detection accuracy.<sup>22</sup> The limitation of this research is that it does not know the specific amino acid bonds between proteins.

## CONCLUSION

The docking of IgG and IgA against *PstS1* protein showed that the most likely and ideal binding was IgG. The structural quality of the IgG and *PstS1* anchorage 3D models met the ideal anchorage requirements. This shows that IgG is more ideal as a basis sero-diagnostic for diagnostic kit saliva based antigen antibody for *M. tuberculosis*.

## ACKNOWLEDGMENTS

The author is grateful and thank to Lembaga Pengelola Dana Pendidikan (LPDP) Republic of Indonesia for supporting this project.

## REFERENCES

1. Nkereuwem E, Kampmann B, Togun T. The need to prioritise childhood tuberculosis case detection. The Lancet 2021;397(10281):1248–1249; doi: 10.1016/S0140-6736(21)00672-3.
2. Tebruegge M, Dutta B, Donath S, et al. Mycobacteria-Specific Cytokine Responses Detect Tuberculosis Infection and Distinguish Latent from Active Tuberculosis. Am J Respir Crit Care Med

- 2015;192(4):485–499; doi: 10.1164/rccm.201501-0059OC.
3. Hendon-Dunn CL, Doris KS, Thomas SR, et al. A Flow Cytometry Method for Rapidly Assessing Mycobacterium Tuberculosis Responses to Antibiotics with Different Modes of Action. *Antimicrob Agents Chemother* 2016;60(7):3869–3883; doi: 10.1128/AAC.02712-15.
4. Dodd PJ, Yuen CM, Sismanidis C, et al. The global burden of tuberculosis mortality in children: a mathematical modelling study. *Lancet Glob Health* 2017;5(9):e898–e906; doi: 10.1016/S2214-109X(17)30289-9.
5. Global Tuberculosis Programme GRC. WHO Consolidated Guidelines on Tuberculosis: Module 5: Management of Tuberculosis in Children and Adolescents. (World Health Organization. ed). 2022.
6. Watson A, Li H, Ma B, et al. Human antibodies targeting a Mycobacterium transporter protein mediate protection against tuberculosis. *Nat Commun* 2021;12(1):602; doi: 10.1038/s41467-021-20930-0.
7. Awoniyi DO, Baumann R, Chegou NN, et al. Detection of a combination of serum IgG and IgA antibodies against selected mycobacterial targets provides promising diagnostic signatures for active TB. *Oncotarget* 2017;8(23):37525–37537; doi: 10.18632/oncotarget.16401.
8. Baumann R, Kaempfer S, Chegou NN, et al. Serologic diagnosis of tuberculosis by combining Ig classes against selected mycobacterial targets. *Journal of Infection* 2014;69(6):581–589; doi: 10.1016/j.jinf.2014.05.014.
9. Chen T, Lin J, Wang W, et al. Cytokine and Antibody Based Diagnostic Algorithms for Sputum Culture-Positive Pulmonary Tuberculosis. *PLoS One* 2015;10(12):e0144705; doi: 10.1371/journal.pone.0144705.
10. World Health Organization. Global Tuberculosis Report 2021. 2021.
11. M. Raras TY, Lyrawati D. Cloning and expression of pab gene of M. tuberculosis isolated from pulmonary TB patient in E. coli DH5 $\alpha$ . *Medical Journal of Indonesia* 2011;247; doi: 10.13181/mji.v20i4.458.
12. Raras TYM, Sholeh G, Lyrawati D. Salivary sIg-A response against the recombinant Ag38 antigen of Mycobacterium tuberculosis Indonesian strain. *Int J Clin Exp Med* 2014;7(1):129–35.
13. Ivanyi J. Function and Potentials of M. tuberculosis Epitopes. *Front Immunol* 2014;5; doi: 10.3389/fimmu.2014.00107.
14. de Araujo LS, de Bárbara Moreira da Silva Lins N, Leung JAM, et al. Close contact interferon-gamma response to the new PstS1(285–374):CPF10: a preliminary 1-year follow-up study. *BMC Res Notes* 2017;10(1):59; doi: 10.1186/s13104-016-2360-4.
15. Coscolla M, Copin R, Sutherland J, et al. M. tuberculosis T Cell Epitope Analysis Reveals Paucity of Antigenic Variation and Identifies Rare Variable TB Antigens. *Cell Host Microbe* 2015;18(5):538–548; doi: 10.1016/j.chom.2015.10.008.
16. Hernández-Santoyo A, Yair A, Altuzar V, et al. Protein-Protein and Protein-Ligand Docking. In: *Protein Engineering - Technology and Application InTech*; 2013; doi: 10.5772/56376.
17. Sailapathi A, Murugan G, Somarathinam K, et al. Proposing the Promiscuous Protein Structures in JNK1 and JNK3 for Virtual Screening in Pursuit of Potential Leads. *ACS Omega* 2020;5(8):3969–3978; doi: 10.1021/acsomega.9b03458.
18. Lakshmi B, Sinduja C, Archunan G, et al. Ramachandran analysis of conserved glyceryl residues in homologous proteins of known structure. *Protein Science* 2014;23(6):843–850; doi: 10.1002/pro.2468.
19. Kitchen DB, Decornez H, Furr JR, et al. Docking and scoring in virtual screening for drug discovery: methods and applications. *Nat Rev Drug Discov* 2004;3(11):935–949; doi: 10.1038/nrd1549.
20. Gunasekaran K, Ramakrishnan C, Balaram P. Disallowed Ramachandran Conformations of Amino Acid Residues in Protein Structures. *J Mol Biol* 1996;264(1):191–198; doi: 10.1006/jmbi.1996.0633.
21. Palma C, Schiavoni G, Abalsamo L, et al. Mycobacterium tuberculosis PstS1 amplifies IFN- $\gamma$  and induces IL-17/IL-22 responses by unrelated memory CD4 $^{+}$  T cells via dendritic cell activation. *Eur J Immunol* 2013;43(9):2386–2397; doi: 10.1002/eji.201243245.
22. Jeon HS, Shin A-R, Son Y-J, et al. An evaluation of the use of immunoglobulin A antibody response against mycobacterial antigens for the diagnosis of Mycobacterium bovis infection in cattle. *Journal of Veterinary Diagnostic Investigation* 2015;27(3):344–351; doi: 10.1177/1040638715578879.



# JOURNAL OF BIOMEDICINE AND TRANSLATIONAL RESEARCH

Available online at JBTR website: <https://jbtr.fk.undip.ac.id>

Copyright©2023 by Faculty of Medicine Universitas Diponegoro, Indonesian Society of Human Genetics and Indonesian Society of Internal Medicine

Original Research Article

## The Effect of Increased Glucose Induction on GSH Levels in Insulin Gaussia Luciferase (iGL) Cells Derived from Rat Pancreatic Beta Cells

Fery Ardiansah<sup>1</sup>, Endin Nokik Stujanna<sup>1\*</sup>, Arief Indra Sanjaya<sup>1</sup>, Erlin Listiyaningsih<sup>1</sup>, Sri Suciati Ningsih<sup>1</sup>, Irena Ujjianti<sup>1</sup> and Dwi Retna Lestari<sup>1</sup>

<sup>1</sup>Faculty of Medicine, University of Muhammadiyah Prof. DR. HAMKA, Indonesia

### Article Info

History

Received: 26 Jul 2023

Accepted: 07 Dec 2023

Available: 31 Dec 2023

### Abstract

**Background:** Prolonged hyperglycaemia can make the pancreatic beta cells work harder and cause fatigue. When this happens, it can trigger oxidative stress reactions, which can produce free radical compounds that can damage pancreatic beta cells. The body compensates by activating protective mechanisms such as the production of antioxidant compounds to reduce the levels of free radicals in the cells. One such compound is glutathione (GSH). Insulin Gaussia Luciferase (iGL) cells are a cell line derived from rat pancreatic beta cells. These cells can be used as a model of oxidative stress in hyperglycaemia to measure GSH levels and there are no studies using iGL cells to measure GSH levels. Therefore, in this study, the iGL cells are used as the object of research. The reason for using serial plasma GSH measurements is to determine gradual differences in changes in GSH levels and to provide variations and new data for further GSH research.

**Objective:** To investigate the effect of GSH levels on glucose toxicity condition through in vitro experiments on iGL cells.

**Methods:** The study used 5 different glucose concentrations of 11, 16.5, 22, 33, and 44 mM with the addition of iGL cell growth medium exposed for 7 days. We measured the amount of intracellular GSH using a colourimetric method (MBS, 2540412) at a wavelength of 405 nm with microplate reader (AMR-100 Allsheng). The analysis used in this study was a one-way ANOVA test. Differences between groups were tested using SPSS.

**Results:** The results of this study showed that there was an increasing trend in total GSH levels on the third and seventh day. with the average increase on third day being 20.16 nmol and the average increase on seventh day being 19.58 nmol.

**Conclusion:** In this study it can be concluded that there was a trend of increasing GSH/cell levels on the first day of observation because the cells were trying to maintain their homeostasis in hyperglycemia conditions. on the third and seventh days the cells experienced a decrease which was thought to be due to glucotoxicity, so that giving high glucose levels had an effect on decreasing GSH.

**Keywords:** Colorimetric method; GSH; Hyperglycaemia; iGL cells; Oxidative stress

**Permalink/ DOI:** <https://doi.org/10.14710/jbtr.v9i3.19644>

### INTRODUCTION

In everyday life, people have a high risk of being exposed to glucose through the consumption of foods with a high glucose content. This makes people susceptible to hyperglycaemia (high blood sugar). When this happens, the body tries to lower blood glucose levels by releasing insulin from the beta cells of the pancreas. Excess glucose in the blood, which continues to rise, can

cause the beta cells to work very hard and lead to fatigue. So, it can cause dysfunction in the beta cells of the pancreas.<sup>10</sup>

\*Corresponding author:

E-mail: [endin\\_stujanna@uhamka.ac.id](mailto:endin_stujanna@uhamka.ac.id)

(Endin Nokik Stujanna)

When this condition occurs continuously, it induces oxidative stress reactions that can produce free radicals through glucose autooxidation and protein glycosylation.<sup>10</sup> Reactive oxygen species (ROS) have the potential to cause dysfunction in affected organs through cell damage and lead to cell apoptosis.<sup>11</sup> In addition to beta-cell fatigue, chronic oxidative stress can cause dysfunction in affected organs. Oxidative stress is also one of the factors leading to decreased intracellular production of insulin biosynthesis due to suppression of pancreatic-duodenal homeobox-1 (PDX-1) gene expression.<sup>6</sup> Thus, the amount of production secreted into the extracellular space is also decreased.<sup>4</sup> The human body can fall into the condition of diabetes mellitus. According to the International Diabetes Federation (IDF), in 2019 there will be an estimated 463 million people aged 20-79 years with a prevalence of 9.3% of the total population of the same age.<sup>2,5</sup> It is estimated that with increasing age, the prevalence will increase by 19.9% or 111.2 million people aged 65-79 years, and it is even estimated that by 2030 it will be 578 million people. In the South-East Asian region, Indonesia is the third most affected country with a prevalence of 11.3%. Diabetes is the most common chronic disease causing death. It can lead to microvascular and macrovascular complications.<sup>15,20</sup>

Therefore, the body compensates by activating the body's defence mechanisms by producing antioxidants. One of these antioxidants is glutathione (GSH), which has the function of maintaining the balance between pro-oxidants and anti-oxidants.<sup>8</sup> In this study, insulin gaussia luciferase (iGL) cells were used. These cells are a subset of cells from the beta cells of the rat pancreas.<sup>9,16</sup> iGL cells have the properties of the Gaussia luciferase protein, which acts as a measure of insulin secretion in a fluorescent state and can be visualised in 2 and 3 dimensions.<sup>16</sup> In addition, these cells can be used to model oxidative stress conditions when exposed to high glucose. This is the reason why we used this cell. It is still very rare for this cell to be used in research, so the data from this research can be used as a reference for further research. The reason for using serial plasma GSH measurements is to determine gradual differences in changes in GSH levels and to provide variations and new data for further GSH research.

## MATERIALS AND METHODS

### 1. Cell culture

The cells used are Insulin Gaussia Luciferase (iGL) cells derived from rat pancreatic beta cells (Cosmo Bio Co., 2020).<sup>3,9</sup> iGL cells are cultured in RPMI 1640 medium incubated at 37°C with 5% CO<sub>2</sub>. RPMI 1640 (Gibco) consists of L-glutamine, phenol red and HEPES.18 Additives were added in the form of 5% FBS, 1 mM pyruvic acid, 500 µM monothiolglycerol and 200 µg/mL G-148. Before culturing the cells in the medium, the cells were thawed in a water bath for two minutes. Then 1 mL of medium was added to the cryotube. The cells were immediately transferred to a 15 mL tube (Corning, 430791 USA) and 10 mL of medium was added. The cells were centrifuged at 300 G for five minutes and the supernatant discarded until cell pellets were visible. 1 mL of media suspension was prepared

from the cells and the number of cells was counted using an automated cell counter (LUNA Automated Cell Counter, Logos Biosystem, South Korea). 8.5 x 10<sup>5</sup> cells were plated in a 100 x 20 mm Petri dish (Corning, 430167 USA). The cultured cells should be replaced on the third or fourth day. Cells that have reached 80-90% confluence can be passaged.

The first thing that has to be done in the cell passaging process is the submersion of the cell media. Cells were rinsed with sterile PBS (Gibco, 181912014 USA). Cells were treated with 0.05% trypsin-EDTA (Gibco, 25300054 USA) at 1:10 and incubated at 37°C for two minutes. Immediately after incubation, 10 mL of medium was added to deactivate the trypsin. Cells removed from the plate are transferred to a 15 mL tube, the cells are centrifuged and the supernatant discarded. Cells used as suspensions were counted using an automatic cell counter. Cells of 8.5 x 10<sup>5</sup> were resuspended in new 100 x 20 mm petridishes.

### 2. Addition of glucose to the culture medium

At this stage, the treatment process was carried out by adding a glucose solution to the RPMI 1640 medium. The RPMI 1640 medium was used as the control medium because it contained 11 mM glucose. The glucose solutions to be prepared were 16.5 mM, 22 mM, 33 mM and 44 mM. The glucose (Sigma, 24895335 USA) required is 19.8, 79.2, 118.2 and 39.6 mg by weighing on an analytical balance. The glucose which has been weighed is then dissolved in 15 ml of medium in a 15 ml tube (Corning, 430829 USA).

### 3. Colorimetric method for measuring GSH levels

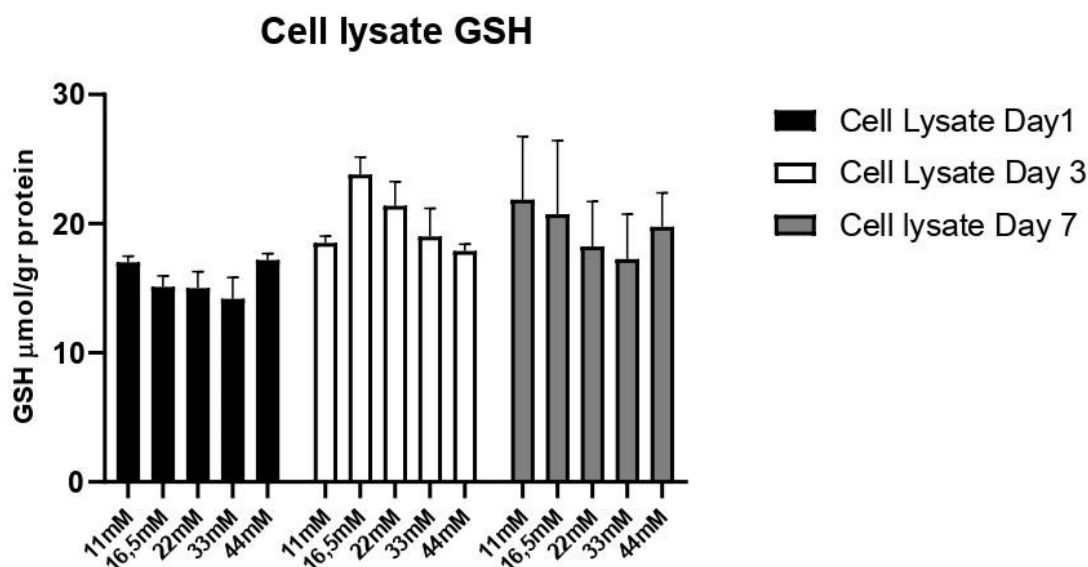
The GSH Colorimetric Assay Kit (MBS, 2540412) was used to measure GSH production. A microplate reader with a wavelength of 405 nm is used for this method. The harvested iGL cells were then rinsed with 0.1 M PBS (Gibco, 181912014 USA); pH 7.4 as much as 0.3 to 0.5 mL. Cells were disrupted by sonicating or grinding by hand in an ice-water bath. Take 0,1 mL of the disrupted cells and add 0,1 mL of Reagent 1 solution. Centrifuge the cells for ten minutes and collect the supernatant for measurement. Prepare the standard solution by dissolving 1 mmol/L GSH standard solution in GSH standard diluent. Standards are prepared in series and then added to the standard wells. Add the supernatant to be measured to the sample well. Allow the evenly mixed wells to stand for five minutes at room temperature. The results of the OD values are plotted on the standard curve and used to calculate the GSH levels.<sup>8</sup>

### Analysis of Statics

Each experiment was performed in triplicate. Software used to analyse normally distributed data, expressed as the standard deviation of the mean (version 19.0; IBM, Chicago, IL, USA). One-way ANOVA analysis was used for group comparisons. A statistically significant difference was defined as  $p < 0.05$ .

**Table 1.** iGL/GSH cell data for each day of observation

Concentration	Days 1			Days 3			Days 7		
	cells	GSH total (μmol)	GSH/C cells (nmol)	cells	GSH total (μmol)	GSH/C cells (nmol)	cells	GSH total (μmol)	GSH/C cells (nmol)
11 mM	257.333	17	0,066	468.000	18,5	0,039	1.553.333	21,9	0,014
16,5 mM	125.000	15,1	0,12	508.333	23,8	0,046	2.000.000	20,7	0,010
22 mM	59.767	15	0,25	391.667	21,4	0,054	956.000	18,2	0,019
33 mM	41.800	14,2	0,339	232.000	19	0,081	625.667	17,3	0,027
44 mM	41.800	17,2	0,411	139.000	17,9	0,128	1.103.333	19,8	0,017

**Figure 1.** iGL cell lysate GSH level at various state of high glucose induction (44, 33, 22, 16,5 and 11mM as control) related times to incubation (1, 3, and 7 days)

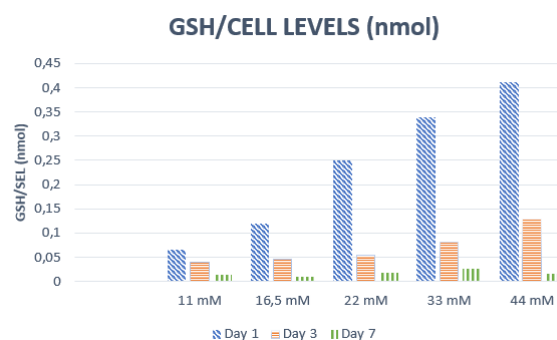
## RESULTS

### Data of total GSH on iGL lysate cells at each concentration

The results of measuring total GSH levels by the colourimetric method showed that there were no significant differences between the groups on a daily basis ( $p > 0.05$ ). These results are shown in Figure 1. However, these data show that there is an increasing trend on the third and seventh day. Table 1 is a description of the value of the results from Figure 1 and Figure 2, where in Figure 2 is the result of the conversion from μmol to nmol.

### Data of GSH/Cell on iGL lysate cells at each concentration

The GSH/Cell value was also obtained from a more detailed analysis by comparing the number of cells with the total GSH content for each concentration. It was then observed in Figure 2 that there was an increasing trend in GSH/Cell levels on the first day when high concentrations of glucose were administered. Then, there was a decreasing trend in GSH/Cell levels each day after exposure to high glucose concentrations for seven days.

**Figure 2.** Graph of Cell Lysate GSH/Cells Measurements in iGL Cells by Comparing the Same on Different Days

## DISCUSSION

Observations on the first day showed that iGL cells were trying to maintain homeostasis by increasing GSH levels. The response of beta cells to acute changes in extracellular glucose is to secrete insulin. High levels of extracellular glucose will increase glucose metabolism in cells. As a result, levels of reactive oxygen species (ROS) increase, advanced glycosylation (AGEs), activation of protein kinase C (PKC), also increase, polyol pathway activity also increases. Hexosamine metabolism and angiotensin II

production are also increased. Hyperglycemia stimulates insulin biosynthesis up to 50-fold in pancreatic beta cells. During this process, three disulfide bonds are formed per insulin molecule, causing the release of millions of ROS molecules per minute or free radicals to increase.

This is because the increase in ROS levels in the cell stimulates the activation of Nrf2 transcription. The Nrf2 protein is a regulator that plays a role in cell defence against oxidants.<sup>12</sup> Nrf2 will regulate the basal and induced expression of a number of genes that play a role in the antioxidant response. ROS will oxidise cysteine, then Nrf2 will phosphorylate serine 40 (ser40) with the help of PKC and then translocate to the nucleus. In this state, Nrf2 forms a complex with the small protein Maf and binds to the antioxidant response element (ARE) located in the regulatory region of the Nrf2 target gene.<sup>1</sup>

Nrf2 regulates more than 100 different genes involved in oxidative stress and cell survival. One of these functions is to control the expression of genes responsible for replenishing the cytosolic pool of NADPH, which is used as a reducing agent to maintain and regenerate cellular detoxification systems and antioxidant defences such as glutathione.<sup>4</sup> The regulated gene expression is glucose-6-phosphate dehydrogenase from the pentose phosphate pathway (hexose monophosphate shunt). One of the main products produced by this pathway is NADPH (nicotinamide adenine dinucleotide phosphate), which is a reduced form of NADPH.<sup>13</sup> Then NADPH is used as a cofactor by glutathione reductase to reduce oxidized glutathione (GSSG  $\rightarrow$  2 GSH).<sup>13,19</sup> After that, the reduced GSH will react with ROS compounds and GSH will be oxidized again to GSSG to reduce intracellular ROS levels, this recycling cycle depends on NADPH.

There is increasing evidence that activation of the Nrf2 pathway during hyperglycaemia and ROS generation is essential for the protection and maintenance of functional  $\beta$  (beta) cell mass. Nrf2 will promote macro-autophagy as an additional  $\beta$  (beta) cell defence mechanism by increasing  $\beta$  (beta) cell proliferation. When iGL cells were further exposed to high concentrations of glucose, there was a downward trend because iGL cells had entered a state of glucotoxicity.<sup>7</sup> This is evidenced by a decrease in antioxidant capacity in hyperglycaemia. A decrease in antioxidant levels can stimulate apoptosis in beta cells through the intrinsic pathway. This stress signal can lead to the activation of the proapoptotic proteins BAK and BAX, which are part of the BCL-2 protein family.<sup>17</sup>

These two proteins mediate mitochondrial outer membrane permeability by forming pores in the mitochondrial outer membrane, and oxidative stress can increase the opening of the mitochondrial permeability transition (mPTP) pores. Prolonged exposure to mPTP can induce cell death by increasing oxidative stress leading to ATP depletion and/or by inducing matrix swelling and subsequent rupture of the mitochondrial outer membrane. Apoptotic molecules such as apoptosis inducing factor (AIF), SMAC/DIABLO or cytochrome c are released during the permeabilization process.<sup>1</sup>

## CONCLUSION

This study concluded that administering high glucose concentrations over a period of 7 days resulted in an increasing trend in GSH/cell levels on the first day of observation. This condition is to maintain homeostasis in acute hyperglycemia. On days 3 to 7 of observation, GSH/cell levels decreased. This condition is thought to be due to glucotoxicity occurring due to a decrease in antioxidants. Giving high glucose has an effect on reducing GSH levels.

## ACKNOWLEDGMENTS

We would like to thank all those who have participated and helped in completing this paper. This research was funded by University of Muhammadiyah Prof. Dr. HAMKA, Jakarta, Indonesia.

## REFERENCES

1. Alterzon SB et al. Nrf2: The Master and Captain of Beta Cell Fate. *Trends Endocrinol Metab.* 2021; DOI:10.1016/j.tem.2020.11.002
2. American Diabetes Association. *Diagnosis and Classification of Diabetes Mellitus.* 2013; Available from: [https://www.diabetesjournals.org/care/issue/37/Supplement\\_1](https://www.diabetesjournals.org/care/issue/37/Supplement_1)
3. Cosmo Bio Co. iGL Cell Line. 2020.
4. Flohé L. *GLUTATHIONE.* 2018; DOI:10.1201/9781351261760
5. International Diabetes Federation. *IDF Diabetes ATLAS.* 2020. Available from: <https://www.diabetesatlas.org/atlas/ninth-edition>
6. Kaneto H, Matsuoka TA. Role of pancreatic transcription factors in maintenance of mature  $\beta$ -cell function. Vol. 16, *International Journal of Molecular Sciences.* MDPI AG; 2015. p. 6281–97. DOI: 10.3390/ijms16036281
7. Lv L, Wang X, Shen J, Cao Y, Zhang Q. MiR-574-3p inhibits glucose toxicity-induced pancreatic  $\beta$ -cell dysfunction by suppressing PRMT1. *Diabetol Metab Syndr.* 2022 Dec 1;14(1). DOI: 10.1186/s13098-022-00869-y
8. My Biosource. *Reduced Glutathione (GSH) Colorimetric Assay Kit.* 2018.
9. Ningsih SS, AR, SEN, LE, YT, & SWS. Evaluation of morphology and viability of spheroid derived from Insulin-GLase cell line: A model system to understand Type 2 Diabetes Mellitus. *Journal of Experimental and Clinical Medicine (Turkey).* 2021;38(3):211–5. DOI:10.52142/omujecm.38.3.1
10. Oyehihi AB AA. *Antioxidant Strategies in the Management of Diabetic Neuropathy.* . Biomed Res Int. 2015; DOI:10.1155/2015/515042
11. Paul RR. *DeGroot's Endocrinology Basic Science and Clinical Practice.* 8th ed. Elsevier; 2022. Available from: [https://www.books.google.co.id/books/about/De\\_groot\\_s\\_Endocrinology](https://www.books.google.co.id/books/about/De_groot_s_Endocrinology)
12. Qiang Ma. *Role of Nrf2 in Oxidative Stress and Toxicity.* 2013; DOI: 10.1146/annurev-pharmtox-011112-140320

- 
13. Robert C. Stanton. Glucose-6-Phosphate Dehydrogenase, NADPH, and Cell Survival. 2012; DOI: 10.1002/iub.1017
  14. Shen CY, Lu CH, Wu CH, Li KJ, Kuo YM, Hsieh SC, et al. The development of maillard reaction, and advanced glycation end product (Age)-receptor for age (rage) signaling inhibitors as novel therapeutic strategies for patients with age-related diseases. Vol. 25, Molecules. MDPI AG; 2020. DOI:10.3390/molecules25235591
  15. Sherwood L. Human Physiology From Cells to Systems 9th Editions. 2016. Available from: <https://www.books.google.co.id/books.id>
  16. Suzuki T, KT, & IS. Quantitative visualization of synchronized insulin secretion from 3D-cultured cells. Biochemical and Biophysical Research Communications, . 2017;486(4):886–92. DOI: 10.1016/j.bbrc.2017.03.105
  17. Tatsuo Tomita. Apoptosis in pancreatic  $\beta$ -islet cells in Type 2 diabetes. Journal of the Association of Basic Medical Sciences. 2016;16. DOI: 10.17305/bjbms.2016.919
  18. Usha Rani MSASSLJAA and SA. Evaluation of Use of RPMI Medium to Preserve Cell Morphology for Pleural/Peritoneal Fluid Cytology. J Cytol. 2022 Feb;39. DOI: 10.4103/joc.joc\_130\_21
  19. Vicent Ribas CGR and JCFC. Gluthathione and Mitochondria. Front Pharmacol. 2014;5: DOI: 10.3389/fphar.2014.00151
  20. WHO. Classification of Diabetes Mellitus 2019. 2019; Available from: <https://www.who.int/publications/i/item/classification-of-diabetes-mellitus>
-

# JOURNAL OF BIOMEDICINE AND TRANSLATIONAL RESEARCH

Available online at JBTR website: <https://jbtr.fk.undip.ac.id>

Copyright©2023 by Faculty of Medicine Universitas Diponegoro, Indonesian Society of Human Genetics and Indonesian Society of Internal Medicine

Case Report

## Recalcitrant Incomplete Secukinumab Administration in a Psoriasis Patient

Joice Sonya Gani Panjaitan<sup>1</sup>, Suhartomi<sup>2\*</sup>

<sup>1</sup> Faculty of Medicine, Universitas HKBP Nommensen, Indonesia

<sup>2</sup> Faculty of Medicine, Dentistry, and Health Sciences, Universitas Prima Indonesia, Indonesia

### Article Info

History

Received: 29 Jun 2023

Accepted: 07 Dec 2023

Available: 31 Dec 2023

### Abstract

**Background:** Psoriasis is an immunologic-mediated disease affected by genetic factors that may affect the skin, joints, and cardiovascular system. Some biological agents have been developed and approved by FDA (Food and Drug Administration) to treat psoriasis. One of these biological agents is Secukinumab, a fully human IgG1κ anti-interleukin-17A(IL-17A) monoclonal antibody.

**Case Presentation:** A seventeen-year-old female teenager came to Dermatovenereology Clinic with scaly patches in the forehead and hairline around ten months ago with a history of repeat Corticosteroid, DMARDs (Disease-Modifying Antirheumatic Drugs), and biologic agent treatment, that was Secukinumab injection. Dermatology examination showed erythema, plaque, and scale in head and extremities with PASI (Psoriasis Area and Severity Index) score of 1.2. The patient was treated with initial and maintenance doses of Secukinumab Injection. After these initial and two maintenance doses, the patient showed a significant clinical improvement by fading off the erythema, plaque, and scale.

**Conclusion:** It can be concluded that the recalcitrant administration of Secukinumab in Psoriasis patients may decrease the treatment response.

**Keywords:** *Psoriasis; Secukinumab; Recalcitrant; PASI; IL17A*

**Permalink/ DOI:** <https://doi.org/10.14710/jbtr.v9i3.19100>

### INTRODUCTION

Psoriasis was known more than 2000 years ago by Hippocrates as psoriasis, which was come from *psora* and *lepra*. Later, psoriasis was described by Ferdinand von Hebra in 1841 as a specialized skin disease. However, recently psoriasis has been defined as an immunologic-mediated disease that is affected by some genetic factors that may affect the skin, joints, and cardiovascular system. Skin clinical presentation of psoriasis is characterized by skin inflammation and epidermal hyperplasia.<sup>1,2</sup>

The prevalence of this disease is different over the world. However, this disease has a lower prevalence rate in Asians. Parisi et al. (2013) reported that the psoriasis prevalence varies in different populations, ranging from 0.91% in the United States to 8.5% in Norway. On the other hand, Bu et al. (2022) also reported that the prevalence of psoriasis ranged from 0.33-0.6% in different races and affected around 125 million people

worldwide. However, psoriasis affects males and females equally.<sup>2,3,4</sup>

The epidemiology data for psoriasis in Indonesia is limited. However, a study has been performed in ten different hospitals in Indonesia to investigate the prevalence of psoriasis. This study was performed from 1996-1998 and reported that the prevalence rate of psoriasis in 1996, 1997, and 1998 were 0.62%, 0.59%, and 0.92%, respectively. On the other hand, psoriasis also increases annually with a remission rate of 17-55% in various duration.<sup>1</sup>

Psoriasis has been classified as a multifactorial disease with various clinical presentations caused by uncontrolled keratinocyte proliferation and excessive inflammatory mediator production.

\*Corresponding author:

E-mail: [suhartomi@unprimdn.ac.id](mailto:suhartomi@unprimdn.ac.id)  
(Suhartomi)



**Table 1.** PASI (Psoriasis Area and Severity Index) Score System

<b>Skin Rash Scoring</b>							
<b>Score</b>	<b>0</b>	<b>1</b>	<b>2</b>	<b>3</b>	<b>4</b>	<b>5</b>	<b>6</b>
Erythema							
Induration	None	Mild	Moderate	Severe	Very Severe	-	-
Desquamation							
True Area (%)	0	1-9	10-29	30-49	50-69	70-89	90-100
<b>Percentage Area Score</b>							
<b>Affected Body</b>				<b>Area Score</b>			
Head (H)				0.1			
Upper Limbs (UL)				0.2			
Trunk (T)				0.3			
Lower Limbs (LL)				0.4			

**Figure 1.** Initial Skin Lesions (Before Initial Dosage of Secukinumab Injection) in (A) Posterior Hairline, (B) Anterior Hairline, (C) Cubital Facies, (D) and (E) Left and Right Cruris

However, the recent postulate believes that the crucial role of psoriasis immunopathogenesis is either CD4+ or CD8+ T Cells. According to psoriasis immunopathogenesis, many drugs have been developed to improve the clinical presentation and quality of life in psoriasis patients.<sup>2,5</sup>

PERDOSKI (*Perhimpunan Dokter Spesialis Kulit dan Kelamin Indonesia*) recently recommended some drugs of choice for psoriasis, including topical, phototherapy, systemic medications, and biological agent. The topical therapy includes emollient, corticosteroid, keratolytic, retinoid, Vitamin D analogue, and tar. Phototherapy uses some types of ultraviolet, including Ultraviolet B broadband (BB-UVB), UVB

narrowband (NB-UVB), and Ultraviolet A (UVA). Meanwhile, the systemic therapy consisted of methotrexate (MTX), cyclosporine, retinoid, some derivatives of mofetil mycophenolate, and sulfasalazine. The last is biologic agents, which can be found in Indonesia as Etarnecept, Ustekinumab, Adalimumab, Infliximab, and Secukinumab.<sup>6</sup>

Some biological agents have targeted some inflammatory mediators, which terminates the inflammation cascade. One of these biological agents is Secukinumab, a fully human IgG1κ anti-interleukin-17A monoclonal antibody. FDA has approved this drug since 2015. However, adherence and persistence to biological agents for psoriasis diseases are still challenging.

Piragine et al. (2022) reported that the adherence and persistence to biological drugs for psoriasis were 61% (95% CI: 48%-73%) and 63% (95% CI: 57%-68%), respectively. Specifically, Piragine et al. also reported that adherence and persistence to Secukinumab were 52% (95% CI: 35%-68%) and 72% (95% CI: 58%-84%), respectively. Another study performed by Huang et al. (2022) also reported that Secukinumab persistence rates in Taiwan were high in the first years of the treatment period and reduced significantly in the second year, which was in contrast to other biologic agents like Ustekinumab, Etanercept, and Adalimumab. Huang et al. (2022) reported that the persistence rate of Secukinumab for psoriasis treatment with a 90-days and 45-days treatment gap was 96.2% (95% CI: 90.7%-100%) and 94.2% (95% CI: 87.7%-100%), respectively. However, the number of patients included in the second year for Secukinumab was very low. Thus the analysis could not be performed.<sup>5,7</sup> Based on these data, it becomes important to report the effect of non-adherence or recalcitrant biologic agent administration, especially Secukinumab. This case report was presented herein to reveal the impact of recalcitrant Secukinumab administration on psoriasis treatment.

### CASE REPORTS

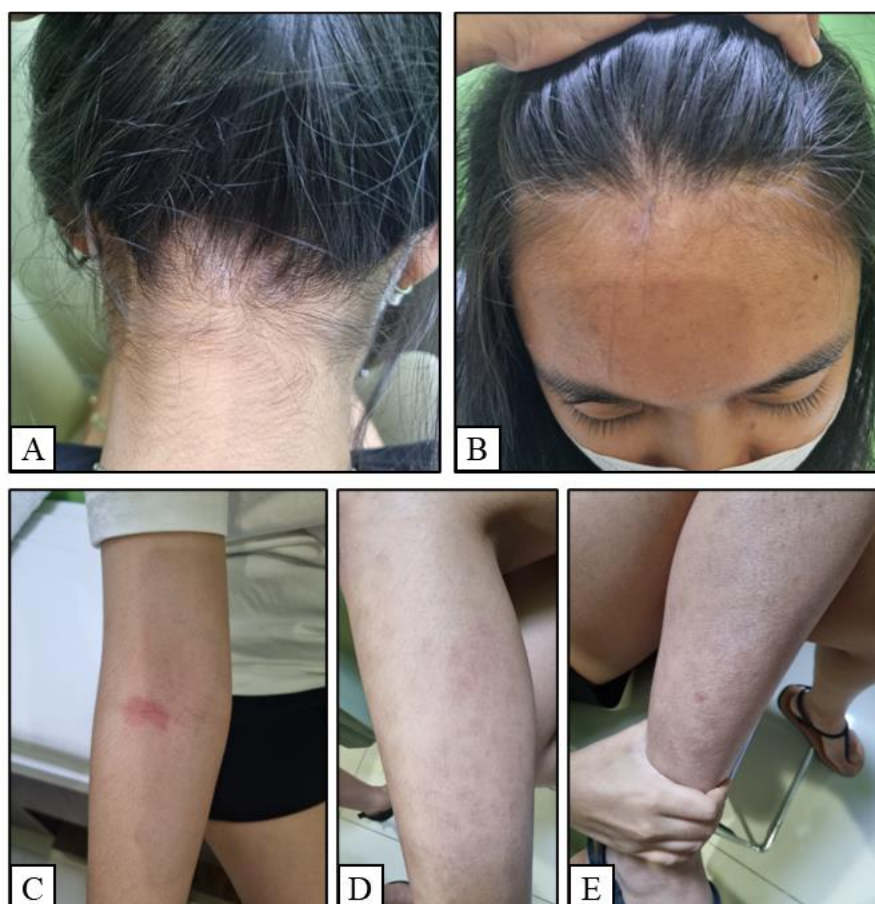
A Seventeen female teenager came to a Dermatovenereology Clinic of a Private Hospital in Medan, North Sumatera, Indonesia, complaining of scaly patches in the forehead and hairline around ten months ago with a history of repeat Corticosteroid,

DMARDs, and biologic agent treatment, that was Secukinumab Injection. There is no family history of similar diseases.

The patient had been diagnosed with psoriasis for seven years and treated with either topical or oral corticosteroid for around two years since the patient was diagnosed, then she did not show any improvement until a few months later. Due to this reason, the patient's treatment was switched to a DMARDs drug that was MTX for two years, and every two months patient underwent routine blood count. The patient showed good clinical improvement against the MTX treatment. Unfortunately, the patients also had the MTX side effects, including appetite loss, hair fall, and severe weight loss after two years of MTX treatment. After that, the patient was suggested to receive a biological agent, Secukinumab. This patient showed a significant clinical improvement after two doses of the initial Secukinumab injection (Fraizeron<sup>TM</sup>). However, she lost follow-up after she finished the initial dosage (Five doses). Hence, she did not receive any maintenance doses.

Dermatology examination showed erythema on the hairline, unilateral cubital facies, and both cruris, plaque on the hairline and unilateral cubital facies, and the last desquamation on the hairline and unilateral cubital facies. This efflorescent of the patient skin can be seen in Figure 1, and the PASI score of this patient was 1.2. Meanwhile, the PASI score system was described in Table 1.

The patient was planned to treat again with the Secukinumab injection. Before the patient received the Secukinumab injection, she underwent some



**Figure 2.** Skin Lesions Before First Maintenance Dose of Secukinumab Injection in (A) Posterior Hairline, (B) Anterior Hairline, (C) Cubital Facies, (D) and (E) Left and Right Cruris

investigation, including full blood count, liver function test, renal function test, randomized blood glucose level, SARS COVID-19 Isothermal Molecular PCR test, IFN-Gamma Release Assay, Electrolytes, and Anti-HCV test. These tests did not show any abnormalities. According to this investigation, the patient was safe to treat again with Secukinumab (Fraizeron™) injection.

This patient received some doses of Secukinumab (Fraizeron™) injection based on the manufacturer's instruction, including initial and maintenance doses. The patient received an initial dose of Secukinumab 300 mg via subcutaneous injection for five doses, including the first visit and every week for a month (first to fourth weeks). Afterwards, the patient received the Secukinumab 300 mg injection via subcutaneous injection as the maintenance dosage in the eighth week and then once every four weeks. After first maintenance dosage, the patient was lost to follow-up for the second maintenance dosage. At the last maintenance injection, the patient showed a significant clinical improvement, that was described in Figure 2. This clinical improvement rate decreased compared to the last year of Secukinumab injection. The patient showed a significant clinical improvement after the second dose of the initial dose at the last secukinumab injection period.

## DISCUSSION

The essential role in the immunopathogenesis of psoriasis is T Cells. The best characterized T Cells in psoriatic lesions are CD4+ and CD8+ with the phenotype memory phenotype (CD45RO+). These cells express cutaneous lymphocyte antigen, a ligand for E Selectin (selectively expressed in skin capillaries). Psoriatic lesion seems to enrich interferon-  $\gamma$  (IFN-  $\gamma$ ) produced by T Helper (Th1). Then, IFN-  $\gamma$  amplifies the dendritic cells to produce Interleukin (IL)-23, which maintains and expands a subset of CD4+ cells (Th17 and Th22). The production of IL-17 and IL-22 characterizes Th17 and Th22. On the other hand, the activated T Cells and Dendritic cells also produce TNF- $\alpha$ . Then, the IL-17, TNF- $\alpha$ , IFN-  $\gamma$ , and IL-22 synergistically promote the activation of innate keratinocyte defence to produce various antimicrobial substances, other cytokines, and chemokines that amplify the last immune responses.<sup>1,2</sup>

Notably, the majority of biological agents with high therapeutic efficacy in psoriasis only target some axes like IL-12-Th1 and IL-23-Th17 axes.<sup>2</sup> PERDOSKI (2017) reported that some biological agents could be found in Indonesia, including Etanercept, Ustekinumab, Adalimumab, Infliximab, and Secukinumab. Etanercept, Adalimumab, and Infliximab are a group of Monoclonal Antibodies that act as Anti-TNF- $\alpha$  monoclonal antibodies. Etanercept is a dimeric fusion protein composed of human IgG1 with the constant region that may fuse to either TNF- $\alpha$  or TNF- $\beta$  receptors. Meanwhile, the adalimumab is a complete IgG1 that blocks TNF- $\alpha$  with the TNF receptor on the cell surface, but the adalimumab does not bind to TNF- $\beta$ . On the other hand, Infliximab is a human-mouse chimeric IgG1 monoclonal antibody possessing human constant (Fc) regions and murine variable regions with the same anti-TNF- $\alpha$  activity as adalimumab and etanercept. However, Etanercept's half-life is shorter than these agents due to its physical form (fusion protein). Other biologic agents

that can be found in Indonesia are Ustekinumab and Secukinumab. Both agents act as anti-Interleukin Monoclonal Antibodies. The ustekinumab is a human IgG1 monoclonal antibody that binds to the p40 subunit of IL-12 and IL-23 cytokines. Furthermore, these blockages inhibit receptor-mediated signalling in lymphocytes.<sup>8</sup> Secukinumab is a fully human IgG1 $\kappa$  anti-interleukin-17A monoclonal antibody that FDA approved in 2015. The current case report used Secukinumab as the biological agent to block the IL-17 activity, preventing T Cells Subset's expansion (Th17). It prevents innate keratinocyte defence from producing various antimicrobial substances, other cytokines, and chemokines.<sup>2,8</sup>

The administration of Secukinumab in the current case report was based on the indication recommended by the local Dermato-Venerology Association (PERDOSKI). PERDOSKI (2017), recommended some indications of biological agent administration for psoriasis treatment. One of these indications is a special consideration in mild psoriasis patients with extensive area on the face that is not responsible for topical treatment, visible location, and any regions that are not unresponsive for topical treatment. In this case report, psoriasis involved the face area that did not respond to topical therapy; thus, the patient was indicated to receive the biologic agent (Secukinumab).<sup>6</sup>

This case report reported that this patient reduced response against the Secukinumab injection. Some hypotheses have been postulated to explain the mechanism of Secukinumab resistance. Berman et al. (2021) believed that the structure of Secukinumab has a lower affinity than another IL-17 monoclonal antibody; hence Secukinumab has a lower equilibrium dissociation constant (Kd) than other IL-17 monoclonal antibodies, allowing a higher potential for IL-17A blockade. Another possible hypothesis is the presence of neutralizing anti-drug antibodies to Secukinumab. Deodhar et al. (2020) reported that Secukinumab has a low incidence of immunogenicity (<1%) within a 52-week course in Psoriatic arthritis and ankylosing spondylitis. Moreover, Deodhar et al. (2020) explained that anti-drug antibodies to Secukinumab may be due to the B cell activation and regulation. However, it remains a theoretical possibility that requires future studies. Although Secukinumab is a fully human antibody, it is still possible that the presence of potential epitopes. It formed within the highly diverse amino acid composition of the complementarity-determining regions (CDRs) of immunoglobulin G (IgG) molecules, the loss of tolerance to self-sequences, and product-specific attributes, such as dosing frequency, dose amount, administration route, and formulation factors such as impurities, host cell proteins, and the tendency to aggregate. A recent study by Reich et al. (2022) reported a similar result as Deodhar (2019). Reich et al. (2022) reported that Secukinumab consistently had low immunogenicity for up to 5 years in moderate-severe psoriasis. However, Reich et al. (2022) concluded that the administration of Secukinumab with low immunogenicity in moderate-severe psoriasis did not affect the efficacy, safety, or pharmacokinetics of this drug.<sup>9,10,11</sup>

Many studies showed various possible hypotheses about the efficacy of Secukinumab. Amschler et al.

(2020) do not agree with the presence of anti-drug antibodies against Secukinumab, which appear not to be relevant as a possible explanation for treatment failure to Secukinumab. Amschler et al. also reported an in-line result to Berman et al. that the affinity of IL-17A also affects the secukinumab resistance, which has 50-100 times lower *in vitro* affinity than the ixekizumab. Moreover, Amschler et al. also explained that their study has limited data on this hypothesis.<sup>9,12</sup>

The patients with mild psoriasis have received an uncompleted dose of Secukinumab. This case report showed the potential mechanism of anti-drug antibody formation. It potentially induces the acquired immune system to eliminate Secukinumab as the low immunogenicity foreign protein. Moreover, this protein with potential epitopes can activate or regulate the B Cells as part of the acquired immune system to produce anti-drug antibodies. However, this case report has limited data to explain this hypothesis, so further study is required to support this hypothesis.

## CONCLUSION

This case report can be concluded that the recalcitrant administration of Secukinumab in Psoriasis patients may decrease the treatment response. This patient revealed a reduced treatment response against the Secukinumab in every course, and in the last course, the patient also showed a significant decrease in treatment response against the Secukinumab. This condition may occur due to either a lower equilibrium dissociation constant of Secukinumab or the formation of anti-drug antibodies against the Secukinumab. This case report showed the importance of adherence and persistence of a biologic agent administration in a clinical setting, especially in psoriasis.

## REFERENCES

1. Jacob TNA. Psoriasis. In: Menaldi SLS, Bramono K, Indriatmi W, eds. *Ilmu Penyakit Kulit Dan Kelamin*. Ketujuh. Badan Penerbit Fakultas Kedokteran Universitas Indonesia; 2015:213-222.
2. Gudjonsson JE, Elder JT. Psoriasis. In: Kang S, Amagai M, Bruckner AL, et al., eds. *Fitzpatrick's Dermatology*. 9th ed. McGraw Hill; 2019:457-497.
3. Parisi R, Symmons DPM, Griffiths CEM, Ashcroft DM. Global epidemiology of psoriasis: A systematic review of incidence and prevalence. *J Invest Dermatol*. 2013;133(2):377-385. doi:10.1038/jid.2012.339
4. Bu J, Ding R, Zhou L, Chen X, Shen E. Epidemiology of Psoriasis and Comorbid Diseases: A Narrative Review. *Front Immunol*. 2022;13(June):1-19. doi:10.3389/fimmu.2022.880201
5. Piragine E, Petri D, Martelli A, et al. Adherence and Persistence to Biological Drugs for Psoriasis: Systematic Review with Meta-Analysis. *J Clin Med*. 2022;11(6). doi:10.3390/jcm11061506
6. Perhimpunan Dokter Spesialis Kulit dan Kelamin Indonesia (PERDOSKI). *Panduan Praktik Klinis Bagi Dokter Spesialis Kulit Dan Kelamin Di Indonesia*. (Widaty S, Soebono H, Nilasari H, et al., eds.). Perhimpunan Dokter Spesialis Kulit dan Kelamin Indonesia (PERDOSKI); 2017.
7. Huang Y-H, Tang C-H, Goh CH, et al. Persistence and Adherence to Biologics in Patients with Psoriasis in Taiwan: A New Biologics User Cohort Study. *Front Pharmacol*. 2022;13(May):1-9. doi:10.3389/fphar.2022.880985
8. Lake DF, Briggs AD, Akporiaye ET. Immunopharmacology. In: Katzung BG, Masters SB, Trevor AJ, eds. *Basic & Clinical Pharmacology*. 12th ed. Mc Graw Hill Lange; 2012:977-1000.
9. Berman J, Furer V, Berman M, et al. Treatment with ixekizumab following secukinumab failure in patients with psoriatic arthritis: Real-life experience from a resistant population. *Biol Targets Ther*. 2021;15:463-470. doi:10.2147/BTT.S326792
10. Deodhar A, Gladman DD, McInnes IB, et al. Secukinumab Immunogenicity over 52 Weeks in Patients with Psoriatic Arthritis and Ankylosing Spondylitis. *J Rheumatol*. 2020;47(4):539-547. doi:10.3899/jrheum.190116
11. Reich K, Blauvelt A, Armstrong A, et al. Secukinumab, a Fully Human Anti-Interleukin-17A Monoclonal Antibody, Exhibits Low Immunogenicity in Psoriasis Patients Treated Up to 5 Years. *J Eur Acad Dermatology Venereol*. 2019;33(9):1733-1741. doi:10.1111/jdv.15637
12. Amschler K, Phillip S, Mohr J, et al. Long-term follow-up of 22 psoriatic patients treated with ixekizumab after failure of secukinumab. *Dermatol Online J*. 2020;26(1):1-5. doi:10.5070/d3262047415



# JOURNAL OF BIOMEDICINE AND TRANSLATIONAL RESEARCH

Available online at JBTR website: <https://jbtr.fk.undip.ac.id>

Copyright©2023 by Faculty of Medicine Universitas Diponegoro, Indonesian Society of Human Genetics and Indonesian Society of Internal Medicine

Review Article

## Exploring Systemic Lupus Erythematosus Pathogenesis through Animal Models: A Systematic Review of Humanized and Pristane-Induced Lupus Mice

Dimas Ikhsan Airlangga<sup>1\*</sup>, Hanifa Rizky Rahmawati<sup>1</sup>, Hani Susianti<sup>1</sup>, Kusworini Handono<sup>1,2</sup>

<sup>1</sup>Faculty of Medicine, Universitas Brawijaya, Indonesia

<sup>2</sup>Saiful Anwar Hospital, Malang, Indonesia

### Article Info

History

Received: 17 Jul 2023

Accepted: 07 Dec 2023

Available: 31 Dec 2023

### Abstract

Studies involving experimental animals to explore the pathogenesis of Systemic Lupus Erythematosus (SLE) which leads to the selection of optimal therapy have been widely conducted. The well-known model used to study SLE includes the pristane-induced mouse model and the more recently developed humanized mouse model that implants human immune cells into immunodeficient mice. The current state of the research has yet to provide a systematic review that analyzes both model and its contribution to our understanding of SLE pathogenesis. This systematic review-based study aims to provide a comprehensive overview of the development and application of pristane-induced and humanized mouse models. We obtained several relevant article sources include: (1) Search Strategy, on databases such as PubMed, MEDLINE, ScienceDirect, and Cochrane by adjusting the protocols listed in the Preferred Reporting Items for Systematic Reviews and Meta-analyses (PRISMA); (2) Eligibility based on exclusion and inclusion criteria; and (3) Data Extraction. The findings show that 30 articles are relevant to the subject matter. Several strains of mice were used in the model of the 0.5 pristane injection method and the humanized mice model. All studies showed similar patterns in the onset and manifestation of SLE in mice models with slight variations. The purpose of using the pristane injection method and humanized mice model is adjusted to the output of each study. A variety of research preferences can be used as a reason for choosing pristane and humanized cells transplanted methods in making SLE model mice.

**Keywords:** *animal models; humanized-mice; pristane; systemic lupus erythematosus (SLE)*

**Permalink/ DOI:** <https://doi.org/10.14710/jbtr.v9i3.19147>

### INTRODUCTION

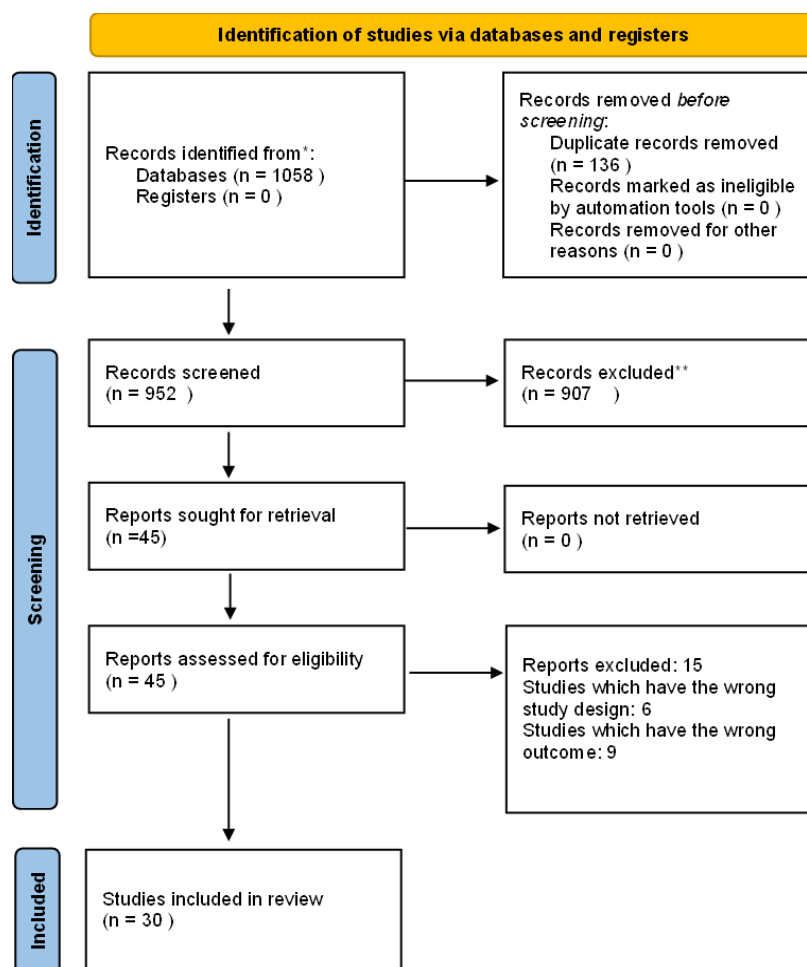
Systemic lupus erythematosus (SLE) is a complex autoimmune disease that affects millions of people worldwide. Despite extensive research efforts, the pathogenesis of SLE remains poorly understood, leading to suboptimal therapy.<sup>1</sup> The use of animal models plays an important role in advancing the understanding of SLE. Many different models have been developed to study the immune dysregulation and multi-organ involvement that characterize the disease.<sup>2</sup> Animal models of SLE can generally be categorized into spontaneous models, transgenic knockout models, induced models, and humanized mouse models.<sup>2</sup> The

focus of each study determines the choice of animal model used. Spontaneous and transgenic models are often used and although they show satisfactory results, they have limitations due to specific SLE manifestations and limited genetic factors.

Spontaneous lupus mice models often do not capture the entire complexity of the disease, including the involvement of specific organs or tissues such as only the kidney. humanized-mice method on creating SLE mice

\*Corresponding author:

E-mail: [dimasikhsanairlangga10@gmail.com](mailto:dimasikhsanairlangga10@gmail.com)  
(Dimas Ikhsan Airlangga)



**Figure 1 PRISMA flow diagram.** There were a total of 1058 articles reviewed from keywords, abstracts, and methods used in research. The types of journals used were original article research and review with a range of years 2013-2023. Based on the flowchart diagram, a final total of 30 articles were included in the review.

Since SLE in humans is not only caused by a single genetic factor but also by the effects of environmental exposures,<sup>2</sup> the induced mouse model was chosen as an alternative. The most commonly used induced mouse model is pristane that represents environmental factors. Pristane is an isopropanol alkaloid that is injected into mice to induce the development of SLE-like symptoms, including autoantibody production, immune complex deposition, and glomerulonephritis.<sup>3,4</sup> Pristane-induced models have been used to study the role of T and B cells in SLE development and environmental factors in disease susceptibility.<sup>3,2</sup> This method has advantages over other methods as an option because of its practicality and the emergence of a more complex spectrum of SLE disease manifestations in different organ systems. Meanwhile, humanized mouse models have also recently been developed by transplanting human immune cells into immunodeficient mice.<sup>5,6</sup> These models provide an opportunity to study the human immune system in vivo and have the potential to advance our understanding of the pathogenesis of SLE, particularly those that are similar to, or close to, the pathogenesis in patients with the disease. This model has also been used to study the role of different immune cell subsets in the development of SLE and to test the efficacy of new therapies.<sup>7,6</sup> Based on these reasons, this

article selects pristane-induced and lupus-induced lupus mice, in addition to both methods having advantages over other methods. Such advantages are relevance to human disease, mimicry of environmental factors, suitability for studying neuropsychiatric lupus, ideal lupus mouse model. The problem with the current state of research is that there is no systematic comprehensive review that analyzes the strengths and limitations of each model, which is important to explore between humanized mice and pristane injection methods. In addition, there is still little information to verify the method of humanizing mice as the use of the method to generate SLE mouse models increases and its contribution to our understanding of generating animal models of lupus associated with SLE pathogenesis.

A systematic review would be very useful for researchers in lupus. It would help to guide future investigations and identify potential areas of research that could lead to new therapeutic targets using animal models. This systematic review aims to take a closer look at the existing studies and provide a comprehensive overview of the development and use of pristane-induced mice and humanized mouse models of lupus in SLE research.



**Table 1.** Summary of results based on the study of research methods in intervening mice to become SLE.

Author and Year of Publication	Animal Models	Method of Induction of Lupus	Research Objective	Result
Aschman <i>et al.</i> , (2021)	(N= 10) Type III IFN receptor-deficient mice (Ifnlr1-/-) and (N= 10) wild-type mice	0.5 ml i.p. pristane injection	Research Objective	Result
Delimitreva <i>et al.</i> , (2021)	(N= 10) Female Balb/c (4 weeks)	0.5 ml i.p. pristane injection	To investigate the function of type III IFN in SLE	Ifnlr1 -/- mice showed a decrease in the number of lipogranulomas, the number of antibody-secreting cells (not significant), natural killer (NK) cells in the kidney, and B cells in the spleen, as well as an increase in survival rate and peripheral CD115+Ly6C+ monocytes compared to wild type mice. Intraperitoneal injections of pristane could show a result in local chronic inflammation and the formation of lipogranulomas.
Dema <i>et al.</i> , (2017)	(N= 12) Female C57/BL/6 mice with diphtheria toxin-induced basophil depletion and MAR-1	0.5 ml i.p. pristane injection	To investigate the effect of SLE on the oocyte maturation process	Decreased activation and apoptosis of T cells, decreased apoptosis of B cells, increased number of plasma cells secreting IgG anti-dsDNA antibodies, increased levels of IgG, IFN- $\gamma$ , and IL10, the onset of proteinuria, increased mesangial proliferation in the glomeruli. Mice with induced lupus exhibited low egg maturation rate
Gunawan <i>et al.</i> , (2017)	(N= 61) NOD scid gamma (NSG) mice	fetal haematopoietic stem cell (HSC) transplantation	Analyzing the contribution of basophil cells to pristane-induced lupus nephritis	After pristane injection, basophils were activated and accumulated in SLOs to promote autoantibody production. Basophils contribute to the development of lupus nephritis by increasing autoantibody production. Basophil depletion decreases autoantibodies and immune complex clearance in the glomerulus

Table 1. Cont...

Author and Year of Publication	Animal Models	Method of Induction of Lupus	Research Objective	Result
Kalim <i>et al.</i> , (2018)	(N= 48) Female Balb/c (8-12 weeks)	0.5 ml i.p. pristane injection	Generation of a human immune system-mediated SLE model induced by pristane injection in humanized mice (hu-mice)	There is a decrease in the number of human lymphocytes in the peripheral blood, hyperactivation of T cells and B cells, an increase in the number of plasma cells and memory T cells, and an increase in pro-inflammatory cytokines and the IFN type 1 gene → resembles lymphopenia in SLE patients. A human immune-mediated SLE model that recapitulates key clinical and immunological features of SLE.
Liou <i>et al.</i> , (2022)	(N= 90) Mice Balb/c (8 weeks)	0.5 ml i.p. pristane injection	Identify the function of regulatory T cells in the pathogenesis of SLE in pristane-induced mice	Th1 and Th17 in the pristane group were higher than the control group at week 8, the percentage of Th1 and Th17 decreased at week 16, Th1 and Th2 increased in the pristane group at weeks 24 and 32, and there was a positive correlation between IL-6 and Treg in the pristane group.
Pannu <i>et al.</i> , (2020)	(N= 10) Mice Balb/c (8 weeks)	0.5 ml i.p. pristane injection	Identifying anti-dsDNA IgG and de-SIA IgG antibodies in SLE mice	The spontaneous lupus model in BALB/c mice summarizes other spontaneous lupus mouse models driven by toll-like receptor 7 and 9. A low SIA/serum IgG anti-dsDNA ratio indicated a high severity of nephritis in the pristane-induced group. High sialylated anti-dsDNA IgG was able to reduce the severity of proteinuria.
Lee <i>et al.</i> , (2020)	Female C57BL/6 and IFNAR1 <sup>-/-</sup> mice	0.5 ml i.p. pristane injection	Investigating the status of oxidative stress, inflammation, immune complex, and histopathological changes in lupus-affected organs	Pristane injection caused the generation of anti-nuclear antibodies, which were apparent from the different immunofluorescence patterns observed. Immune deposits were evident in all the vital organs stating the similarity this model holds with SLE patients. Pristane injection mimics the two main manifestations of lupus, oxidative stress and inflammation.
Peixoto <i>et al.</i> , (2019)	(N= 26) female Balb/c (6-8 weeks)	0.5 ml i.p. pristane injection	To understand how inflammation in SLE mice models affects red blood cell (RBC) alloimmunization.	Pristine challenge upregulates the secretion of NGAL by macrophages and splenocytes. Pristane induction of a lupus-like phenotype promoted alloimmunization to the KEL RBC antigen in an IFN $\alpha$ /b-dependent manner

Table 1. Cont...

Author and Year of Publication	Animal Models	Method of Induction of Lupus	Research Objective	Result
Tang <i>et al.</i> , (2021)	(N= 5) Female Balb/c (6-8 weeks) mice	0.5 ml i.p. pristane injection	analyzing the expression of CD4+ CD69+ T cells and Treg cells as well as multiple interleukin profiles of SLE model mice	Compared with the controls, SLE-induced animals presented increased numbers of CD4+ CD69+ T cells in the blood on T90 and T120 and in the spleen on T120, but there were decreased numbers in the PL on T120. T90. Increased numbers of CD4 + CD69+ T cells in the PL were positively associated with high IL-2.
Ma <i>et al.</i> , (2021)	female C57BL/6J (C57), NOD-SCID IL2R $\gamma$ null (NSG), B6.SJL-Ptprca Pepcb/BoyJ, Il17rc-/- (IL-17RC KO, with C57), mice MRL/MPJ, and MRL/MpJ-Faslpr/J (MRL/Lpr mice)	Humanized lupus mouse model by transferring Th17 cell-depleted PBMCs from SLE patients	examining changes in the thymus and potential mechanisms responsible for immuno-logical abnormalities in Pristane Induced Lupus (PIL) mice.	The modification in the thymus in PIL and elucidated the immunologic abnormalities of increased B cells, potentially providing insight into the associated molecular mechanisms and facilitating further research.
Leiss <i>et al.</i> , (2013)	(N= 57) BALB/c mice received pristane (PIL group) and were analyzed for serum autoantibodies (anti-chromatin-, -histone, -Sm, -dsDNA)	injected intraperitoneally (i.p.) with either 0.5 ml of pristane or saline (as a control)	identified a novel function of IL-17 in enhancing plasma cell survival for autoantibody production in SLE pathogenesis	novel function of IL-17 in enhancing plasma cell survival for autoantibody production in SLE pathogenesis. IL-17 significantly promoted plasma cell survival via p38-mediated Bcl-xL transcript stabilization.

Table 1. Cont...

Author and Year of Publication	Animal Models	Method of Induction of Lupus	Research Objective	Result
Yun <i>et al.</i> , (2023)	(N= 12) Female (4 weeks) BALB/c mice	0.5 mL pristane injection intraperitoneally (i.p.)	To characterize the clinical and histological features of arthritis associated with systemic lupus and to compare with models of rheumatoid arthritis (RA)	BALB/c PIL mice developed clinical arthritis within 3 months and correlated with areas of inflammation, erosion, cartilage damage, osteoclast number, and severity. PIL mice with arthritis also showed signs of pulmonary (100%) and renal (46%) lupus.
Luciano <i>et al.</i> , (2019)	(N= 54) Female BALB/c mice 8–12 weeks old	i.p 0.5 mL pristane injection	To investigate the neuropsychiatric symptoms in the PIL mouse model for the Neuropsychiatric Systemic Lupus Erythematosus (NPSLE) study	Pristane can induce mice to exhibit olfactory dysfunction and an anxiety- and depression-like phenotype, along with increased expression of cytokines, BBB leakage, activation of microglia and astrocytes and aberrant deposition of IgG and lipofuscin in the brain.
Summers <i>et al.</i> , (2014)	(N= 7) Female wild-type (WT) and (N= 6) IL-17A <sup>-/-</sup> mice	Injected with 500 µl of pristane	To analyze the NMDA subunit receptors, finding a downregulation of NR2A subunit related to learning and memory disturbance when were exposed to lipopolysaccharides (LPS).	Pristane-induced lupus BALB/c mice had the downregulation of hippocampal NR2A/2B subunits which related to cognitive impairment i.e., learning and memory disturbance. Moreover, Downregulation of the NR2A subunit was more pronounced when they were exposed to LPS.
Han <i>et al.</i> , (2015)	(N= 2-6) BALB/cBy J and BALB/c TLR7 <sup>-/-</sup> mice	Injected with 0.5 mL pristane (i.p.)	To define the role of IL-17A in experimental lupus induced by pristane administration.	Seven months after treatment with Pristane, humoral autoimmunity was reduced in the absence of IL-17A with reduced levels of immunoglobulin (Ig)G and anti-dsDNA antibodies. IL-17A is required for the maximal production of humoral and cellular autoimmunity and IL-17A is even produced early in the disease process, predominantly by innate immune cells.

Table 1. Cont...

Author and Year of Publication	Animal Models	Method of Induction of Lupus	Research Objective	Result
Liu <i>et al.</i> , (2022)	(N= 3-5) BALB/c, C57BL/6 mice, and TCR $\alpha$ <sup>-/-</sup> mice	Injected by 0.5 mL pristane	To address anti-ribonucleoprotein/Smith (anti-Sm/RNP) and other SLE autoantibodies levels are maintained over time.	B cells with a switched "memory-like" (CD19+ CD138- IgM- IgD-) (sMB) phenotype were increased in pristane-treated mice and expressed higher levels of Toll-like receptor 7 (TLR7) than cells with this phenotype from untreated mice. Also, B cells are hyper-responsive to synthetic TLR7 ligands and apoptotic cells.
Rodriguez <i>et al.</i> , (2018)	(N= 7-9) Cd38 <sup>-/-</sup> and Art2 <sup>-/-</sup> mice	intraperitoneal injection of pristane	To investigate the manners of CD4+ T cells in antibody production in a lupus-like mouse model by pristane injection	CD4+ T cells in pristane-treated mice play important roles in IgG production, which implies the critical roles in the induction of pathological autoantibodies in MHC-independent and ICAM-1-dependent manners.
Kienhöfer <i>et al.</i> , (2017)	Both Ncf1-mutated and PAD4-deficient mice	Injected i.p. alkane pristane	To investigate the role of CD38 in a pristane-induced murine model of SLE.	Reveal a new role for CD38 in promoting aberrant inflammation and lupus-like autoimmunity via an apoptosis-driven mechanism
McClung <i>et al.</i> , (2021)	(N= 14) female C57BL/6 mice	Pristane 0.5mL injection (i.p.)	To investigate the functional impact of neutrophils and NETs on a mouse model of SLE triggered by intraperitoneal injection of the cell death-inducing alkane pristane.	Hydrocarbon oil pristane induces chronic peritonitis by the production of autoantibodies directed against DNA- and RNA-associated autoantigens and chronic inflammation, resulting in a disease closely resembling and meeting the classification criteria of SLE. The aberrant NET is one of the factors that promotes experimental lupus-like autoimmunity through the uncontrolled release of inflammatory mediators.
Bossaler <i>et al.</i> , (2013)	Wild-type BALB/c and C57BL/6 mice as well as B6gld/gld and BALB/c Rag2 <sup>-/-</sup>	single i.p. injection of 0.5 ml of pristane	The pristane-inducible model of SLE would develop hypertension and vascular dysfunction as the disease progressed.	Seven months after pristane administration, mice developed various autoantibodies (including anti-dsDNA IgG, anti-ssDNA IgG, and anti-nRNP IgG, as well as hypergammaglobulinemia) and immunological changes (increased circulating neutrophils and increased CD4-CD8-)

Table 1. Cont...

Author and Year of Publication	Animal Models	Method of Induction of Lupus	Research Objective	Result
Bossaler <i>et al.</i> , (2016)	(N= 29) Tlr92/2 BALB/c mice	injected i.p. with TMPD (pristane)	evaluated the effect of FasL-deficiency, as well as FasL overexpression, on TMPD-injected BALB/c mice.	FasL-deficiency significantly reduced the early inflammatory exudate induced by TMPD injection. In contrast, $\Delta$ CS mice developed a markedly exacerbated disease profile, associated with a higher frequency of splenic neutrophils and macrophages, a profound change in ANA specificity, and a more pronounced
Kanno <i>et al.</i> , (2020)	Male wild type ( $\alpha$ 2AP+/+) and $\alpha$ 2AP <sup>-/-</sup> mice	Injected 500 $\mu$ l of pristane (i.p.)	To evaluate the negative regulatory role of TLR9 in murine SLE	Develop more severe autoimmunity than do their TLR-sufficient cohorts (increased production of neutrophils, anti-neutrophil Abs, and the development and progression of renal disease). Thus, the BALB/c Pristine model recapitulates other TLR7-driven spontaneous models of SLE and is negatively regulated by TLR9.
Amarilyo <i>et al.</i> , (2014)	(N= 12-16) Wild-type (WT) C57BL/6 (B6) and syngeneic IL-17-deficient (IL-172/2) mice	one i.p. injection of 500 ml pristane	identification functions of Alpha2-antiplasmin ( $\alpha$ 2AP) and to be associated with immune and inflammatory responses in Lupus Nephritis (LN).	The levels of plasmin- $\alpha$ 2AP complex and $\alpha$ 2AP were elevated in the lupus model mice. In addition, $\alpha$ 2AP deficiency attenuated pristane-induced glomerular cell proliferation, mesangial matrix expansion, collagen production, fibrin deposition, immunoglobulin G deposition and pro-inflammatory cytokine production in the model mice. This also correlated with the function of pristane known to induce LN.
Smith <i>et al.</i> , (2018)	(N= 8) C57BL/6 (B6) mice	i.p. injection of 500 ml pristane	Identification the role of IL-17 in SLE mice that were genetically deficient of this cytokine.	Pristane-treated IL-172/2 mice had significantly reduced titers of IgG and low anti-ssDNA, anti-nRNP, and anti-chromatin Autoantibodies. Pro-inflammatory IL-17 after Pristane administration. administration, it appeared to involve multiple immune cell populations.



Table 1. Cont

Author and Year of Publication	Animal Models	Method of Induction of Lupus	Research Objective	Result
Lu <i>et al.</i> , (2017)	<i>Nlrp3</i> <sup>R258W</sup> mouse	one i.p. injection of 500 µl of pristane	Identification a role for IL-16/mir-125a in SLE pathology and show not only that IL-16 is a target for miR-125a but that reduced miR-125a expression in SLE patients is associates with lung involvement.	In the pristane model of acute “SLE-like” lung inflammation and alveolar hemorrhage, there is reducing pulmonary miR-125a, neutrophil infiltration was markedly reduced, and enhanced IL-16 expression. miR-125a/IL-16 in the regulation of lung inflammation and suggest that this axis may be a may be a therapeutic target for the treatment of acute lung injury in SLE.
Kluger <i>et al.</i> , (2016)	(N= 12) <i>Foxp3</i> <sup>Cre</sup> × <i>Stat3</i> <sup>fl/fl</sup> mice	one i.p. injection of pristane	Explore the role of NLRP3 in the development of SLE using the pristane-induced experimental lupus model.	<i>Nlrp3</i> <sup>-R258W</sup> mutant mice exhibited significantly higher mortality upon pristane challenge because developed a much more severe lupus-like syndrome in the pristane-induced SLE model. NLRP3 functions to drive kidney inflammation in lupus are primarily myeloid cells, including macrophages, neutrophils and some dendritic cells. This can be confirmed in the future using conditional NLRP3 knockout mice.
Zhang <i>et al.</i> , (2018)	BALB/c and C57BL/6 Female (6–8 weeks old) mice	Injected by 0.5 ml pristane (i.p.)	To identify the function of the newly defined Stat3-dependent Th17-specific regulatory T cells (Treg17).	Establishes a role of Treg17 cells for the control of Th17 responses and tissue protection during acute inflammatory and chronic autoimmune-mediated stages of pristane-induced SLE.
Zhou <i>et al.</i> , (2021)	Balb/c WT mice and BALB/c nude mice (CAnN.Cg-Foxn1nu/CrlVr),	Mice were prepared to be immunodeficient by UVB exposure. Then, PBMC cells from cutaneous lupus patients and healthy controls were transplanted.	to investigate whether MDSCs are involved in the process of podocyte injury in the development of Lupus Nephritis (LN)	MDSCs induce podocyte injury by ROS and were involved for the first time in the subsequent development of proteinuria in LN of pristane-induced lupus mice. Furthermore, TLR-7-activated MDSCs enhanced podocyte injury by activating p-38MAPK and NF-kB pathways through ROS.

**Table 1.** Cont...

Author and Year of Publication	Animal Models	Method of Induction of Lupus	Research Objective	Result
Zhuang <i>et al.</i> , (2016)	(N= 4-8) C57BL/6 (B6), B6 (mu;MT), B6 (C3-/-), and B6 (CD18-/-) mice	Injection of Purified human IgM or murine IgG (200 mu;g/mouse) i.v. into mu;MT mice. Then 0.5 ml pristane injection i.p.	Establishment of humanized mice (hu-mice) model for the development of rapid onset induction murine against cutaneous lupus	Humanized mice develop lupus-like cutaneous lesions under UVB radiation, present cutaneous lupus lesions of Hu-LE mice show B cell clusters and CD11b+ B220+ cell infiltration exhibits prominent expansion

- PIL : Pristane Induced Lupus
- hu-mice : humanized mice
- LN : Lupus Nephritis
- NPSLE : Neuropsychiatric Systemic Lupus Erythematosus

**Table 2.** List of clinical manifestations that emerged or were the focus of studies with SLE mice model

Disease Manifestation		Pristane-Induced Model (N = 27) N (%)	Humanized Model (N = 3) N (%)
<b>Onset</b>			
-	< 8 weeks	2 (7%)	1 (33%)
-	8-16 weeks	15 (55%)	1 (33%)
-	>16 weeks	8 (31%)	1 (33%)
-	N/A	2 (7%)	-
<b>Clinical</b>			
-	Proteinuria/lupus nephritis	17 (63%)	2 (67%)
-	Arthritis	4 (15%)	N/A
-	Lung (i.e., pleuritis, vasculitis, alveolar hemorrhage)	3 (11%)	1 (33%)
-	Skin lesion and/or alopecia	2 (7%)	1 (33%)
-	Behavioural/neuronal	2 (7%)	N/A
-	Cardiovascular (i.e., hypertension)	1 (4%)	N/A
<b>Serological</b>			
-	ANA and/or Anti-dsDNA	20 (74%)	3 (100%)
-	Anti-RNP/Anti-Sm	10 (37%)	1 (33%)
-	Anti-histone	2 (7%)	N/A
<b>Immunohistochemistry</b>			
-	Kidney and/or other organs (i.e., spleen, liver)	20 (74%)	3 (100%)

N/A: not mentioned in the article

**Table 3.** Summary of the advantage and the disadvantage of pristane induced lupus model and humanized lupus model

Model	Advantage	Disadvantage
Pristane Induced Lupus	<ul style="list-style-type: none"> <li>● Pristane Induced Lupus (PIL) mice are relatively easy to generate and maintain in the laboratory.</li> <li>● The development of lupus-like symptoms in PIL mice is highly reproducible, allowing researchers to conduct consistent experiments.</li> <li>● Pristane triggers the autoimmune response seen in lupus-like symptoms, including the production of autoantibodies and kidney damage.</li> <li>● PIL mice develop lupus-like symptoms within a predictable timeframe, which is advantageous for studying disease progression and assessing the effects of experimental interventions.</li> </ul>	<ul style="list-style-type: none"> <li>● PIL mice do not spontaneously develop SLE, but rather exhibit lupus-like symptoms and thus do not fully capture the complexity and heterogeneity of human disease.</li> <li>● The autoimmune response in PIL mice is induced by pristane, which is different from the human lupus trigger.</li> <li>● PIL mice lack the genetic disorders characteristic of human SLE.</li> <li>● PIL mice often show kidney disease as a manifestation of lupus-like symptoms, whereas human SLE can affect multiple organs.</li> </ul>
Humanized Lupus	<ul style="list-style-type: none"> <li>● Mice models transplanted with human immune cells allow researchers to study SLE in a more human-relevant context</li> <li>● Humanized mice can display a variety of disease manifestations, including autoantibody production, tissue damage and organ involvement, reflecting the multifaceted nature of human SLE.</li> <li>● This model provides a platform to evaluate the efficacy and safety of potential therapeutic interventions for SLE prior to human clinical trials.</li> <li>● Humanized mice models can be created using immune cells from SLE patients, facilitating the investigation of individualized treatment approaches.</li> </ul>	<ul style="list-style-type: none"> <li>● The creation and maintenance of humanized mice will be technically challenging and time consuming due to the need for human cell transplantation and subsequent maintenance.</li> <li>● Other physiological and genetic differences between mice and humans may limit the applicability of findings from this model to human SLE.</li> <li>● Use of humanized mice models raises ethical concerns</li> </ul>

## METHODS

### Search Strategy

We conducted a comprehensive search on databases such as PubMed, MEDLINE, ScienceDirect, and Cochrane with a publication period from January 2013 to April 2023. The search for published articles in English was conducted with the following keywords: "lupus mouse model"; "lupus mice model"; "humanized mouse model of lupus"; "pristane induced mouse lupus"; "Pathogenesis of systematic lupus erythematosus"; and "Pathophysiology of systematic lupus erythematosus". This study followed the protocol listed in the Preferred Reporting Items for Systematic Reviews and Meta-analyses (PRISMA).

### Eligibility

The research criteria included: (1) Studies that used humanized lupus mice models and pristane induction; (2) Studies that successfully induced SLE in mice models; (3) Studies that reported outcomes related to SLE manifestations such as autoantibody production, immune cell disorders, and tissue damage; (4) and studies with statistically significant or non-significant results.

We excluded studies that (1) used spontaneous lupus mice model; (2) used therapeutic interventions that affected improving the condition of the mice; (3) had other autoimmune disorders; (4) did not present primary data; and (5) included reviews, systematic reviews, meta-analyses, commentaries, letters to the editor, books, doctoral dissertations, conference abstracts, and study protocols.

### Data Extraction

Data extracted independently using a standardized form that includes the following information: (a) authors and year of publication (b) animal model used, (c) SLE induction method, (d) study objectives, and (e) main results and findings.

## RESULTS

### Study Selection

Relevant articles were identified based on the database and registers through screening with the Rayyan.ai tool (<https://www.rayyan.ai/>) resulting in total of 1058 articles (Figure 1). A total of 136 duplicate records were removed to obtain articles that were suitable for the screening process. The 952

articles were separated based on exclusion and inclusion criteria, resulting in 45 articles that met the criteria. A more thorough assessment of reports eligibility excluded studies that had the wrong study design ( $n = 6$ ) and studies that had the wrong outcome ( $n = 9$ ). Thus, the final results of articles by the inclusion criteria were 30, which were used as the subject of discussion in the systematic review.

### Pristane-induced Lupus Mice Model

Mouse models of lupus induced by intraperitoneal (i.p.) injection of 0.5 ml of pristane cause different onset and clinical manifestations of the disease. Twenty-seven articles are using pristane-induced mice as animal models of SLE. All pristane-model mice showed success in developing lupus-like disease manifestations. The onset of lupus disease in this model most commonly occurred between 8 and 16 weeks after induction, as reported in 15 studies. This was followed by an onset above 16 weeks in 8 studies and 2 studies showing an onset below 8 weeks.<sup>16,20</sup> The most commonly reported or investigated clinical manifestations were the onset of proteinuria and symptoms of lupus nephritis in 17 studies, followed by arthritis ( $n=4$ ),<sup>1,16,18,19</sup> lung disease ( $n=3$ ),<sup>18,31,33</sup> skin lesions and/or alopecia ( $n=2$ ),<sup>1,14</sup> neuronal or behavioral disorders ( $n=2$ ),<sup>19,20</sup> and cardiovascular disorders ( $n=1$ ).<sup>26</sup> The most commonly investigated serological signs of SLE were ANA and/or anti-ds-DNA antibody levels ( $n=20$ ), followed by anti-Rnp/anti-Sm ( $n=10$ ) and anti-histone ( $n=2$ ). Immunohistochemistry was used in 20 studies to examine morphological changes in kidney tissue and other organs such as the spleen, brain, and liver.

### Humanized lupus mice models

Three articles discuss the use of lupus mice models using humanized mice. This model is obtained by transferring human cells, such as hematopoietic stem cells and PBMC cells, into immunodeficient mice so that human cells can be reconstituted in mice.<sup>7,11,17</sup> All three humanized-modeled mice also showed the progressivity of SLE disease. The onset of lupus and SLE manifestations in each study was different, with an onset of less than 8 weeks,<sup>17</sup> onset between 8 and 16 weeks,<sup>7</sup> and onset more than 16 weeks after stem cell transplantation.<sup>11</sup> Clinical manifestations include proteinuria and lupus nephritis,<sup>11,17</sup> pleuritis,<sup>11</sup> and skin lesions or alopecia.<sup>7</sup> The serological markers used in each study were ANA antibodies, anti-ds-DNA, and anti-RNP/anti-Sm. The use of immunohistochemistry to examine morphological changes in kidney, spleen tissue,<sup>11,17</sup> and skin tissue.<sup>7</sup>

## DISCUSSION

The review systematically examines studies based on two methods of making animal models such as mice of various strains into SLE. The two types of methods are pristane induction and transferring cells from SLE patients into immunodeficient mice. Although both have the potential to develop lupus-like disease, the result is that the mice models made humanized lupus have similarities to those suffered by humans. Interestingly, the majority of mice used as animal models are female. Several factors make the selection of female mice as

animal models in SLE, including (1) mice have similar characteristics to humans in terms of gene composition, cells, and organs. Lupus in humans often affects women compared to men,<sup>2</sup> (2) high levels of the hormone estrogen in female mice correlate with SLE,<sup>36</sup> (3) in general, women and most female SLE mice models are more susceptible to disease,<sup>37</sup> (4) autoantibodies increase in female mice with SLE which is inversely proportional to male mice.<sup>38</sup>

Regarding the role of estrogen hormones in SLE, the mechanism of action of these hormones, namely through estrogen receptor alpha (ER $\alpha$ ), promotes the development of SLE and contributes to female sex bias in the loss of tolerance and immune cell activation caused by the Sle1b lupus susceptibility locus.<sup>39</sup> Multiple preferences may serve as reasons for choosing pristane and humanized cells transplanted SLE methods in creating SLE model mice. Pristane injection may be preferred when the study aims to create a widely used murine model for the induced disease, as the pristane-induced model is one of the most widely used SLE models (2). Human cell transplantation may be preferred when studying the pathogenesis of human SLE and testing new therapies, as it can provide a more human-like model of SLE,<sup>6</sup> and transplantation of humanized cells is likely to be chosen when studying the interaction between human immune cells and other cells in the body, such as kidney cells, which are difficult to replicate in pristane-induced models.<sup>11</sup>

### Pristane Induced Mice Model

The results of several studies that discuss the effects of pristane injection on animal models of mice are shown in Table 2. According to the summary table, the pristane injection method of 0.5 mL (i.p.) can cause various onset and clinical manifestations of the disease. Pristane (2,6,10,14-tetramethylpentadecane) is a type of isoprenoid alkane commonly found in mineral oil. The mineral oil is injected intraperitoneally into the mice to induce peritoneal irritation and increase the yield of monoclonal antibodies from ascites when hybridomas are injected, which can induce autoimmunity.<sup>2,40</sup> The activation of polyclonal B cells elicited by pristane can lead to autoantibodies and the development of autoimmune diseases. In addition, immunologic factors, such as the development of SLE in mice after pristane injection, are associated with modulation of the immune response, including the expression of activated and inhibited Fc receptors.<sup>41</sup> In summary, the onset of SLE in animal models of mice following injection of 0.5 mL of pristane is a complex process involving multiple factors, including pristane injection, polyclonal B cell activation, and immunological factors. The percentage of success rate by using pristane method varies depending on the study and the strain of mice used. A study has shown that the murine lupus model can be successfully established in female BALB/c mice with a single i.p. injection of 0.5 mL of Pristane, and that the specific autoantibody anti-dsDNA for SLE has appeared in the sera of BALB/c mice.<sup>42</sup> The key features of SLE, including the

production of human anti-nuclear autoantibodies, lupus nephritis and pulmonary serositis, were recapitulated when pristane was injected into immunodeficient mice reconstituted with the human immune system (humanized mice).<sup>42</sup> Overall based on previous study result pristane injection is a well-established method to induce lupus-like disease in mice, it may not fully reflect the complexity of the disease in humans.

Various studies from 27 relevant articles used pristane injection with a dose of 0.5 mL that induced peritoneal irritation and increase monoclonal antibody yield from ascites when hybridomas were injected.<sup>2,43</sup> The dose has been taken as the optimal dose to induce the desired effect of each study. Pristane has the ability to activate membranes through its interaction with the lipid bilayer of cells, as well as trigger programmed cell death in lymphoid cell types through the mitochondrial caspase activation pathway.<sup>3</sup> In the process, this triggers the development of autoimmune conditions similar to systemic lupus erythematosus. Regarding the clinical manifestations that appear in the model mice given pristane induction, most of them develop proteinuria and symptoms of lupus nephritis. The mechanism that occurs behind lupus nephritis due to pristane induction is related to the production of autoantibodies against several polynuclear antigens that can form immune complexes deposited in the kidneys due to inflammation and tissue damage.<sup>11,44</sup> Cytokine dysregulation triggers blood-brain barrier (BBB) disruption, IgG deposition, glial activation in nerves, and nerve damage.<sup>45</sup> Basophil activation can lead to autoreactive B cell expansion and autoantibody production, triggering the development of lupus nephritis.<sup>45</sup> A previous study by Yan *et al.* (2020) explained that coptisine, a natural compound, slowed disease progression in pristane-induced lupus mice by inhibiting the Rho/ROCK pathway.<sup>44</sup> Activation of the Rho/ROCK pathway may contribute to the development of lupus nephritis. Other clinical manifestations include arthritis, pulmonary disorders caused by pulmonary hemorrhage within a few weeks in C57BL/6 mice,<sup>46</sup> the appearance of glaucous lesions and/or alopecia, neuronal and behavioral disorders, and cardiovascular disorders. Serologically, the clinical manifestations that appear in pristane-injected mice are antinuclear antibody (ANA) levels and/or anti-ds-DNA, anti-Rnp/Anti-Sm, and anti-histone. ANA measurement with Indirect immunofluorescence (IIF) is usually scored as 0 to 4+ or as a titer (referring to the number of times the blood is diluted and still yields a positive result). An ANA of 0, 1+ or 2+, or at a titer of less than 1:80 (diluted 80 times) does not usually indicate a significant problem.<sup>47</sup> ANA titers at higher levels are more likely to indicate the presence of an autoimmune disease. In cases of lupus, ANA is present in approximately 95% of patients with active disease. Specific antibodies that need to be checked and become the hallmark of SLE are anti-Sm/anti-Rnp, which are non-specific antibodies that appear in many patients with lupus and other rheumatic diseases with an incidence percentage of 25%.<sup>48</sup> Anti-histone shows that the characteristics of drug-induced lupus, namely pristane in lupus model mice.<sup>49</sup> The time required to develop mice as SLE model animals after pristane injection (**Table 2**) at a certain dose varies

depending on the study and the strain of mice used. Some relevant study results explain that pristane-induced mice (PIL) show olfactory dysfunction accompanied by phenotypic symptoms, such as anxiety and depression at the 2nd or 4th month.<sup>19</sup> There are drawbacks to creating pristane-injected mice as a lupus model animal: exposure to hydrocarbon adjuvants can trigger inflammatory or autoimmune responses in humans,<sup>40</sup> and pristane-induced mice are unlikely to fully replicate the complexities of human SLE.<sup>50</sup> Thus, to produce SLE model mice that are similar to humans, other methods are carried out by humanized-lupus mice.

### Humanized Mice Model of Lupus

The humanized mice model (hu-mice) is a mice model in which human cells are transplanted into immunodeficient mice. The term "humanized" is used to indicate that these mice can produce cells that have characteristics similar to humans. For example, by transplanting human immune cells, it is expected that the mice will exhibit characteristics of the human immune system. The use of this humanized mice model can assist researchers in conducting human immune system and stem cell research *in vivo*.<sup>5</sup> The development of humanized mice models is still carried out in limited numbers and involves mice that have been designed to experience immunodeficiency, followed by the transfer and transplantation of human cells.<sup>6</sup> From the findings of related articles, only three articles were relevant to the topic of this systematic review. There is a great opportunity for researchers to use this method as it can provide a platform to study the pathogenesis of SLE and test potential therapeutic agent interventions.<sup>4</sup> In addition, using the hu-mice model can also help identify genetically susceptible loci and targets for future drug development.<sup>51</sup> Thus, this model can further clarify the pathogenesis of SLE and provide new strategies for the prevention and treatment of SLE, especially the development of new drugs for which there are still very few challenges in the form of biological therapies for SLE.

In general, there are currently two main methods used to create hu-mice lupus models. The first method involves the transfer of human peripheral blood mononuclear cells (PBMCs) or peripheral blood lymphocytes (PBLs) from SLE patients to immunodeficient mice. The second method involves the transfer of human hematopoietic stem cells (HSCs) to immunodeficient mice, followed by intraperitoneal administration of pristane to induce SLE.<sup>6,11</sup> The difference between the two characteristics of the PBMC cell transfer method and HSC cells followed by pristane administration according to Chen *et al.* (2022) is that the PBMC method from the patient's blood cells is injected intravenously (i.v.) or intraperitoneally (i.p.) into immunodeficient mice,<sup>6</sup> while in the HSC method, blood stem cells are injected i.v. into immunodeficient mice followed by i.p. pristane administration. The purpose of giving pristane in the HSC method is to stimulate SLE in mice so that it is expected that animal models will produce human anti-nuclear autoantibodies, lupus

nephritis, and pulmonary serositis.<sup>11</sup> Based on the immune cells involved, the HSC + pristane method involves various immune cells in the body, such as T cells, memory B cells, NK cells, Human CD19+ CD20- CD27hi CD38hi plasma blasts/plasma cell, Human CD27+ memory B cells and CD27- IgD- B cells, and human CD27- IgD + naive compared to the PBMC method, namely Human CD45+ cells, CD4+, T cells and CD8+ cells, and IL-17+.<sup>6</sup> In terms of survival rate, mice given PBMCs are more vulnerable than HSCs which can survive up to 13 weeks.<sup>11</sup>

The clinical manifestations that appear in Table 2 are similar to the pristane-injected mice model, among others: Clinical manifestations include proteinuria and lupus nephritis,<sup>11,17</sup> pleuritis,<sup>11</sup> and skin lesions or alopecia.<sup>52</sup> Serological signs in each study studied were ANA antibodies and anti-ds-DNA and anti-RNP/anti-Sm. Each strain of mice used gives rise to the onset of SLE with different times. Some factors may cause differences in onset, namely genetic, environmental and immunological. According to Chen *et al.* (2022), genetic studies in susceptible human or mouse populations show that disease susceptibility is multifactorial, involving complex interactions between several genes along with environmental factors, especially the importance of non-MHC loci that play a role in increasing or suppressing susceptibility to SLE.<sup>6</sup> Environmental factors, such as infections, medication-induced, and UV exposure can be genetically triggered in at-risk individuals.<sup>53</sup> Other immunologically related factors due to T and B cell activation, autoantibody production, and immune complex formation may contribute to the development of SLE in different mouse strains.<sup>2</sup>

There are some advantages (Table 3) of using human stem cells transplanted into mice as an animal model. Cells with cellular defects in SLE humans can provide a SLE model that is more similar to humans, as they are derived from SLE patients and can mimic the complexity of human SLE.<sup>6,11</sup> Transplanted cells from the patients can be used as a method of studying the pathogenesis of SLE and testing new therapies, and the interactions between human immune cells and other cells in the body, such as the kidney that are difficult to replicate in pristane-induced models, can be studied through this method.<sup>11</sup> However, the use of transplanted human SLE cells also has some limitations, such as difficulties in establishing and characterizing models, cell variability among patients, and the cost and ethical considerations associated with using human cells in animal models.

Considering the advantages and disadvantages of both models, it is important to consider the synergy between them. SLE is a complex autoimmune disorder characterized by a multifaceted pathogenesis, which includes an elaborate immune response, autoantibody production and tissue damage. Humanized mouse models of lupus offer a unique opportunity to study disease mechanisms in a more human-like context. This allows researchers to explore the interaction of genetic and environmental factors that contribute to the development of SLE. By contrast, pristane-induced lupus models, which mimic the disease through chemical triggers, provide insights into the immune dysregulation and autoantibody production that are central to SLE pathology. By combining these models, we can attain a

deeper understanding of SLE, bridging the gap between fundamental immunological processes and environmental influences. This integrative approach not only improves our understanding of SLE pathophysiology, but also offers a promising path to evaluate potential therapeutic strategies from a more comprehensive point of view.

## CONCLUSION

Pristane-induced lupus mice offers simplicity, reproducibility, and a predictable time course for studying lupus-like symptoms and autoimmune responses. However, they lack genetic predisposition, relevance to human SLE triggers, and comprehensive organ involvement. On the other hand, humanized mice models with engrafted human immune cells provides a more human-relevant context, complex disease manifestations, and opportunities for drug testing and personalized medicine. Nevertheless, technical challenges, heterogeneity, species differences, and ethical concerns limit their applicability. Choosing between these models depends on the research goals, aspects of the disease being studied, and available resources, while a combination of models can offer a more comprehensive understanding of SLE.

## ACKNOWLEDGMENTS

We like to express our sincere gratitude to Ristekdikti (Ministry of Research, Technology, and Higher Education in Indonesia) for providing a research grant SPK INDUK 087/E5/PG/02.00.PT/2002 and SPK TURUNAN 1071.22/UN10.C10/TU/2022.

## REFERENCES

1. Tang WY, Zhang YH, Zhang YS, Liao Y, Luo JS, Liu JH, et al. Abnormal thymic B cell activation and impaired T cell differentiation in pristane-induced lupus mice. *Immunol Lett* [Internet]. 2021;231(November 2020):49–60. doi: 10.1016/j.imlet.2020.12.012
2. Richard ML, Gilkeson G. Mouse models of lupus: what they tell us and what they don't. *Lupus Sci Med*. 2018;5(1):199. doi: 10.1136/lupus-2016-000199
3. Freitas EC, Oliveira, Souza M, Monticeli OA. Pristane-induced lupus: considerations on this experimental model. *Clin Rheumatol*. 2017;1(2). doi: 10.1007/s10067-017-3811-6
4. Halkom A, Wu H, Lu Q. Contribution of mouse models in our understanding of lupus. *Int Rev Immunol*. 2020;1(1):1–14. doi: 10.1080/08830185.2020.1742712
5. Pittenger MF, Discher DE, Péault BM, Phinney DG, Hare JM, Caplan AI. Mesenchymal stem cell perspective: cell biology to clinical progress. *NPJ Regen Med*. 2019;2(3):22. doi: 10.1038/s41536-019-0083-6
6. Chen J, Liao S, Zhou H, Yang L, Guo F, Chen S, et al. Humanized Mouse Models of Systemic Lupus Erythematosus: Opportunities and Challenges. *Front Immunol*. 2022;18(12):816–956. doi: 10.3389/fimmu.2021.816956



7. Zhou S, Li Q, Zhou S, Zhao M, Lu L, Wu H, et al. A novel humanized cutaneous lupus erythematosus mouse model mediated by IL-21-induced age-associated B cells. *J Autoimmun* [Internet]. 2021;123(July):102686. doi: 10.1016/j.jaut.2021.102686
8. Aschman T, Schaffer S, Georgallis SIB, Triantafyllopoulou A, Staeheli P, Voll RE. Interferon lambda regulates cellular and humoral immunity in pristane-induced lupus. *Int J Mol Sci*. 2021;22(21). doi: 10.3390/ijms222111747
9. Delimitreva SM, Boneva G V., Chakarova I V., Hadzhinesheva VP, Zhivkova RS, Markova MD, et al. Defective oogenesis in mice with pristane-induced model of systemic lupus. *J Reprod Immunol* [Internet]. 2021;148(July):103370. doi: 10.1016/j.jri.2021.103370
10. Dema B, Lamri Y, Pellefigues C, Pacreau E, Saidoune F, Bidault C, et al. Basophils contribute to pristane-induced Lupus-like nephritis model. *Sci Rep* [Internet]. 2017;7(1):7969. doi: 10.1038/s41598-017-08516-7
11. Gunawan M, Her Z, Liu M, Tan SY, Chan XY, Tan WWS, et al. A Novel Human Systemic Lupus Erythematosus Model in Humanised Mice /631/250/38 /631/250/256/2515 /13/21 article. *Sci Rep* [Internet]. 2017;7(1):1–11. doi: 10.1038/s41598-017-16999-7
12. Kalim H, Pratama MZ, Nugraha AS, Prihartini M, Chandra A, Sholihah AI, et al. Regulatory T cells compensation failure cause the dysregulation of immune response in pristane induced lupus mice model. *Malaysian J Med Sci*. 2018;25(3):17–26. doi:10.21315/mjms2018.25.3.3
13. Liou L bang, Chen C chieh, Chiang W yu, Chen M hsin. De-sialylated and sialylated IgG anti-dsDNA antibodies respectively worsen and mitigate experimental mouse lupus proteinuria and possible mechanisms. *Int Immunopharmacol* [Internet]. 2022;109(6):108837. Available from: doi: 10.1016/j.intimp.2022.108837
14. Pannu N, Bhatnagar A. Oxidative stress and immune complexes: Pathogenic mechanisms in pristane induced murine model of lupus. *Immunobiology* [Internet]. 2020;225(1):151871. doi: 10.1016/j.imbio.2019.11.006
15. Lee JY, Madany E, El Kadi N, Pandya S, Ng K, Yamashita M, et al. Type 1 Interferon Gene Signature Promotes RBC Alloimmunization in a Lupus Mouse Model [Internet]. Vol. 11, *Frontiers in Immunology*. 2020. doi: 10.3389/fimmu.2020.584254
16. Peixoto TV, Carrasco S, Botte DAC, Catanozi S, Parra ER, Lima TM, et al. CD4+CD69+ T cells and CD4+CD25+FoxP3+ Treg cells imbalance in peripheral blood, spleen and peritoneal lavage from pristane-induced systemic lupus erythematosus (SLE) mice. *Adv Rheumatol (London, England)*. 2019;59(1):30. doi:10.1186/s42358-019-0072-x
17. Ma K, Du W, Xiao F, Han M, Huang E, Peng N, et al. IL-17 sustains the plasma cell response via p38-mediated Bcl-xL RNA stability in lupus pathogenesis. *Cell Mol Immunol* [Internet]. 2021;18(7):1739–50. doi: 10.1038/s41423-020-00540-4
18. Leiss H, Niederreiter B, Bandur T, Schwarzecker B, Blüml S, Steiner G, et al. Pristane-induced lupus as a model of human lupus arthritis: evolvement of autoantibodies, internal organ and joint inflammation. *Lupus*. 2013 Jul;22(8):778–92. doi: 10.1177/0961203313492869
19. Yun Y, Wang X, Xu J, Jin C, Chen J, Wang X, et al. Pristane induced lupus mice as a model for neuropsychiatric lupus (NPSLE). *Behav Brain Funct* [Internet]. 2023;19(1):3. doi: 10.1186/s12993-023-00205-y
20. Luciano-Jaramillo J, Sandoval-García F, Vázquez-Del Mercado M, Gutiérrez-Mercado YK, Navarro-Hernández RE, Martínez-García EA, et al. Downregulation of hippocampal NR2A/2B subunits related to cognitive impairment in a pristane-induced lupus BALB/c mice. *PLoS One* [Internet]. 2019 Sep 9;14(9):e0217190. doi: 10.1371/journal.pone.0217190
21. Summers SA, Odobasic D, Khouri MB, Steinmetz OM, Yang Y, Holdsworth SR, et al. Endogenous interleukin (IL)-17A promotes pristane-induced systemic autoimmunity and lupus nephritis induced by pristane. *Clin Exp Immunol*. 2014 Jun;176(3):341–50. doi: 10.1111/cei.12287
22. Han S, Zhuang H, Xu Y, Lee P, Li Y, Wilson JC, et al. Maintenance of autoantibody production in pristane-induced murine lupus. *Arthritis Res Ther* [Internet]. 2015;17(1):384. doi: 10.1186/s13075-015-0886-9
23. Liu S, Li Y, Li J, Wang S, Ji P, Zhang M, et al. CD4<sup>+</sup> T Cells Promote IgG Production in MHC-Independent and ICAM-1-Dependent Manners in Pristane-Induced Lupus Mice. Kato Y, editor. *Mediators Inflamm* [Internet]. 2022;2022:9968847. doi: 10.1155/2022/9968847
24. García-Rodríguez S, Rosal-Vela A, Botta D, Cumba Garcia LM, Zumaquero E, Prados-Maniviesa V, et al. CD38 promotes pristane-induced chronic inflammation and increases susceptibility to experimental lupus by an apoptosis-driven and TRPM2-dependent mechanism. *Sci Rep* [Internet]. 2018;8(1):3357. doi: 10.1038/s41598-018-21337-6
25. Kienhöfer D, Hahn J, Stoof J, Csepregi JZ, Reinwald C, Urbonaviciute V, et al. Experimental lupus is aggravated in mouse strains with impaired induction of neutrophil extracellular traps. *JCI Insight*. 2017;2(10):1–13. doi: 10.1172/jci.insight.92920

26. McClung DM, Kalusche WJ, Jones KE, Ryan MJ, Taylor EB. Hypertension and endothelial dysfunction in the pristane model of systemic lupus erythematosus. *Physiol Rep*. 2021;9(3):1–13. doi: 10.14814/phy2.14734
27. Bossaller L, Rathinam VAK, Bonegio R, Chiang P-I, Busto P, Wespiser AR, et al. Overexpression of membrane-bound fas ligand (CD95L) exacerbates autoimmune disease and renal pathology in pristane-induced lupus. *J Immunol*. 2013 Sep;191(5):2104–14. doi:10.4049/jimmunol.1300341
28. Bossaller L, Christ A, Pelka K, Nündel K, Chiang P-I, Pang C, et al. TLR9 Deficiency Leads to Accelerated Renal Disease and Myeloid Lineage Abnormalities in Pristane-Induced Murine Lupus. *J Immunol* [Internet]. 2016 Aug 15;197(4):1044–53. doi: 10.4049/jimmunol.1501943
29. Kanno Y, Miyashita M, Seishima M, Matsuo O.  $\alpha$ 2AP is associated with the development of lupus nephritis through the regulation of plasmin inhibition and inflammatory responses. *Immunity, Inflamm Dis*. 2020 Sep;8(3):267–78. doi: 10.1002/iid3.302
30. Amariljo G, Lourenço E V, Shi F-D, La Cava A. IL-17 Promotes Murine Lupus. *J Immunol* [Internet]. 2014 Jul 15;193(2):540–3. doi: 10.4049/jimmunol.1400931
31. Smith S, Wu PW, Seo JJ, Fernando T, Jin M, Contreras J, et al. IL-16/miR-125a axis controls neutrophil recruitment in pristane-induced lung inflammation. *J Clin Invest*. 2018;3(15):1–15. doi: 10.1172/jci.insight.120798
32. Lu A, Li H, Niu J, Wu S, Xue G, Yao X, et al. Hyperactivation of the NLRP3 Inflammasome in Myeloid Cells Leads to Severe Organ Damage in Experimental Lupus. *J Immunol* [Internet]. 2017 Feb 1;198(3):1119–29. doi: 10.4049/jimmunol.1600659
33. Kluger MA, Melderis S, Nosko A, Goerke B, Luig M, Meyer MC, et al. Treg17 cells are programmed by Stat3 to suppress Th17 responses in systemic lupus. *Kidney Int* [Internet]. 2016 Jan 1;89(1):158–66. doi: 1038/ki.2015.296
34. Zhang L, Wu M, Hu B, Chen H, Pan J-R, Ruan W, et al. Identification and molecular typing of *Naegleria fowleri* from a patient with primary amebic meningoencephalitis in China. *Int J Infect Dis* [Internet]. 2018;72:28–33. doi:10.1016/j.ijid.2018.05.001
35. Zhuang H, Han S, Li Y, Kienhöfer D, Lee P, Shumyak S, et al. A Novel Mechanism for Generating the Interferon Signature in Lupus: Opsonization of Dead Cells by Complement and IgM. *Arthritis Rheumatol*. 2016;68(12):2917–28. doi: 10.1002/art.39781
36. Perry D, Sang A, Yin Y, Zheng Y-Y, Morel L. Murine models of systemic lupus erythematosus. *J Biomed Biotechnol*. 2011;1(1):271694. doi: 10.1155/2011/271694
37. Rottman JB, Willis CR. Mouse Models of Systemic Lupus Erythematosus Reveal a Complex Pathogenesis. *Vet Pathol* [Internet]. 2010 May 6;47(4):664–76. doi: 10.1177/0300985810370005
38. Dent EL, Taylor EB, Sasser JM, Ryan MJ. Temporal hemodynamic changes in a female mouse model of systemic lupus erythematosus. *Am J Physiol Physiol* [Internet]. 2020 Mar 9;318(5):F1074–85. doi: 10.1152/ajprenal.00598.2019
39. Graham JH, Yoachim SD, Gould KA. Estrogen Receptor Alpha Signaling Is Responsible for the Female Sex Bias in the Loss of Tolerance and Immune Cell Activation Induced by the Lupus Susceptibility Locus *Sle1b*. *Front Immunol*. 2020;11(2):582214. doi:10.3389/fimmu.2020.582214
40. Reeves WH, Lee PY, Weinstein JS, Satoh M, Lu L. Induction of autoimmunity by pristane and other naturally occurring hydrocarbons. *Trends Immunol* [Internet]. 2009;30(9):455–64. doi:10.1016/j.it.2009.06.003
41. Hoffmann MH, Tuncel J, Skriner K, Tohidast-Akrad M, Türk B, Pinol-Roma S, et al. The Rheumatoid Arthritis-Associated Autoantigen hnRNP-A2 (RA33) Is a Major Stimulator of Autoimmunity in Rats with Pristane-Induced Arthritis1. *J Immunol* [Internet]. 2007 Dec 1;179(11):7568–76. doi: 10.4049/jimmunol.179.11.7568
42. Alves da Costa T, Lang J, Torres RM, Pelanda R. The development of human immune system mice and their use to study tolerance and autoimmunity. *J Transl Autoimmun*. 2019;2:100021. doi: 10.1016/j.jtauto.2019.100021.
43. Sang A, Yin Y, Zheng YY, Morel L. Animal models of molecular pathology systemic lupus erythematosus. *Prog Mol Biol Transl Sci*. 2012;105:321–370. doi:10.1016/B978-0-12-394596-9.00010-X
44. Yan Y, Zhang Z, Chen Y, Hou B, Liu K, Qin H, et al. Coptisine Alleviates Pristane-Induced Lupus-Like Disease and Associated Kidney and Cardiovascular Complications in Mice [Internet]. Vol. 11, *Frontiers in Pharmacology*. 2020. doi: 10.3389/fphar.2020.00929
45. Dema B, Lamri Y, Pellefigues C, Pacreau E, Saidoune F, Bidault C, et al. Basophils contribute to pristane-induced Lupus-like nephritis model. *Sci Rep*. 2017;7(1):1–9. doi: 10.1038/s41598-017-08516-7
46. Shi Y, Tsuboi N, Furuhashi K, Du Q, Horinouchi A, Maeda K, et al. Pristane-Induced Granulocyte Recruitment Promotes Phenotypic Conversion of Macrophages and Protects against Diffuse Pulmonary Hemorrhage in Mac-1 Deficiency. *J Immunol* [Internet]. 2014 Nov 15;193(10):5129–39. doi: 10.4049/jimmunol.1401051

- 
47. Wijaya C. The Role of Antinuclear Antibody (ANA) Profile in Diagnosis of Systemic Lupus Erythematosus. *Adv Cytol Pathol.* 2017;2(5):133–4. doi: 10.15406/acp.2017.02.00035
  48. Kattah NH, Kattah MG, Utz PJ. The U1-snRNP complex: structural properties relating to autoimmune pathogenesis in rheumatic diseases. *Immunol Rev.* 2010 Jan;233(1):126–45. doi: 10.1111/j.0105-2896.2009.00863.x
  49. Cozzani E, Drosera M, Gasparini G, Parodi A. Serology of Lupus Erythematosus: Correlation between Immunopathological Features and Clinical Aspects. *Autoimmune Dis.* 2014;2014:321359. doi: 10.1155/2014/321359
  50. Moore E, Putterman C. Are lupus animal models useful for understanding and developing new therapies for human SLE? *J Autoimmun.* 2020 Aug;112(1):102490. doi: 10.1016/j.jaut.2020.102490
  51. Celhar T, Fairhurst A-M. Modelling clinical systemic lupus erythematosus: similarities, differences and success stories. *Rheumatology [Internet].* 2017 Apr 1;56(suppl\_1):i88–99. doi: 10.1093/rheumatology/kew400
  52. Zhou T, Liao C, Li HY, Lin W, Lin S, Zhong H. Efficacy of mesenchymal stem cells in animal models of lupus nephritis: a meta-analysis. *Stem Cell Res Ther.* 2020;11(1):1–10. doi:10.1186/s13287-019-1538-9
  53. Barbhaiya M, Costenbader KH. Environmental exposures and the development of systemic lupus erythematosus. *Curr Opin Rheumatol.* 2016;28(5):497-505. doi:10.1097/BOR.0000000000000318
-